UCRL-ID-154357

Hydrologic Resources Management Program and Underground Test Area Project FY 2001 – 2002 Progress Report

T.P. Rose, A.B. Kersting, L.J. Harris, G.B. Hudson, D.K. Smith, R.W. Williams, D.R. Loewen, E.J. Nelson, P.G. Allen, F.J. Ryerson, G.A. Pawloski, C.A. Laue, J.E. Moran

August 15, 2003

U.S. Department of Energy

Lawrence Livermore National Laboratory

DISCLAIMER

This work was performed under the auspices of the U. S. Department of Energy by the University of California, Lawrence Livermore National Laboratory under Contract No. W-7405-Eng-48.

Table of Contents

Introduction: Hydrologic Resources Management Program and Underground Test Area Project FY 2001–2002 Progress Report ..... *i*

Chapter 1: FY 2001-2002 Hot Well Data Summary 1

Chapter 2: Xenon Isotope Measurements of Near-Field Groundwater Samples 19

Chapter 3: Distribution, Concentration, and Isotope Ratios of Uranium and Plutonium in a Nuclear Test Cavity and Collapse Chimney 27

Chapter 4: The Redox State Of Nuclear Melt Glass 41

Chapter 5: α-Autoradiography: A Simple Method to Monitor the Migration of α-Emitters in the Environment 61

Chapter 6: ^{241}Am Analyses by Multi-Collector Inductively Coupled Plasma Mass Spectrometry 77

Chapter 7: A Chlorine-36 Study of Vertical Groundwater Transport in Frenchman Flat, Nevada Test Site 81

Chapter 8: Stable Isotope Investigation of Precipitation and Recharge Processes in Central Nevada 113

Introduction

Hydrologic Resources Management Program and Underground Test Area Project FY 2001–2002 Progress Report

Timothy P. Rose and Annie B. Kersting

This report contains highlights of FY 2001 and 2002 technical studies conducted by the Analytical and Nuclear Chemistry Division (ANCD) at Lawrence Livermore National Laboratory (LLNL) in support of the Hydrologic Resources Management Program (HRMP) and the Underground Test Area (UGTA) Project. These programs are administered by the U.S. Department of Energy, National Nuclear Security Administration, Nevada Site Office (NNSA/NSO) through the Defense Programs and Environmental Restoration Divisions, respectively. HRMP-sponsored work emphasizes the Defense Programs goal of responsible management of natural resources at the NTS, while UGTA-funded work focuses on defining the extent of radionuclide contamination in NTS groundwater resulting from underground nuclear testing.

The report is organized on a topical basis, and contains eight chapters that reflect the range of technical work performed by LLNL-ANCD in support of HRMP and UGTA. While we have emphasized investigations led by ANCD, we also participate in a number of collaborative studies with other contract organizations including the Energy and Environmental Sciences Directorate at LLNL, Los Alamos National Laboratory (LANL), the Desert Research Institute (DRI), the U.S. Geological Survey (USGS), Shaw Environmental, Inc., and Bechtel Nevada.

Chapter 1 describes recent hot well sampling efforts at the NTS, and presents the results of chemical and isotopic analyses of groundwater samples from six near-field wells. These include the Cambric (UE-5n), Bilby (U-3cn PS#2), Bourbon (UE-7nS), Nash (UE-2ce), Tybo/Benham (ER-20-5 #3), and Almendro (U-19v PS#1ds) sites. The data generated by the hot well program is vital to the development and validation of contaminant transport models at the NTS.

Chapter 2 discusses the results of xenon isotope measurements of groundwater samples from the six near-field wells described in Chapter 1. This work demonstrates that fission xenon is present in the water at levels that are readily measurable and highlights the significant differences in xenon concentrations and isotopic abundances at different sites. These differences provide insight into the early cooling history of nuclear test cavities, and may assist in predicting the distribution of the source term in the near-field environment.

Chapter 3 is an investigation of the distribution and abundance of actinides in a nuclear test cavity and chimney. This work demonstrates that early-time processes can widely

disperse actinides at low concentrations outside the melt glass, implying that melt glass dissolution may not be the sole mechanism for the release of actinides to groundwater. The study also provides evidence for the isotopic fractionation of plutonium under the extreme conditions accompanying nuclear explosions.

In Chapter 4, X-ray absorption spectroscopy measurements were used to determine the redox state of Fe and U in nuclear melt glass samples from the NTS. Both elements were found to occur in mixed valence states (Fe^{2+}/Fe^{3+} and U^{5+}/U^{6+}) in all samples. Comparison of the Fe and U redox states with published redox studies of synthetic glasses suggests that plutonium is predominantly in the Pu^{4+} oxidation state in the melt glasses.

In Chapter 5, alpha autoradiography is used in a NTS field study to investigate the spatial distribution and transport of actinides in soils, and to help identify the size distribution and morphology of the actinide particles. It was found that α-emitting radionuclides have moved to at least 39 cm depth in the soil profile, far deeper than expected. The methodology that was developed could easily be applied to other field locations where actinides are dispersed in the soil zone.

Chapter 6 summarizes the development of a method for measuring environmental levels of ^{241}Am on the multi-collector inductively coupled plasma mass spectrometer. The method detection limit of 0.017 pCi/L is about two times lower than the best analyses possible by alpha spectrometry.

Chapter 7 describes a chlorine-36 study of vertical groundwater transport processes in Frenchman Flat. Mass balance calculations developed from a ^{36}Cl mixing model at well ER-5-3 #2 are used to estimate vertical transport fluxes and average vertical flow velocities through the thick volcanic section underlying the basin. The study also documents the variations in $^{36}Cl/Cl$ ratios within the three principal hydrostratigraphic units in Frenchman Flat.

Chapter 8 discusses an ongoing stable isotope investigation of precipitation and recharge processes in central Nevada. Precipitation, spring water, and shallow infiltration samples have been collected at four locations on a biannual basis since 1999. The results show that winter precipitation accounts for >90% of the recharge at these sites. Lysimeter data suggest that most of the evaporation occurring during recharge is due to water vapor loss through the soil zone during periods of slow infiltration.

In addition to the topical investigations described above, LLNL-ANCD contributed to several other major collaborative technical products during FY 2001 and 2002.

One of the landmark achievements was the publication of an unclassified radionuclide inventory for the six principal geographic testing centers at the NTS: Frenchman Flat, Pahute Mesa Area 19, Pahute Mesa Area 20, Rainier Mesa/Shoshone Mountain, Yucca Flat – above the water table, and Yucca Flat – below the water table. This inventory, published by LANL (Bowen et al., 2001), provides a calculated estimate of radioactivity

remaining underground at the NTS after underground nuclear testing ceased on September 23, 1992. The report is the culmination of a multi-year effort by LLNL, LANL, DOE/NV, DOE/HQ, and DOD to address technical concerns and administrative requirements associated with formal approval of the declassification request. These data were also recently published in the peer-reviewed literature (Smith et al., 2003). In addition to the unclassified inventory report, LLNL and LANL also collaborated on the publication of a revised classified radionuclide inventory for all individual nuclear tests conducted at the NTS (Miller et al., 2002).

In 2002, we completed a multi-year investigation of colloid-facilitated transport of actinides in NTS groundwater. This report provides a compilation of results from a series of field, laboratory and modeling studies designed to evaluate the potential for inorganic colloids to transport low-solubility radionuclides, such as Pu, at the NTS (Kersting and Reimus, 2003). This work showed the Pu can exist as it own colloid (intrinsic), or sorb to inorganic colloids (pseudocolloid) and be transported under groundwater conditions expected at the NTS. Colloid-facilitated transport of Pu (intrinsic or pseudo colloids) is the dominant mechanism by which Pu is transported.

Also during FY 2002, LLNL participated in a multi-agency geochemical investigation to determine groundwater flow paths in the Pahute Mesa – Oasis Valley flow system. Using a combination of conservative tracer and reactive transport geochemical models, water budget and travel time estimates were developed for the flow path between the underground testing area on Pahute Mesa and the Oasis Valley discharge area. This work was performed in collaboration with DRI, Shaw Environmental, the USGS, and the Harry Reid Center for Environmental Studies at UNLV. The draft report (Rose et al., 2002) is currently undergoing revision, and will be released as a LLNL UCRL report in 2003.

Finally, we also wish to note the publication of a review document that summarizes our current understanding of the radiochemistry of near-field groundwater samples at the NTS (Smith, 2002). This document provides a historical perspective on the three decades of radionuclide migration studies at the NTS, and assesses variations in radionuclide concentrations over time in the context of the processes governing radionuclide mobility. Discussion of site-specific investigations is included for a number of near-field wells that have extensive sampling histories.

References

Bowen, S.M., Finnegan, D.L., Thompson, J.L., Miller, C.M., Baca, P.L., Olivas, L.F., Geoffrion, C.G., Smith, D.K., Goishi, W., Esser, B.K., Meadows, J.W., Namboodiri, N., and Wild, J.F. (2001) Nevada Test Site Radionuclide Inventory, 1951-1992. Los Alamos National Laboratory Report, LA-13859-MS, September 2001, 28 p.

Kersting, A.B., and Reimus, P.W., eds. (2003) Colloid-facilitated transport of low-solubility radionuclides: A field, experimental, and modeling investigation. Lawrence Livermore National Laboratory Report, UCRL-ID-149688, February 2003, 270 p.

Miller, C.M., Bowen, S.M., Finnegan, D.L., Thompson, J.L., Baca, P.L., Olivas, L.F., Geoffrion, C.G., Smith, D.K., Goishi, W., Esser, B.K., Meadows, J.W., Namboodiri, N., and Wild, J.F. (2002) Total Radionuclide Inventory Associated with Underground Nuclear Tests Conducted at the Nevada Test Site, 1951-1992 (U). Los Alamos National Laboratory Report, LA-13989, Secret/Restricted Data, October 2002, 966 p.

Rose, T.P., Benedict, F.C., Jr., Thomas, J.M., Sicke, W.S., Hershey, R.L., Paces, J.B., Farnham, I.M., and Peterman, Z.E. (2002) Geochemical data analysis and interpretation of the Pahute Mesa – Oasis Valley groundwater flow system, Nye County, Nevada. Lawrence Livermore National Laboratory, draft report prepared for the U.S. Department of Energy, National Nuclear Security Administration, Nevada Operations Office, August 2002, 607 p.

Smith, D.K. (2002) Evaluation of the radiochemistry of near-field water samples at the Nevada Test Site applied to the definition of a hydrologic source term. Lawrence Livermore National Laboratory Report, UCRL-ID-149049, July 2002, 49 p.

Smith, D.K., Finnegan, D.L., and Bowen, S.M. (2003) An inventory of long-lived radionuclides residual from underground nuclear testing at the Nevada test site, 1951-1992. Journal of Environmental Radioactivity, v. 67, p. 35-51.

Chapter 1

FY 2001-2002 Hot Well Data Summary

Timothy P. Rose and Lennox J. Harris

Introduction

This report summarizes the results of chemical and isotopic analyses of groundwater samples collected from near-field "hot" wells during FY 2001 and FY 2002. The objective of this effort is to develop a database that describes the state of the hydrologic source term in wells located near underground nuclear tests (also referred to as near-field wells). These data are subsequently used to support groundwater contaminant transport models at the Nevada Test Site (NTS).

LLNL has participated in radionuclide migration studies at the NTS since the 1970s, and all of the sites described in this report were previously sampled at various times during the history of this effort. A total of 14 near-field wells are now part of a long-term monitoring program wherein samples are collected at defined time intervals in order to develop a long-term perspective on temporal variations in the hydrologic source term. This effort is coordinated by the Environmental Management Program of the U.S. Department of Energy, National Nuclear Security Administration, Nevada Site Office, and is supported by LLNL in cooperation with Los Alamos National Laboratory (LANL), the U.S. Geological Survey (USGS), the Desert Research Institute (DRI), Bechtel Nevada, and Shaw Environmental, Inc.

Samples were collected from a total of six near-field wells at the NTS during FY 2001 and 2002. These include pumped samples from UE-5n (Cambric), U-3cn PS#2 (Bilby), and ER-20-5 #3 (Tybo/Benham), and bailed samples from UE-7nS (Bourbon), UE-2ce (Nash), and U-19v PS1ds (Almendro). LLNL analyzes these samples in accordance with laboratory protocols found in the Underground Test Area Project Standard Operating Procedures Manual (LLNL, 2001). Well data and analytical results for hot well samples collected between FY 2000 and FY 2002 are summarized in Tables 1 through 5 at the end of this chapter. We chose to include the FY 2000 data because additional analyses were performed on several samples since the time of our last report. Descriptions of FY 2000 sampling activities are found in Rose et al. (2002). The samples described here are also being analyzed for ^{129}I, but the data were not available at the time this report was being prepared. The ^{129}I results will be summarized in our next annual report.

Los Alamos National Laboratory also publishes an annual report summarizing hot well data for samples collected concurrently with LLNL. The LANL report includes a different set of parameters than those measured by LLNL, as well as comparative tritium data, and is a valuable compliment to this report. The reader is referred to Finnegan and Thompson (2002) for a discussion of the FY 2001 LANL hot well data.

Well UE-5n (Cambric)

The Cambric test was detonated in Frenchman Flat alluvium on 14 May 1965 at a depth of 294 m below the surface and ~70 m below the water table. In 1974, a cavity re-entry hole (RNM-1) and satellite hole (RNM-2S) were drilled at the Cambric site, and starting in 1975, a 16-year pumping experiment was initiated at RNM-2S to study the migration of radionuclides under induced groundwater flow conditions. Data gathered during this experiment have been the topic of a number of radionuclide transport studies (e.g., Burbey and Wheatcraft, 1986; Ogard et al., 1988; Bryant, 1992; Tompson et al., 1999; Guell and Hunt, 2003).

Well UE-5n was drilled in 1976 at a location ~560 m southeast of the Cambric emplacement hole. It is situated ~100 m NE of the Cambric ditch, an unlined canal that was used to drain the discharge from RNM-2S to Frenchman Lake playa. Radionuclides were not detected in UE-5n groundwater until 1989, and are inferred to reflect infiltration of water from Cambric ditch. Recent modeling of vadose zone transport from Cambric ditch to UE-5n strongly supports this hypothesis (Tompson et al., 2002).

Groundwater characterization samples were collected at UE-5n on 19 April 2001 using the DRI Bennett pump, which was set at the top of the water table (702 ft below the surface). Approximately 4730 L of water were purged prior to sampling, at a pump rate of 1.3 L/min. The major ion chemistry of UE-5n groundwater is dominated by Na^+ and HCO_3^- ions with moderate levels of SO_4^{2-}, as is characteristic of water produced from the alluvial aquifer in Frenchman Flat. The stable isotope (δD and $\delta^{18}O$) composition of the water indicates it has undergone moderate amounts of evaporation relative to other Frenchman Flat groundwaters (see also Rose et al., 2002). This observation is consistent with the presence of recycled water from Cambric ditch.

Two separate measurements of the tritium activity in UE-5n groundwater yielded values of 1.38×10^5 and 1.40×10^5 pCi/L (corrected to the sample date). These results are comparable to values reported by Finnegan and Thompson (2002). Tritium decay produces a local accumulation of ^3He in the groundwater that can be used to estimate the mean residence time of the groundwater. The $^3He/^4He$ ratio in UE-5n groundwater was >800 times above the natural atmospheric ratio in April 2001, from which a mean ^3H-^3He age of 9.7 years was calculated. This age is consistent with the observed arrival of tritium at UE-5n approximately one decade before the samples were collected.

Dissolved inorganic carbon (DIC) in UE-5n groundwater has a very low ^{14}C value (28.4 pmc) relative to the amount of tritium in the water. Given the likelihood that the tritium in UE-5n originated from Cambric ditch, it is plausible that the test-derived ^{14}C was removed by isotopic exchange with calcite during infiltration through the ~200 meter thick vadose zone (see Rose et al., 2002). In contrast, the amount of ^{36}Cl in the water ($^{36}Cl/Cl = 5.4 \times 10^{-10}$) is approximately three orders of magnitude above the natural background level, implying that ^{36}Cl is far more conservative than ^{14}C during vadose zone transport.

UE-5n groundwater has an $^{87}Sr/^{86}Sr$ ratio (0.71039) that is similar to other groundwater samples from the alluvial and volcanic aquifers in Frenchman Flat (e.g. Rose et al., 1997), reflecting equilibration of the water with the volcanic-rich basin fill sediments. The isotopic composition of dissolved uranium in UE-5n groundwater is consistent with natural abundances.

U-3cn PS#2 (Bilby)

The Bilby test was conducted in on 09 September 1963 at a depth of 713 m beneath the surface of Yucca Flat, and ~240 m below the water table. The working point lithology consists of zeolitized non-welded ash-flow tuff (tuff-confining unit). U-3cn PS#2 was drilled within the Bilby collapse chimney soon after the test, and was originally completed in the test cavity. Shortly after completion, the casing crimped at 587 m, presumably due to shifting blocks within the chimney rubble (Garber, 1971). The following year, a packer was inserted above the broken casing, and new perforations were made between 512 and 527 m depth. Groundwater samples were collected sporadically between 1964 and 1985 (e.g. Buddemeier and Isherwood, 1985), and in January 1997 the well was rehabilitated and sampled for the UGTA project (DOE/NV, 1998).

On 18 December 2001, groundwater samples were collected from U-3cn PS#2 using a submersible pump with a discharge rate of ~35.5 L/min (9.4 gal/min). Approximately 5.4×10^4 L of water was purged from the well prior to sampling. The well produces a sodium-potassium-bicarbonate groundwater that is low in Cl and SO_4, and is typical of the water found in tuffaceous volcanic rocks beneath Yucca Flat (Winograd and Thordarson, 1975). U-3cn PS#2 groundwater has stable isotope (δD and $\delta^{18}O$) values that are depleted in heavy isotopes relative to modern precipitation in Yucca Flat (Ingraham et al., 1991). Assuming the water was locally recharged (as opposed to "imported" via regional flow), the stable isotope data imply recharge under much cooler climatic conditions than present-day southern Nevada.

The tritium activity of U-3cn PS#2 groundwater was 9.9×10^6 pCi/L in December 2001, as compared to 1.3×10^7 pCi/L in January 1997 (corrected to the respective sample dates). Decay correcting both measurements to the Bilby zero time produces nearly identical values, implying little groundwater circulation through the Bilby chimney. Dissolved helium in the water has a $^3He/^4He$ ratio 10^5 times the natural atmospheric ratio, reflecting significant in-growth of ^3He from tritium decay. However, the calculated ^3H-^3He age of the water was only 23.6 years in December 2001, or 38% lower than expected. This suggests that some helium gas was lost from the system.

U-3cn PS#2 groundwater has a radiocarbon value that is 878 times the modern atmospheric level (8.78×10^4 pmc). This is equivalent to a ^{14}C activity of 303 pCi/L (at a DIC concentration of 287 mg/L HCO_3). The ^{14}C value measured in 1997 was only 515 times modern, although the increase in the 2001 sample may simply reflect an improvement in our analytical method. When we ran the Bilby sample in 1997, the sample was not diluted prior to analysis, and the detectors on the accelerator mass

spectrometer (AMS) were saturated by the high ^{14}C count rate. Samples are now diluted with ^{14}C-absent CO_2 prior to analysis, and the actual ^{14}C concentration is later calculated based on the dilution amount. This provides a more accurate method of measuring extremely "hot" samples. An analogous dilution method is used to measure $^{36}Cl/Cl$ ratios on the AMS. However, we failed to produce a reliable $^{36}Cl/Cl$ ratio for the U-3cn PS#2 sample collected in 2001 due to a lack of adequate dilution. A more highly diluted sample will be re-analyzed in the near future. The groundwater sample collected from U-3cn PS#2 in 1997 had a $^{36}Cl/Cl$ ratio of 1.24×10^{-9} and an activity of 0.3 pCi/L.

Strontium and uranium analytical results showed very little change between 1997 and 2001. The $^{87}Sr/^{86}Sr$ ratio in U-3cn PS#2 groundwater is consistent with groundwater in equilibrium with the volcanic host rock. Uranium isotope measurements indicate the dissolved uranium is natural in origin, although the U concentration in the water is higher than average for the NTS (10.7 μg/L). The total plutonium concentration (colloidal + dissolved) in U-3cn PS#2 groundwater is below the detection limit of 0.6×10^{-12} g/L (0.6 pg/L). Hence, reliable Pu isotope ratios and activities could not be determined.

A satellite hole near the Bilby test (U-3cn #5) is completed in Paleozoic carbonate rocks and has been periodically monitored for radionuclides since the mid-1960s. When LLNL last sampled this hole in 1997, we found a tritium activity of only 80 pCi/L. More recently, LANL collected samples from this U-3cn #5 and reported tritium values were below 40 Bq/L (1.08×10^3 pCi/L; Finnegan and Thompson, 2001). These results suggest that little or no contamination is moving downward from the test cavity to the underlying carbonate aquifer.

UE-7nS (Bourbon)

The Bourbon (U-7n) test was detonated on 20 January 1967 at a depth of 560 m beneath Yucca Flat. The test was conducted in unsaturated Paleozoic carbonate rock, and the base of the cavity is inferred to be "near" the water table, although it is uncertain whether it is in direct contact with the groundwater (e.g. Buddemeier and Isherwood, 1975). The satellite well UE-7nS was drilled at a location 137 m SE of the Bourbon emplacement hole in 1976. The total depth of UE-7nS is 672 m, and the static water level is at 601 m. The stratigraphic contact between the overlying tuff and carbonate rock occurs at a depth of 503 m.

Groundwater samples were collected from UE-7nS on 21 August 2001 using the USGS wireline bailer. The sampling depth was 617.2 m below the surface. The major ion chemistry of UE-7nS groundwater is dominated by Na^+ and HCO_3^-, with modest amounts of Ca^{2+} and Cl^-, and very low SO_4^{2-}. The most striking aspect of these data is that they do not look like a typical carbonate aquifer groundwater, but instead resemble groundwater from the overlying volcanic tuffs (with slightly elevated Ca^{2+}). It is possible that groundwater is moving laterally from the volcanic tuff to the carbonate rock in this area, although we lack detailed information on the geology and local hydraulic gradient to support this hypothesis.

The δD and $\delta^{18}O$ values of UE-7nS groundwater are depleted in heavy isotopes relative to local precipitation, and strongly resemble other lower carbonate aquifer (LCA) groundwaters in Yucca Flat (e.g. Rose et al., 1997). Although depleted δD-$\delta^{18}O$ values are not unique to the carbonate aquifer, it is notable that the dissolved inorganic carbon is highly enriched in ^{13}C ($\delta^{13}C$ = -2.0‰), implying the water is in isotopic equilibrium with the carbonate rock. Hence, the UE-7nS stable isotope data are generally consistent with a carbonate aquifer source, even though the water chemistry is not typical of the LCA.

Two separate tritium analyses on the UE-7nS samples collected in 2001 gave values of 4.6×10^3 pCi/L (at the lab in Mercury) and 8.0×10^2 pCi/L (at LLNL). Finnegan and Thompson (2002) reported tritium activities ranging from ~2.7×10^2 to 3.2×10^3 pCi/L for the same sampling event, and noted that the activity increased with each successive bailer run. When UE-7nS was last sampled in 1993, the tritium activity was 4.6×10^2 pCi/L. Correcting the 1993 and 2001 results to t = 0 suggests the tritium value may be increasing with time, although the trend is inconclusive given the apparent lack of mixing in the borehole. The $^3He/^4He$ ratio in UE-7nS groundwater is remarkably high given the low tritium concentration in the sample ($R/R_a = 5.71 \times 10^3$). The calculated ^3H-^3He age of the water is ~95 years, or almost three times the age of the test! This may suggest that ^3He is somehow getting to the well in advance of the tritium. Given that the working point of the Bourbon test is above the water table, it is possible that helium is being preferentially transported relative to tritium through the unsaturated zone, perhaps by a diffusive mechanism. However, we have no supporting evidence for this suggestion.

The ^{14}C value of dissolved inorganic carbon (DIC) in UE-7nS is 69.7 percent modern, which is slightly less than the atmospheric value (100 pmc). As noted above, the $\delta^{13}C$ value suggests the groundwater DIC has equilibrated with the carbonate rock. This equilibration process normally yields ^{14}C values <50 pmc on very short timescales, and <10 pmc on 1,000-year timescales. We therefore conclude that a small fraction of test-derived radiocarbon is present in the sample. A similar argument can be made for ^{36}Cl, which shows a slight enrichment in UE-7nS groundwater ($^{36}Cl/Cl = 1.9 \times 10^{-12}$) relative to natural environmental levels (~ 5.0×10^{-13}). The uranium concentration in UE-7nS groundwater is low (0.04 μg/L) compared to most groundwaters in southern Nevada (e.g. Paces et al., 2002), and the measured $^{235}U/^{238}U$ ratio indicates the uranium is natural in origin. The plutonium concentration is below the detection limit of 0.6 pg/L.

To quote Buddemeier and Isherwood (1985) regarding the UE-7nS site: "It is safe to say that there is no indication of significant radionuclide migration from the cavity to the satellite well and that the low water yield makes the site inappropriate for a serious pumping experiment. Further analysis is probably not justified unless routine tritium monitoring indicates the breakthrough of higher activity water or new questions or techniques are developed". These words were written nearly two decades ago, but are probably just as true now as they were then. Given the possible tritium increase in the 2001 samples, it is timely to attempt pumping the UE-7nS well again. This would provide the most reliable means of comparing the current state of radionuclide migration at this site with the historical data.

UE-2ce (Nash)

The Nash (U-2ce) test was conducted in unsaturated carbonate rock on 19 January 1967 at a depth of 367.6 m below the surface of Yucca Flat. In 1977, the satellite well UE-2ce was drilled at a location 183 m south of the Nash emplacement hole to a total depth of 503 m. The depth to the water table is ~448 m. UE-2ce was pumped and sampled intermittently between 1977 and 1984, and a cumulative volume of more than 4×10^7 L was pumped from the well during that time period (Buddemeier and Isherwood, 1985). The tritium activity in April 1984 was reported to be 7.3×10^7 pCi/L. In August 1993, samples were collected from UE-2ce using a wireline bailer, at which time the tritium activity had dropped to 1.3×10^5 pCi/L.

We returned to UE-2ce on 21 August 2001 and collected a suite of groundwater samples using the USGS wireline bailer. The sampling depth was 472.5 m below the surface. The water chemistry is typical of most LCA groundwaters, Ca^{2+} and HCO_3^- being the dominant dissolved ions, although substantial amounts of Na^+, Mg^{2+}, and K^+ ions are also present. UE-2ce has δD and $\delta^{18}O$ values that are enriched in heavy isotopes compared with most Yucca Flat waters, particularly those from the LCA. Even so, comparable δD and $\delta^{18}O$ values were observed in the LCA within the shallowest of three pumped intervals in well UE-10j (691 to 699 m depth) in March 1997. Both UE-2ce and UE-10j are located in northern Yucca Flat, and the water produced from these wells may reflect the "typical" isotopic composition of groundwater in the upper part of the LCA in this area.

The tritium activity in UE-2ce groundwater was 1.4×10^5 pCi/L in August 2001, and is nearly identical to the value observed in 1993. The 2001 sample of course has a higher decay corrected value (at t = 0) relative to the 1993 sample, but is still well below the values observed during pumping in the 1980s. UE-2ce has a $^3He/^4He$ ratio that is 1500 times the atmospheric value, yielding a ^3H-^3He age of 16.3 years (as of August 2001). The actual time elapsed between the test date and sample date was ~34.5 years. Hence, the ^3H-^3He age is less than half of the expected value, indicating that some fraction of the parent tritium and daughter helium were somehow separated.

UE-2ce groundwater shows a modest ^{14}C enrichment of 217 percent modern that is somewhat lower than expected based on the tritium activity. As with wells UE-7nS and UE-5n, it is probable that ^{14}C transport is being attenuated by isotopic exchange reactions with carbonate minerals in the aquifer. These data suggest it is unlikely that ^{14}C will ever represent a major contamination issue in aquifers containing large amounts of carbonate minerals, such as the LCA. In contrast to radiocarbon, ^{36}Cl appears to be transported conservatively in UE-2ce groundwater. The $^{36}Cl/Cl$ ratio (1.62×10^{-9}) is higher than expected based on the observed tritium activity, and is comparable to values recently observed at Cheshire (U-20n) and Almendro (U-19v). Interestingly, the ^{14}C and ^{36}Cl in UE-2ce groundwater have identical activities of 0.8 pCi/L. UE-2ce groundwater has a relatively low uranium concentration (0.39 μg/L) and the measured $^{235}U/^{238}U$ ratio indicates the uranium is natural in origin. The plutonium concentration in the water is below the detection limit of 0.6 pg/L.

UE-2ce remains the only site where substantial radionuclide migration has been documented in the lower carbonate aquifer (LCA). As such, it is perhaps the best location available for performing forced gradient studies of radionuclide migration within the LCA. The 8.625" diameter casing in the hole can readily accommodate a submersible pump, and installation of a pump would vastly improve the quality of samples collected during routine hot well monitoring.

ER-20-5 #3 (Tybo/Benham)

ER-20-5 #3 is one of a cluster of three holes that were drilled by the U.S. Department of Energy, Nevada Operations Office in support of the Nevada Environmental Restoration Project at the NTS. ER-20-5 #3 is located ~290 m WSW of ground zero for the Tybo test (U-20y), which was detonated on 14 May 1975 at a depth of 765 m beneath the surface of Pahute Mesa. The Tybo working point was ~135 m below the water table, in zeolitized non-welded Topopah Spring Tuff (DOE/NV, 1997). Well ER-20-5 #3 was completed in 1996 at a depth of 1,308.8 m, with one screened interval from 1,045.6 to 1,183.2 m in a lava-flow aquifer of the Calico Hills Formation.

Groundwater samples were previously collected from ER-20-5 #3 in 1996, 1997, and 1998 using a downhole Moyno pump. Tritium activities during sampling were consistently in the range of 1.1 to 1.6×10^5 pCi/L. It was initially assumed that the radioactivity in groundwater from the ER-20-5 well cluster originated from the Tybo test. However, Kersting et al. (1999) demonstrated that the $^{240}Pu/^{239}Pu$ isotopic ratio of groundwater from ER-20-5 #1 and ER-20-5 #3 uniquely matches that of the Benham test, located 1.3 km NNE of the ER-20-5 well cluster, and does not match that of the Tybo test or any other potential sources in the area. Plutonium transport is facilitated by sorption to colloidal-size mineral particles (cf. Kersting and Reimus, 2003), which also carry detectable amounts of ^{60}Co and ^{137}Cs in the ER-20-5 #3 samples.

Pumped groundwater samples were collected at well ER-20-5 #3 on 15 November 2001. Approximately 5.6×10^4 L of water was purged from the well (at ~38 L/min) prior to sample collection. Well ER-20-5 #1 was originally scheduled for concurrent sampling, but the dedicated Moyno pump in the hole failed shortly after start-up. Well ER-20-5 #3 produces a sodium bicarbonate groundwater with modest levels of Cl^- and SO_4^{2-} that is characteristic of tuffaceous volcanic rocks beneath Pahute Mesa. The δD and $\delta^{18}O$ values of ER-20-5 #3 groundwater are consistent with regional groundwater underflow from north of the Nevada Test Site (Blankennagel and Weir, 1973; Thomas et al., 2002).

The tritium activity in the 2001 sample was 1.4×10^5 pCi/L at the time of sampling, and is within the range of previously observed values. It is notable that the decay corrected tritium values appear to show a slight increasing trend over time. The $^3He/^4He$ ratio is 784 times the atmospheric ratio, and the calculated ^3H-^3He age is 25 years. This age closely matches the time elapsed since the 1975 Tybo test, but is somewhat lower than the age of the Benham test, which was conducted in December 1968. If we assume the

tritium is derived from Benham, as the plutonium data suggest, then some helium gas loss must have occurred.

Dissolved inorganic carbon in ER-20-5 #3 groundwater has a ^{14}C value of 1,570 pmc, or approximately 15 times the modern atmospheric level. This corresponds to a radiocarbon activity of 2 pCi/L, given the DIC concentration of 110 mg/L HCO_3^-. As with tritium, the ^{14}C concentration in this well has remained fairly constant over time, although the 2001 sample does show a slight enrichment over previous years (earlier values range from 1,350 to 1,460 pmc). The $^{36}Cl/Cl$ ratio at ER-20-5 #3 was 3.49×10^{-11} in the 2001 sample, which is a factor of two higher than the last time the well was sampled. When considered together, the conservative radionuclide data (^3H, ^{14}C, and ^{36}Cl) suggest that groundwater activities may be slowly increasing with time at ER-20-5 #3.

The $^{87}Sr/^{86}Sr$ ratio in the ER-20-5 #3 sample (0.70864) reflects the equilibration of the groundwater with strontium in the host rock, and is comparable to other volcanic aquifer groundwaters at the NTS (e.g. Rose et al., 1997). ER-20-5 #3 groundwater has a high uranium concentration (12.8 μg/L), but the $^{235}U/^{238}U$ ratio indicates an environmental source for the uranium. Uranium enrichments are not uncommon in rhyolitic tuffs. The total plutonium concentration in the water is below our current method detection limit of 0.6 pg/L.

The ER-20-5 wells are strategically located near the NTS boundary on Pahute Mesa, and will continue to be a valuable asset for long-term monitoring of radionuclide migration. It will be interesting to return to ER-20-5 #3 within the next several years to determine whether the apparent trend toward increasing concentrations of conservative radionuclides continues. In addition, there would be considerable value in replacing the broken Moyno pump in ER-20-5 #1 given that this well has a history of producing groundwater with higher concentrations of radionuclides than the ER-20-5 #3 well.

U-19v PS#1ds (Almendro)

The Almendro test was conducted on 06 June 1973 at a depth of 1,063 m beneath the surface of Pahute Mesa. The lithology at the working point consists of a devitrified lava flow breccia of the Bullfrog Tuff. Post-shot re-entry hole U-19v PS#1ds was drilled through the Almendro cavity to a vertical depth of 1,169.5 m (corrected for borehole slant). The water table was tagged at ~667 m vertical depth in May 2001. Prior to 2001, the water level had shown a gradual increase since the time of the test, reaching a maximum value of ~661 m depth (see Fenelon et al., 2000). The 2001 measurement is the first documented instance of an apparent drop in water level at this site, and should be verified.

Well U-19v PS#1ds was sampled on a number of occasions in recent years, including 1996, 1998, 1999, and 2000 (see Smith et al., 1998, 1999; Rose et al., 2001). Tritium activities have remained fairly constant over this time period, ranging from 1.5 to 2.1×10^8 pCi/L at the time of sampling. The most remarkable feature of the Almendro

site is the anomalous groundwater temperature, which has remained elevated for nearly three decades since the test was fired. A borehole temperature log in 1996 recorded a maximum value of 157°C at 1,073 m vertical depth. These data imply the Almendro test cavity is effectively isolated from the surrounding groundwater environment.

Groundwater samples were again collected at U-19v PS#1ds on 31 May 2001 using the USGS wireline bailer. The sampling depth was 941.5 m below the surface (vertical). The major ion chemistry of the water is dominated by Na^+ and HCO_3^- but contains high concentrations of Cl^- (66.5 mg/L) and low SO_4^{2-} (2.5 mg/L). Also notable is the unusual enrichment in selected trace elements, including As (0.14 mg/L), Mo (1.2 mg/L) and Pb (0.25 mg/L). The enrichments in Cl and soluble trace elements probably reflect prolonged hydrothermal leaching of the wall rock adjacent to the test cavity. Almendro groundwater also shows a pronounced enrichment in ^{18}O relative to water from other deep wells on Pahute Mesa, but lacks a correlated enrichment in deuterium. This observation almost certainly reflects oxygen isotope exchange between the groundwater and the wall rock, as is widely observed in natural geothermal systems.

The tritium activity in U-19v PS#1ds groundwater was 1.8×10^8 pCi/L in May 2001. As noted above, this value has not varied appreciably over the past 6 years. Decay corrected values have also remained fairly steady since 1996. The $^3He/^4He$ ratio in the water is 1.8×10^5 times the ratio in air, but the actual concentration of dissolved helium is much lower than expected. Hence, the calculated ^3H-^3He age of the water is only 2 years, indicating that helium is being lost from the system. Conversely, the concentration of ^{130}Xe in the water is approximately twice the predicted value based on atmospheric equilibrium (see also Chapter 2 of this report).

Dissolved inorganic carbon in Almendro groundwater is characterized by unusually high $\delta^{13}C$ values (+30‰ in the most recent samples) that are consistent with methanogenic reduction of CO_2. The large isotopic fractionation between CH_4 and CO_2 causes the DIC remaining in the system to become enriched in ^{13}C. The ^{14}C value of the DIC is 3.11×10^4 pmc, corresponding to an activity of 93 pCi/L. This ^{14}C activity is lower than expected for the amount of tritium in the groundwater, which may suggest some loss of radiocarbon to the gas phase during methanogenesis. The $^{36}Cl/Cl$ ratio in U-19v PS#1ds groundwater is 1.63×10^{-9}, and the ^{36}Cl activity is 3.6 pCi/L. Both ^{14}C and ^{36}Cl have remained relatively constant during recent sampling history.

The uranium concentration in U-19v PS#1ds groundwater is very low (0.03 μg/L in the 2001 sample) and may be a reflection of the redox state of the system. Methanogenesis occurs only in anoxic environments, indicating that the test cavity environment must be fairly reducing. The stable oxidation state of uranium under reducing conditions is U^{4+}, which has a much lower solubility in water than the more oxidized U^{6+}. The $^{235}U/^{238}U$ ratio indicates the uranium is natural, but it is notable that low level ^{236}U from the device was detected in both the 2000 and 2001 samples.

Plutonium was once again detected in the 2001 Almendro sample at a concentration of 2.12 ± 0.27 pg/L, with a combined $^{239,240}Pu$ activity of 0.18 pCi/L. However, this is

considerably less in than the 1999 Almendro sample, where the Pu concentration was 58.2 ± 3.9 pg/L with a ^{239,240}Pu activity of 9.4 pCi/L. We note that the 2001 sample contained a considerable amount of grayish particulate matter even after acidifying the sample with HNO_3 to a pH < 2. It is possible that much of the Pu was associated with the insoluble particulates, accounting for the difference in concentration between the 1999 and 2001 samples.

References

Blankennagel, R.K, and Weir, J.E., Jr. (1973) Geohydrology of the eastern part of Pahute Mesa, Nevada Test Site, Nye County, Nevada. U.S. Geological Survey Professional Paper 712-B, 35 p.

Bryant, E.A. (1992) The Cambric Migration Experiment – A Summary Report. Los Alamos National Laboratory Report, LA-12335, September 1992.

Buddemeier, R.W., and Isherwood, D. (1985) Radionuclide Migration Project – 1984 Progress Report. Lawrence Livermore National Laboratory Report, UCRL-53628, April 1985, 71 p.

Burbey, T.J., and Wheatcraft, S.W. (1986) Tritium and chlorine-36 migration from a nuclear explosion cavity. Desert Research Institute, Water Resources Center Publication #45050, University of Nevada, Reno, April 1986, 103 p.

DOE/NV (1997) Completion Report for Well Cluster ER-20-5. U.S. Department of Energy, Nevada Operations Office, Environmental Restoration Project, DOE/NV-466, Las Vegas, NV, March 1997.

DOE/NV (1998) Recompletion Report for BILBY. U.S. Department of Energy, Nevada Operations Office, Environmental Restoration Project, DOE/NV-500, Las Vegas, NV, February 1998.

Fenelon, J.M. (2000) Quality assurance and analysis of water levels in wells on Pahute Mesa and vicinity, Nevada Test Site, Nye County, Nevada. U.S. Geological Survey Water-Resources Investigations Report 00-4014, 68 p.

Finnegan, D.L., and Thompson, J.L. (2001) Laboratory and Field Studies Related to Radionuclide Migration at the Nevada Test Site in Support of the Underground Test Area Program and Hydrologic Resources Management Project. Los Alamos National Laboratory Report, LA-13787-PR, January 2001, 19 p.

Finnegan, D.L., and Thompson, J.L. (2002) Laboratory and Field Studies Related to Radionuclide Migration at the Nevada Test Site in Support of the Underground Test Area and Hydrologic Resources Management Projects. Los Alamos National Laboratory Report, LA-13919-MS, June 2002, 25 p.

Garber, M.S. (1971) Hydraulic-test and quality-of-water data from hole U-3cn PS#2, Bilby site, Nevada Test Site. U.S. Geological Survey Report USGS-474-102 (NTS-230), Denver, CO.

Guell, M.A., and Hunt, J.R. (2003) Groundwater transport of tritium and krypton 85 from a nuclear detonation cavity. Water Resources Research, v. 39, p. 1175-1185.

Ingraham, N.L., Lyles, B.F., Jacobson, R.L., and Hess, J.W. (1991) Stable isotopic study of precipitation and spring discharge in southern Nevada. Journal of Hydrology, v. 125, p. 243-258.

Kersting, A.B., Efurd, D.W., Finnegan, D.L., Rokop, D.J., Smith, D.K., and Thompson, J.L. (1999) Migration of plutonium in groundwater at the Nevada Test Site. Nature, v. 397, p. 56-59.

Kersting, A.B., and Reimus, P.W., eds. (2003) Colloid-facilitated transport of low-solubility radionuclides: A field, experimental, and modeling investigation. Lawrence Livermore National Laboratory Report, UCRL-ID-149688, February 2003, 270 p.

LLNL (2001) Analytical Measurements: Standard Operating Procedures, Underground Test Area Project. Lawrence Livermore National Laboratory, unpublished report, September 2001.

Ogard, A.E., Thompson, J.L., Rundberg, R.S., Wolfsberg, K., Kubic, P.W., Elmore, D., and Bentley, H.W. (1988) Migration of chlorine-36 and tritium from an underground nuclear test. Radiochimica Acta, v. 44/45, p. 213-217.

Paces, J.B., Ludwig, K.R., Peterman, Z.E., and Neymark, L.A. (2002) $^{234}U/^{238}U$ evidence for local recharge and patterns of groundwater flow in the vicinity of Yucca Mountain, Nevada, USA. Applied Geochemistry, v. 17, p. 751-779.

Rose, T.P., Kenneally, J.M., Smith, D.K., Davisson, M.L., Hudson, G.B., and Rego, J.H. (1997) Chemical and isotopic data for groundwater in southern Nevada. Lawrence Livermore National Laboratory Report, UCRL-ID-128000, July 1997, 35 p.

Rose, T.P., Eaton, G.F., and Yamamoto, R.I., eds. (2002) Hydrologic Resources Management Program and Underground Test Area Project FY 2000 Progress Report. Lawrence Livermore National Laboratory Report, UCRL-ID-145167, June 2002, 141 p.

Smith, D.K., Kersting, A.B., Rose, T.P., Kenneally, J.M., Hudson, G.B., Eaton, G.F., and Davisson, M.L. (1998) Hydrologic Resources Management Program and Underground Test Area Operable Unit FY 1997 Progress Report. Lawrence Livermore National Laboratory Report, UCRL-ID-130792, May 1998, 92 p.

Smith, D.K., Eaton, G.F., Rose, T.P., Kenneally, J.M., Hudson, G.B., Davisson, M.L., Benedict, F.C., Jr., and Criss, R.E. (1999) Hydrologic Resources Management Program and Underground Test Area FY 1998 Progress Report. Lawrence Livermore National Laboratory Report, UCRL-ID-135170, July 1999, 76 p.

Thomas, J.M., Benedict, F.C., Jr., Rose, T.P., Hershey, R.L., Paces, J.B., Peterman, Z.E., Farnham, I.M., Johannesson, K.H., Singh, A.K., Stetzenbach, K.J., Hudson, G.B., Kenneally, J.M., Eaton, G.F., and Smith, D.K. (2002) Geochemical and isotopic interpretations of groundwater flow in the Oasis Valley flow system, southern Nevada. Desert Research Institute, Water Resources Center Publication No. 45190

Tompson, A.F.B., Bruton, C.J., and Pawloski, G.A., eds. (1999) Evaluation of the hydrologic source term from underground nuclear tests in Frenchman Flat at the Nevada Test Site:

The CAMBRIC test. Lawrence Livermore National Laboratory Report, UCRL-ID-132300, March 1999, 355 p.

Tompson, A.F.B., Smith, D.K., and Hudson, G.B. (2002) Analysis of radionuclide migration through a 200-m vadose zone following a 16-year infiltration event. Lawrence Livermore National Laboratory Report, UCRL-ID-146979, January 2002, 27 p.

Winograd, I.J., and Thordarson, W. (1975) Hydrogeologic and hydrochemical framework, south-central Great Basin, Nevada-California, with special reference to the Nevada Test Site. U.S. Geological Survey Professional Paper 712-C, 126 p.

Table 1. Hot well construction data and sampling information.

Well name	Test Name	Test Date	Latitude (d m s)	Longitude (d m s)	Surface Elevation (m)	Well Depth (m bgs)	Open Interval (m bgs)	Water Depth (m bgs)	Sample Method	Sample Depth (m bgs)	Sample date
Frenchman Flat											
UE5n	Cambric	14-May-65	36 49 34	116 06 59	949	515	219-223	214	pump	214	19-Apr-01
UE5n	Cambric	14-May-65	36 49 34	116 06 59	949	515	219-223	215	pump	223	09-Sep-99
RNM-1	Cambric	14-May-65	36 49 28	115 58 01	956	397 †	324-328 †	241 †	pump	---	28-Jun-00
RNM-2S	Cambric	14-May-65	36 49 21	115 58 01	955	341	316-341	220	pump	---	14-Jun-00
RNM-2S	Cambric	14-May-65	36 49 21	115 58 01	955	341	316-341	220	pump	224	11-Oct-99
Yucca Flat											
U4u PS2a	Dalhart	13-Oct-88	37 05 13	116 02 51	1255	695	472-501	499	pump	500	16-Aug-99
UE-7ns	Bourbon	20-Jan-67	37 05 56	116 00 09	1332	672	608-670	601	bailer	617	21-Aug-01
UE-2ce	Nash	19-Jan-67	37 08 31	116 08 07	1452	503	422-495	448	bailer	472	22-Aug-01
U-3cn PS#2	Bilby	13-Sep-63	37 03 38	116 01 19	1217	793	512-527	472	pump	504-505	18-Dec-01
Pahute Mesa											
U20n PS1 DDh	Cheshire	14-Feb-76	37 14 25	116 25 24	1971	1296	1250-1253	625	pump	1250	12-Oct-99
U19v PS1ds	Almendro	06-Jun-73	37 14 53	116 20 57	2085	1170*	---	667*	bailer	942*	31-May-01
U19v PS1ds	Almendro	06-Jun-73	37 14 53	116 20 57	2085	1170*	---	661*	bailer	942*	26-Sep-00
U19v PS1ds	Almendro	06-Jun-73	37 14 53	116 20 57	2085	1170*	---	661*	bailer	914*	18-Aug-99
ER-20-5 #3	Tybo	14-May-75	37 13 11	116 28 38	1903	1309	1045-1183	628	pump	1031-1038	15-Nov-01

* well depth, water depth, and sampling depth are corrected for borehole slant assuming vertical depth = slant depth × 0.936.
† data are not corrected for borehole slant

Table 2. Water chemistry and anion concentrations.

Well name	Test	Sample date	pH	T (°C)	Cond. (mS/cm)	TDIC as HCO_3^- (mg/L)	F (mg/L)	Cl (mg/L)	Br (mg/L)	NO_3 (mg/L)	SO_4 (mg/L)
Frenchman Flat											
UE5n	Cambric	19-Apr-01	8.7	23.0	408	162	0.7	12.9	<0.1	6.7	32.0
UE5n	Cambric	09-Sep-99	8.4	26.5	453	183	0.8	12.0	<0.03	8.1	31.8
RNM-1	Cambric	28-Jun-00	8.0	26.0	416	---	0.3	12.3	0.2	16.2	36.5
RNM-2S	Cambric	14-Jun-00	7.8*	---	429*	130	0.4	14.8	0.2	14.3	36.8
RNM-2S	Cambric	11-Oct-99	8.2	24.6	440	168	0.6	13.7	<0.03	13.9	37.0
Yucca Flat											
U4u PS2a	Dalhart	16-Aug-99	8.2*	---	352*	160	0.7	5.8	<0.03	18.5	12.0
UE-7ns	Bourbon	21-Aug-01	8.0*	---	375*	166	0.8	22.9	<0.1	<0.09	1.6
UE-2ce	Nash	22-Aug-01	7.9*	---	435*	308	0.3	15.5	<0.1	<0.09	11.1
U-3cn PS#2	Bilby	18-Dec-01	8.1*	---	490*	287	0.8	8.6	0.57	5.8	20.3
Pahute Mesa											
U20n PS1 DDh	Cheshire	12-Oct-99	8.2	38.2	324	108	3.6	11.1	<0.03	2.3	28.2
U19v PS1ds	Almendro	31-May-01	---	---	---	250	9.7	66.5	<0.1	<0.09	2.5
U19v PS1ds	Almendro	26-Sep-00	9.3*	---	742*	262	9.5	48.2	<0.1	<0.09	3.8
U19v PS1ds	Almendro	18-Aug-99	8.2*	---	728*	120	9.9	40.5	<0.03	<0.02	3.9
ER-20-5 #3	Tybo/Benham	15-Nov-01	8.0*	---	345*	110	3.6	18.9	0.76	2.6	35.3

A dashed line indicates the sample was not analyzed for the listed parameter
Cond. = conductivity
Asterisks (*) on pH and conductivity data indicate values measured in the laboratory

Table 3. Major ion chemistry and trace element data. Note that concentrations are given in units of milligrams, micrograms, or picograms.

Well Name	Test	Sample Date	Na (mg/L)	K (mg/L)	Ca (mg/L)	Mg (mg/L)	Al (mg/L)	As (µg/L)	B (mg/L)	Ba (mg/L)	Fe (mg/L)	I (µg/L)	Li (mg/L)	Mn (µg/L)	Mo (µg/L)	Pb (µg/L)	Pu (pg/L)	Se (µg/L)	Si (mg/L)	Sr (µg/L)	U (µg/L)
Frenchman Flat																					
UE5n	Cambric	19-Apr-01	76	8.0	8.6	2.0	<0.05	22	---	0.021	<0.04	---	0.02	<6	4	---	---	---	27.4	22	0.41
UE5n	Cambric	09-Sep-99	86	8.0	7.5	2.0	<0.02	9	0.34	<0.005	0.06	30	<0.05	10	5	0.37	---	<2	---	50	4.0
RNM-1	Cambric	28-Jun-00	44	8.0	26.0	9.4	0.37	---	---	---	0.18	---	0.03	---	---	---	---	---	20	300	4.0
RNM-2S	Cambric	14-Jun-00	62	9.70	18.0	5.2	0.38	---	---	---	0.18	---	0.02	---	---	---	---	---	35	140	5.0
RNM-2S	Cambric	11-Oct-99	63	9.2	17.0	5.6	<0.02	5	0.24	<0.005	0.01	11	<0.05	<2	3	0.24	---	<2	---	110	4.0
Yucca Flat																					
U4u PS2a	Dalhart	16-Aug-99	72	14.0	13.1	2.7	12	4	0.12	0.03	1.3	3.1	0.14	90	<1	8.6	8.7	<1	37	30	4.2
UE-7ns	Bourbon	21-Aug-01	67.4	4.9	20.9	3.6	<0.05	21	---	0.077	0.21	19.4	0.06	55	26	<14	<0.6	<24	10	70	0.04
UE-2ce	Nash	22-Aug-01	45.6	21.8	49.1	25.4	<0.05	<20	---	0.047	0.11	7.4	0.10	66	17	<14	<0.6	<24	22.2	160	0.39
U-3cn PS#2	Bilby	18-Dec-01	98.4	18.3	14.4	3.3	0.26	<20	---	0.004	0.30	---	0.045	78	3.5	<14	<0.6	<24	28.7	24	10.67
Pahute Mesa																					
U20n PS1 DDh	Cheshire	12-Oct-99	65	2.2	4.7	0.1	0.07	3	0.14	<0.005	1.4	13	<0.05	110	10	0.67	7.0	<2	24	10	2.3
U19v PS1ds	Almendro	31-May-01	173	14.0	1.5	0.2	0.29	140	---	0.06	3.7	---	0.28	330	1200	250	2.1	<24	2.0	44	0.03
U19v PS1ds	Almendro	26-Sep-00	131	11.6	0.7	0.1	0.25	50	---	0.02	0.19	1.2	0.24	---	1100	22	---	<24	6.6	---	0.02
U19v PS1ds	Almendro	18-Aug-99	162	9.8	0.9	0.2	0.52	1716	1.54	0.07	12.0	1.7	0.42	250	1226	63	58.2	8	11	40	<0.5
ER-20-5 #3	Tybo/ Benham	15-Nov-01	87.1	3.3	4.4	0.1	3.6	23	---	0.017	1.9	<1	0.07	75	5.8	<14	<0.6	<24	29	31	12.80

A dashed line indicates the sample was not analyzed for the listed parameter

Table 4. Stable isotope and noble gas data.

Well name	Test	Sample Date	δD_{SMOW} (‰)	$\delta^{18}O_{SMOW}$ (‰)	$\delta^{13}C_{PDB}$ (‰)	^{3}He (atoms/g)	^{4}He (atoms/g)	R/R_a ($^{3}He/^{4}He$ sample/air)	^{20}Ne (atoms/g)	^{40}Ar (atoms/g)	^{130}Xe (atoms/g)	$^{87}Sr/^{86}Sr$ (ratio)	$\delta^{87}Sr$ (‰)
Frenchman Flat													
UE5n	Cambric	19-Apr-01	-105	-13.4	-6.7	2.70E+09	2.34E+12	8.36E+02	4.66E+12	8.30E+15	4.22E+10	0.71039	1.68
UE5n	Cambric	09-Sep-99	-106	-13.4	-8.3	1.95E+09	3.16E+12	4.48E+02	7.25E+12	1.04E+16	4.42E+10	---	---
RNM-1	Cambric	28-Jun-00	-104	-12.7	---	1.43E+09	2.05E+12	5.05E+02	4.15E+12	7.63E+15	---	---	---
RNM-2S	Cambric	14-Jun-00	-105	-13.0	-5.3	2.50E+10	6.43E+12	2.84E+03	5.50E+12	9.11E+15	---	---	---
RNM-2S	Cambric	11-Oct-99	-104	-12.9	-9.3	2.35E+10	6.40E+12	2.65E+03	4.35E+12	8.09E+15	---	---	---
Yucca Flat													
U4u PS2a	Dalhart	16-Aug-99	-100	-12.8	-8.7	---	---	---	---	---	---	---	---
UE-7ns	Bourbon	21-Aug-01	-106	-14.0	-2.0	1.93E+10	2.45E+12	5.71E+03	6.52E+12	9.30E+15	4.08E+10	---	---
UE-2ce	Nash	22-Aug-01	-100	-12.9	-5.3	4.78E+09	2.36E+12	1.47E+03	7.14E+12	9.31E+15	4.06E+10	---	---
U-3cn PS#2	Bilby	18-Dec-01	-108	-13.9	-3.8	5.98E+11	3.59E+12	1.21E+05	7.41E+12	9.30E+15	3.73E+10	0.70974	0.76
Pahute Mesa													
U20n PS1 DDh	Cheshire	12-Oct-99	-113	-15.0	-6.0	2.01E+12	1.01E+13	1.44E+05	5.70E+12	6.45E+15	---	0.71078	1.39
U19v PS1ds	Almendro	31-May-01	-112	-13.3	+30.1	3.75E+11	1.50E+12	1.81E+05	4.42E+12	1.45E+16	8.13E+10	---	---
U19v PS1ds	Almendro	26-Sep-00	-111	-13.4	+30.2	---	---	---	---	---	---	---	---
U19v PS1ds	Almendro	18-Aug-99	-111	-13.4	+45.0	---	---	---	---	---	---	---	---
ER-20-5 #3	Tybo/ Benham	15-Nov-01	-114	-15.0	-4.0	8.09E+09	7.48E+12	7.84E+02	7.49E+12	---	4.20E+10	0.70864	-0.79

A dashed line indicates the sample was not analyzed for the listed parameter

Table 5. Radiochemical data.

Well name	Test	Sample date	^{3}H	^{3}H	^{14}C	^{14}C	$^{36}Cl/Cl$	^{36}Cl	^{85}Kr	^{99}Tc
Units		*date*	*(pCi/L)*	*(pCi/L)*	*(pmc)*	*(pCi/L)*	*ratio*	*(pCi/L)*	*(pCi/L)*	*(pCi/L)*
Half-life (a)		*collected*	*12.32*	*12.32*	*5730*	*5730*		*3.01E+05*	*10.73*	*2.13E+05*
Ref. date		*in field*	*collect.*	*time zero*	*collect.*	*collect.*		*collect.*	*collect.*	*collect.*
Frenchman Flat										
UE5n	Cambric	19-Apr-01	1.4E+05	1.1E+06	2.84E+01	5.53E-02	5.38E-10	2.29E-01	---	---
UE5n	Cambric	09-Sep-99	---	---	1.88E+01	4.14E-02	6.01E-10	2.38E-01	<40	2.29E-03
RNM-1	Cambric	28-Jun-00	2.8E+04	2.1E+05	---	---	1.06E-12	4.30E-04	---	---
RNM-2S	Cambric	14-Jun-00	1.9E+05	1.4E+06	---	---	1.62E-10	7.92E-02	---	---
RNM-2S	Cambric	11-Oct-99	2.3E+05	1.6E+06	4.13E+02	8.34E-01	1.64E-10	7.40E-02	<40	9.72E-04
Yucca Flat										
U4u PS2a	Dalhart	16-Aug-99	1.6E+07	3.1E+07	1.19E+05	2.29E+02	4.45E-08	8.52E+00	---	---
UE-7ns	Bourbon	21-Aug-01	4.6E+03	3.2E+04	6.97E+01	1.39E-01	1.85E-12	1.40E-03	---	---
UE-2ce	Nash	22-Aug-01	1.4E+05	9.9E+05	2.17E+02	8.01E-01	1.62E-09	8.27E-01	---	---
U-3cn PS#2	Bilby	18-Dec-01	9.9E+06	8.6E+07	8.78E+04	3.03E+02	---	---	---	---
Pahute Mesa										
U20n PS1 DDh	Cheshire	12-Oct-99	5.1E+07	1.9E+08	1.54E+05	2.00E+02	1.15E-09	4.20E-01	2.77E+04	2.20E+01
U19v PS1ds	Almendro	31-May-01	1.8E+08	9.0E+08	3.11E+04	9.33E+01	1.63E-09	3.58E+00	---	---
U19v PS1ds	Almendro	26-Sep-00	1.5E+08	7.1E+08	3.19E+04	1.01E+02	2.30E-09	3.66E+00	---	---
U19v PS1ds	Almendro	18-Aug-99	1.6E+08	6.8E+08	2.47E+04	3.56E+01	1.60E-09	2.14E+00	---	---
ER-20-5 #3	Tybo/ Benham	15-Nov-01	1.4E+05	6.3E+05	1.57E+03	2.08E+00	3.49E-11	2.18E-02	---	---

A dashed line indicates the sample was not analyzed for the listed parameter

Table 5. Radiochemical data (continued).

Well name	Test	Sample date	$^{129}I/^{127}I$	$^{234}U/^{238}U$	$^{234}U/^{238}U$ activity ratio	$^{234}U/^{235}U$	$^{235}U/^{238}U$	^{234}U	^{235}U	^{238}U	$^{239,240}Pu$ total
Units *Half-life (a)* *Ref. date*		*date collected in field*	*ratio*	*ratio*	*ratio*	*ratio*	*ratio*	*(pCi/L)* *2.46E+05* *collect.*	*(pCi/L)* *7.04E+08* *collect.*	*(pCi/L)* *4.47E+09* *collect.*	*(pCi/L)* *collect.*
Frenchman Flat											
UE5n	Cambric	19-Apr-01	---	1.130E-04	2.06	1.558E-02	7.252E-03	0.29	0.006	0.14	---
UE5n	Cambric	09-Sep-99	3.51E-09	---	---	---	---	---	---	---	---
RNM-1	Cambric	28-Jun-00	---	1.363E-04	2.48	1.869E-02	7.292E-03	3.33	0.06	1.33	---
RNM-2S	Cambric	14-Jun-00	---	1.233E-04	2.24	1.693E-02	7.285E-03	3.77	0.08	1.66	---
RNM-2S	Cambric	11-Oct-99	2.12E-07	---	---	---	---	---	---	---	---
Yucca Flat											
U4u PS2a	Dalhart	16-Aug-99	---	---	---	---	---	---	---	---	1.2
UE-7ns	Bourbon	21-Aug-01	---	1.687E-04	3.08	2.312E-02	7.297E-03	0.046	0.0007	0.015	<0.04
UE-2ce	Nash	22-Aug-01	---	2.049E-04	3.74	2.823E-02	7.258E-03	0.50	0.006	0.13	<0.04
U-3cn PS#2	Bilby	18-Dec-01	---	1.600E-04	2.92	2.206E-02	7.254E-03	10.53	0.17	3.56	<0.04
Pahute Mesa											
U20n PS1 DDh	Cheshire	12-Oct-99	---	1.888E-04	3.44	2.633E-02	7.171E-03	3.00	0.04	0.86	0.5
U19v PS1ds	Almendro	31-May-01	---	1.771E-04	3.24	2.443E-02	7.251E-03	0.034	0.0005	0.010	0.2
U19v PS1ds	Almendro	26-Sep-00	---	1.723E-04	3.15	2.384E-02	7.226E-03	0.017	0.0003	0.005	---
U19v PS1ds	Almendro	18-Aug-99	---	---	---	---	---	---	---	---	9.4
ER-20-5 #3	Tybo/ Benham	15-Nov-01	---	6.353E-05	1.16	8.759E-03	7.253E-03	5.01	0.20	4.27	<0.04

A dashed line indicates the sample was not analyzed for the listed parameter

Chapter 2

Xenon Isotope Measurements of Near-Field Groundwater Samples

G. Bryant Hudson

Introduction

The noble gas xenon (Xe) has nine stable isotopes with atomic masses ranging from 124 to 136, all of which occur naturally in the atmosphere. During actinide fission, the four heaviest Xe isotopes (masses 131, 132, 134, and 136) or their radioactive precursors are produced in abundance. Differences in the half-lives and volatilities of the Xe-precursors lead to different distributions of fission Xe among post-explosion debris. Because of these differences, the relative abundances of fission $^{131\text{-}136}$Xe in recovered samples have the potential to provide insights into the geochemistry and cooling history of an explosion cavity after a nuclear test. In this work, we report measurements of fission Xe observed in groundwater samples recovered in the near-field environment of past underground nuclear explosions.

During the nuclear test program, LLNL routinely measured xenon isotope ratios on recovered gas samples to determine the device total fission yield. The mass 136 chain has been used for diagnostic measurements since the decay of the mass 136 chain to ^{136}Xe is very rapid. Essentially all of the fission ^{136}Xe ends up in the cavity gas phase following a nuclear explosion, and this fact greatly simplifies its interpretation and makes it useful for fission yield determinations. This is not the case for the other more slowly decaying chains of fission products where trapping within liquid or solid phases prevents or delays the release of the stable Xe daughters to the gas phase. The mass 131-136 decay chains are as follows:

$$^{131}\text{Sn} \xrightarrow{58\,\text{s}} {}^{131}\text{Sb} \xrightarrow{23\,\text{m}} {}^{131}\text{Te} \xrightarrow{1.35\,\text{d}} {}^{131}\text{I} \xrightarrow{8.02\,\text{d}} {}^{131}\text{Xe (stable)}$$

$$^{132}\text{Sn} \xrightarrow{40\,\text{s}} {}^{132}\text{Sb} \xrightarrow{4.2\,\text{m}} {}^{132}\text{Te} \xrightarrow{3.2\,\text{d}} {}^{132}\text{I} \xrightarrow{137\,\text{m}} {}^{132}\text{Xe (stable)}$$

$$^{134}\text{Sb} \xrightarrow{10.4\,\text{s}} {}^{134}\text{Te} \xrightarrow{42\,\text{m}} {}^{134}\text{I} \xrightarrow{52.6\,\text{m}} {}^{134}\text{Xe (stable)}$$

$$^{136}\text{Sb} \xrightarrow{0.8\,\text{s}} {}^{136}\text{Te} \xrightarrow{17.5\,\text{s}} {}^{136}\text{I} \xrightarrow{1.4\,\text{m}} {}^{136}\text{Xe (stable)}\,.$$

The stable isotopes ^{124}Xe, ^{126}Xe, ^{128}Xe, and ^{130}Xe have negligible fission contributions, and the fission contribution to ^{129}Xe is held up by the very slow β-decay of ^{129}I (half life = 1.57×10^7 yrs). Table 1 summarizes direct fission yields and half-lives of the relevant isotopes. Figures 1 through 4 show the ideal behavior of the isotope abundances for each

of the decay chains. Prior to now, we have not attempted to measure Xe isotope abundances in near-field groundwater samples. Groundwater that contains excess fission-derived xenon should show isotopic enrichments at masses 131, 132, 134, and 136 relative to atmospheric Xe values.

Results

Xenon data for seven near-field groundwater samples are presented in Tables 2 and 3. In Table 2, the measured Xe isotopic compositions are reported as ratios relative to ^{132}Xe. The natural Xe isotope ratios in air (as measured in a laboratory standard of water in equilibrium with the atmosphere) are shown for comparison. Four near-field groundwaters show detectable enrichments in heavy Xe isotopes relative to air (Table 2), indicating that fission xenon is present. These include samples from UE-2ce, U-3cn PS#2, UE-7nS, and U-19v PS1ds.

In Table 3, the fission Xe concentrations are calculated by subtracting air-composition Xe assuming that all the ^{130}Xe is due to atmospheric Xe. We observe that the samples from wells UE-2ce, UE-7nS, and U-19v PS1ds are all enriched in the longer-lived chain yield nuclides relative to ^{136}Xe. The most striking fission Xe enrichments are observed at U-19v PS1ds (Almendro), a site known for its anomalous thermal and chemical characteristics. In contrast, U-3cn PS#2 is depleted in the same species relative to ^{136}Xe. This suggests a substantially different thermal history for the U-3cn test with the simplest scenario being that the U-3cn cavity cooled much more rapidly than the other events examined here. Conversely, for the events where the long-lived decay chains are enriched relative to ^{136}Xe, we must invoke a gas loss scenario, where gas is effectively lost from the system at early times allowing the subsequent decay of the long-lived chains to be enhanced.

Discussion

Drawing upon prior experience with gas diagnostic measurements, we can also evaluate the observed fission Xe concentrations. From the use of noble gas tracers and D_2O tracers in the nuclear testing diagnostics program, we have developed estimates of post-explosion gas phase volumes and the volume of water available to isotopically exchange with D_2O.

$$V_{gas} = 1.5 \times 10^4 \text{ m}^3/\text{kt}$$
$$V_{water} = 3.0 \times 10^3 \text{ m}^3/\text{kt}$$

For a pure fission explosion there are 1.4×10^{23} fissions/kt, which corresponds to the production of about 8.4×10^{21} atoms of ^{136}Xe/kt, or a gas phase concentration of 5.6×10^{17} ^{136}Xe/m^3. The solubility of Xe is temperature dependent and the predicted fission ^{136}Xe concentration for water in equilibrium with the gas phase at ~100 °C is about 6×10^{10} ^{136}Xe/gram H_2O. This is of the same order of magnitude observed in the recovered groundwater samples. We should recognize that this estimate for the fission ^{136}Xe concentration is almost certainly an upper bound. Between dilution with other water sources and gas loss, we should expect values lower than 6×10^{10} ^{136}Xe/g. However, this

again points to the anomalous behavior observed at U19v. In this case, the fission ^{136}Xe concentration is a full order of magnitude greater than our estimate (Table 3). The atmospheric contribution of Xe to this sample is also anomalously high. For non-fission gases we expect concentrations similar to that predicted by equilibrium solubility with the atmosphere. This is observed in all other samples, where ^{130}Xe concentrations are around 4×10^{10} atoms/gram. The U19v sample has twice the ^{130}Xe concentration (Table 3). This sample also shows a modest enrichment in Ar. Conversely, He and Ne are depleted relative to our expectations based on atmospheric equilibrium. The He depletion is also observed in an extreme fashion with the low abundance of ^{3}He from ^{3}H decay and its apparent $^{3}H/^{3}He$ age of only 2 years (see also Chapter 1 of this report).

Three near-field samples (two from UE-5n and one from ER-20-5 #3) have Xe isotope ratios nearly identical to air, indicating fissiogenic Xe is not present (Tables 2 and 3). This result is not surprising at UE-5n, whose radionuclides are derived from the infiltration of water pumped from RNM-2S. Water brought to the surface would have re-equilibrated with atmospheric Xe long before re-infiltrating the aquifer. The lack of excess fission Xe in ER-20-5 #3 is not as readily explained, but we can largely rule out atmospheric re-equilibration given the results for ^{3}He. The $^{3}H/^{3}He$ age of the water (~25 years) indicates little re-equilibration

Examining the data more closely, we see that fission ^{132}Xe is enriched relative fission ^{131}Xe when compared to chain yields for UE-2ce, UE-7nS, and U-19v PS1ds. The most straightforward explanation comes from examining Table 1 and Figures 1 and 2. The long half-life of ^{131}I is likely responsible. Here the ^{131}I may be incorporated in solids that have cooled sufficiently that the ^{131}Xe remains trapped and unavailable to either the gas or water phase.

Future Work

This report is not intended to provide a detailed evaluation of the fission Xe data presented. Our goal is to demonstrate that fission Xe is present at levels that are readily measurable and that significant differences are present in the relative abundances of the different Xe isotopes from one event to the next. Future investigations may be able to develop more detailed geochemical models that the fission Xe can help to calibrate and constrain. In turn, these calibrated models may be able to significantly improve our understanding of the early cooling histories of nuclear explosion cavities.

Table 1. Fission product yields and half-lives

		mass 131	**mass 132**	**mass 134**	**mass 136**
		direct fission product yield *(as a percentage of the total fission yield)*			
Xenon	(Z=54)	0.00%	0.01%	0.48%	3.25%
Iodine	(Z=53)	0.17%	0.88%	4.39%	2.70%
Tellurium	(Z=52)	2.29%	3.63%	1.65%	0.09%
Antimony	(Z=51)	1.29%	0.62%	0.03%	0.00%
full chain yield		3.77%	5.14%	6.55%	6.05%
		isotope half-life (sec)			
Xenon	(Z=54)	stable	stable	stable	stable
Iodine	(Z=53)	6.9E+05	8.2E+03	3.2E+03	8.6E+01
Tellurium	(Z=52)	1.2E+05	2.8E+05	2.5E+03	1.8E+01
Antimony	(Z=51)	1.4E+03	2.5E+02	1.0E+01	<1

Table 2. Xenon isotopic data for NTS Wells

Sample Name	Sample Date	^{132}Xe (atoms/gram)		^{124}Xe/^{132}Xe	^{126}Xe/^{132}Xe	^{128}Xe/^{132}Xe	^{129}Xe/^{132}Xe	^{130}Xe/^{132}Xe	^{131}Xe/^{132}Xe	^{134}Xe/^{132}Xe	^{136}Xe/^{132}Xe
UE-5n	09/09/1999	2.9E+11		0.00353	0.00334	0.07109	0.98058	0.15117	0.78841	0.38889	0.33091
			±	0.00003	0.00003	0.00004	0.00013	0.00006	0.00014	0.00007	0.00006
UE-5n	04/19/2001	2.8E+11		0.00358	0.00329	0.07109	0.98035	0.15117	0.78839	0.38895	0.33089
			±	0.00003	0.00004	0.00005	0.00010	0.00005	0.00006	0.00007	0.00005
ER-20-5 #3	11/15/2001	2.8E+11		0.00345	0.00320	0.07109	0.98112	0.15121	0.78867	0.38898	0.33091
			±	0.00003	0.00004	0.00004	0.00010	0.00004	0.00008	0.00006	0.00006
UE-2ce	08/22/2001	3.1E+11		0.00306	0.00289	0.06188	0.85337	0.13185	0.78078	0.52783	0.34839
			±	0.00004	0.00004	0.00005	0.00008	0.00003	0.00008	0.00004	0.00005
U3cn PS #2	12/18/2001	2.6E+11		0.00335	0.00316	0.06789	0.93643	0.14471	0.79290	0.53678	0.53780
			±	0.00003	0.00004	0.00004	0.00008	0.00003	0.00006	0.00005	0.00006
UE-7ns	08/21/2001	2.8E+11		0.00342	0.00317	0.06814	0.93969	0.14491	0.78799	0.42191	0.34341
			±	0.00003	0.00004	0.00005	0.00009	0.00004	0.00009	0.00005	0.00005
U19v PS1ds	05/31/2001	2.8E+12		0.00068	0.00064	0.01373	0.18888	0.02956	0.46496	0.44680	0.25423
			±	0.00000	0.00000	0.00000	0.00002	0.00001	0.00005	0.00005	0.00003
water	06/13/2003	2.7E+11		0.00353	0.00330	0.07106	0.98008	0.15106	0.78808	0.38866	0.33044
(18.4C, 183m)			±	0.00003	0.00004	0.00004	0.00014	0.00004	0.00010	0.00004	0.00005

Table 3. Fission Xe concentrations.

Sample Name	**Sample Date**	**^{130}Xe** *Non-fission Xe from air* **(atoms/gram)**	**^{131}Xe (atoms/gram)**	**^{132}Xe (atoms/gram)**	**^{134}Xe (atoms/gram)**	**^{136}Xe (atoms/gram)**
UE-5n	09/09/1999	4.42E+10	<1.0E+08	<1.0E+08	<1.0E+08	<1.0E+08
UE-5n	04/19/2001	4.22E+10	<1.0E+08	<1.0E+08	<1.0E+08	<1.0E+08
ER-20-5 #3	11/15/2001	4.20E+10	<1.0E+08	<1.0E+08	<1.0E+08	<1.0E+08
UE-2ce	08/22/2001	4.06E+10	2.9E+10	4.0E+10	5.8E+10	1.8E+10
U3cn PS #2	12/18/2001	3.73E+10	1.0E+10	1.2E+10	4.2E+10	5.7E+10
UE-7ns	08/21/2001	4.08E+10	9.1E+09	1.2E+10	1.4E+10	7.4E+09
U19v PS1ds	05/31/2001	8.13E+10	8.6E+11	2.2E+12	1.0E+12	5.2E+11

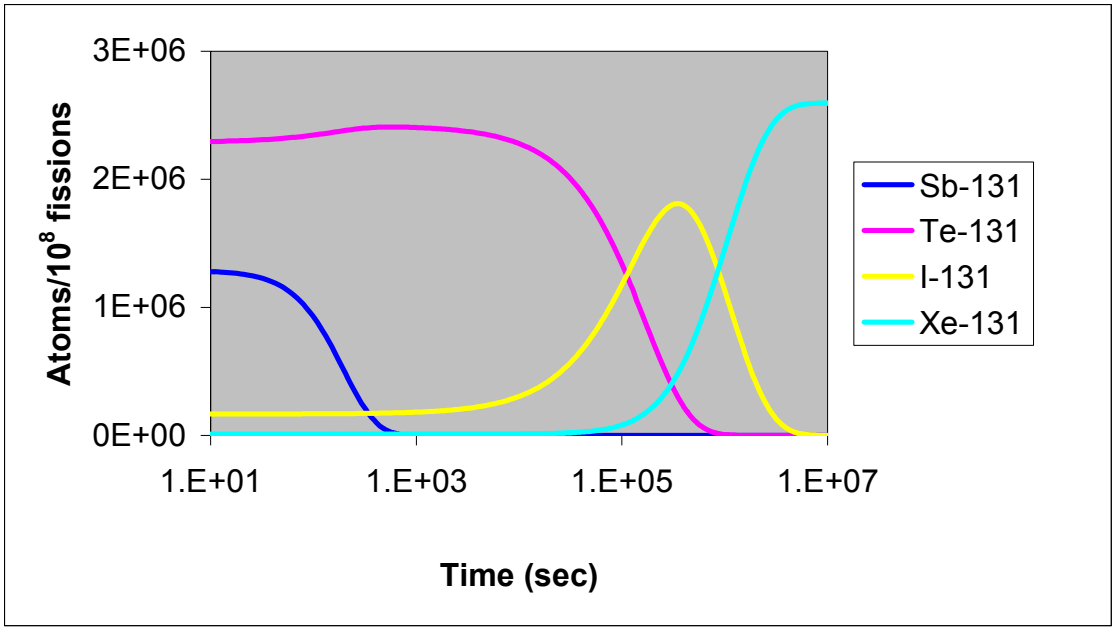

Figure 1. Decay and in-growth of nuclides as a function of time for the mass 131 decay chain.

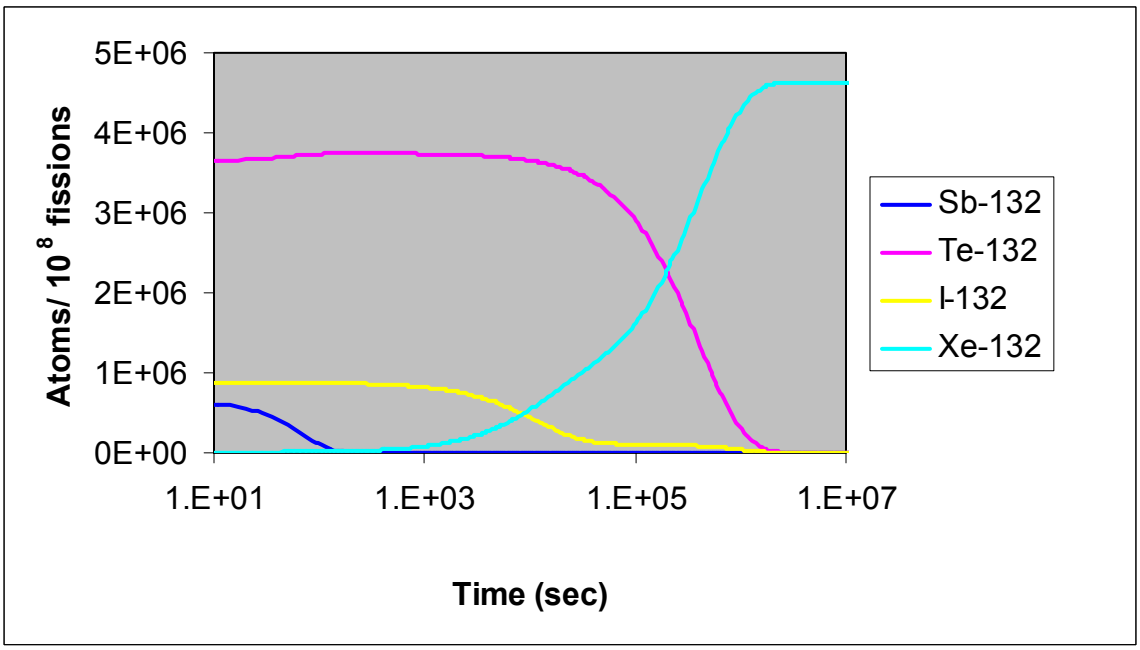

Figure 2. Decay and in-growth of nuclides as a function of time for the mass 132 decay chain.

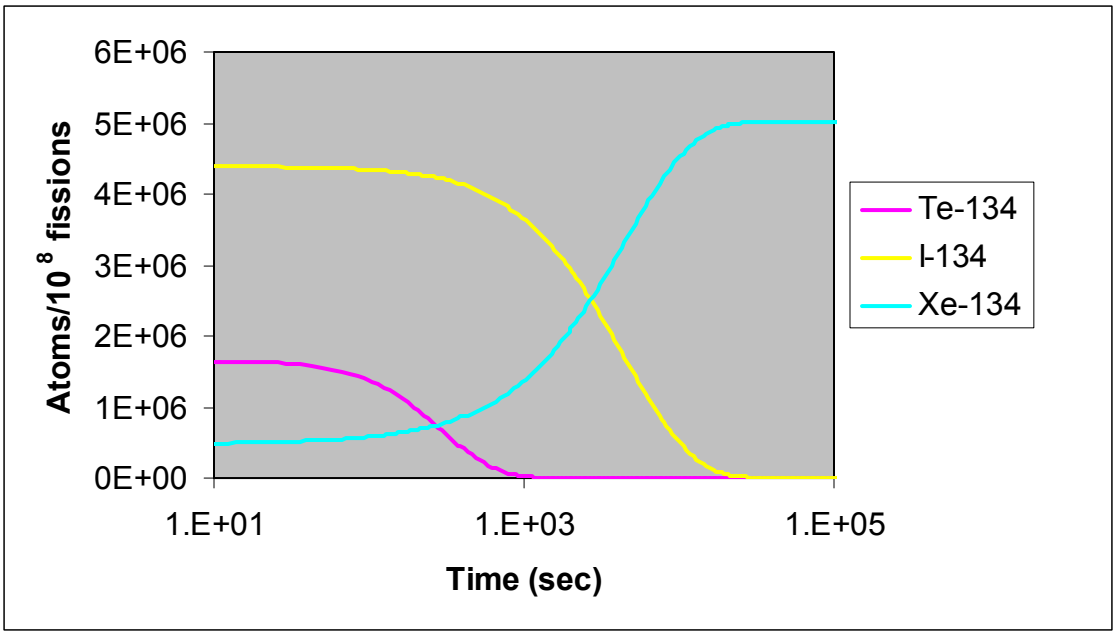

Figure 3. Decay and in-growth of nuclides as a function of time for the mass 134 decay chain.

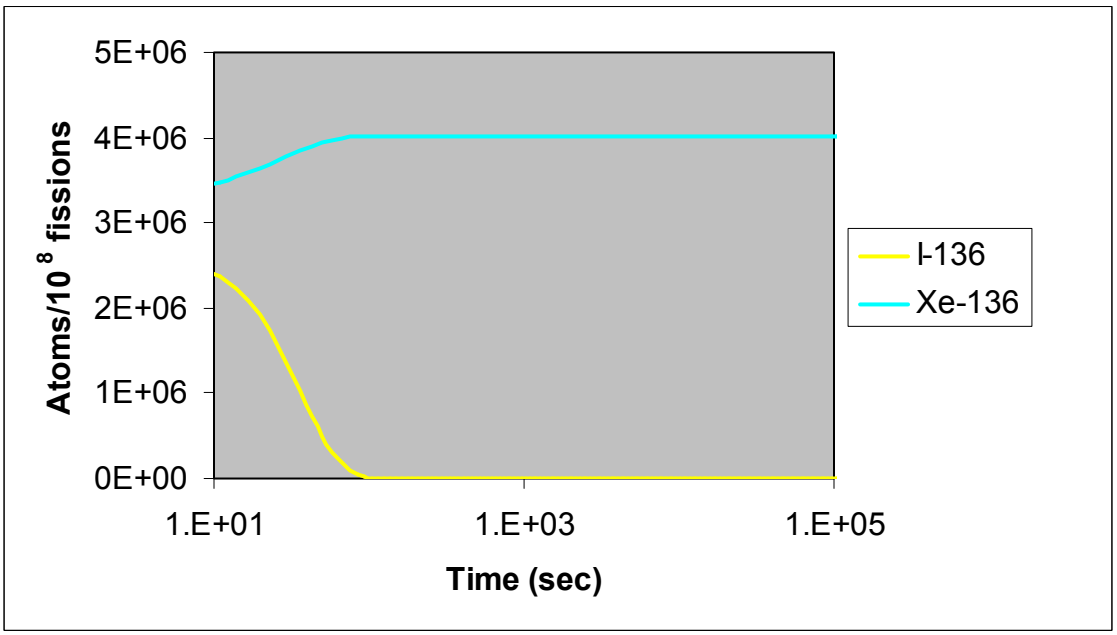

Figure 4. Decay and in-growth of nuclides as a function of time for the mass 136 decay chain.

Chapter 3

Distribution, Concentration, and Isotope Ratios of Uranium and Plutonium in a Nuclear Test Cavity and Collapse Chimney

David K. Smith, Ross W. Williams, and Diane R. Loewen

Introduction

The migration of radionuclides associated with underground tests involves transport processes that occur at or near the time of the detonation as well as hydrologic processes that occur over longer time scales. The ability to make credible predictions of radionuclide mobility necessitates characterizing the relative importance of each. While much effort has been devoted to study and assessments of transport of radionuclides in groundwater (e.g., Borg et al., 1976; Buddemeier et al., 1991; IAEA, 1998; Kersting et al., 1999; Tompson et al., 1999) there has been less effort focused on studying early-time processes affecting the dispersal radionuclides within and adjacent to an underground explosion.

At ground-zero and zero-time of a nuclear explosion, pressures may exceed 1 Mbar and temperatures may exceed 1M degrees Kelvin (Sawyer et al., 1999). These extreme conditions can mobilize radionuclides by prompt process associated with underground explosion phenomenology. Prompt transport represents extreme thermodynamic conditions not driven by geochemical reactions that characterize radionuclide release at lower temperature and near-equilibrium conditions. Understanding of prompt processes comes exclusively from site-based measurements made in the near-field, largely involving drilling into expended nuclear test cavities and chimneys. The end-member pressure and temperature regimes accompanying dynamic transport are impossible to reproduce in the laboratory. Hence the opportunity to study the distribution of radionuclides following an underground nuclear test is severely limited by the lack of accessibility to these sites, and by the limited availability of samples that are appropriate for understanding these processes.

Many questions hinge on the results of a study of this kind. Numerical models of the release and transport of radionuclides from underground nuclear explosions are extremely sensitive to where radionuclides are distributed following the explosion. In particular radionuclides that are not volumetrically incorporated in the melt glass produced by fusion of host rock during the detonation are susceptible to release by surface reactions involving ion exchange with groundwater. Radionuclides are known to have been transported as much as 350 m from ground zero by prompt injection (Nimz and Thompson, 1992). There is the perceived concern that radionuclides may be directly injected into groundwater at the time of explosion, although temperatures associated such transport would likely be high enough to displace or vaporize any condensed water phase.

At the Nevada Test Site prompt injection has been documented at many sites of underground nuclear explosions since radionuclide investigations began in the mid-1970's (e.g., Nimz and Thompson, 1992; Thompson and Gilmore, 1991; Smith, 2001).

The implications of such transport are significant. A lingering and unresolved question associated with the 1997 discovery of colloidal facilitated transport of plutonium beneath Pahute Mesa is the role of explosion phenomenology in the observed migration of radionuclides (Kersting et al., 1999). While the plutonium in groundwater at the ER-20-5 well cluster can unambiguously be traced back to the BENHAM test due to characteristic $^{240}Pu/^{239}Pu$ isotope ratios common to each, colloidal transport between the test and the wells requires that plutonium be released from the BENHAM cavity prior to or concurrently with its migration downgradient. The distribution of plutonium at the time of the BENHAM test is not known, nor is the extent to which plutonium may have been transported within or outside of the cavity at the time of the explosion. If plutonium was mobilized away from ground-zero by processes other than by colloidal-transport, the saturated transport distance may be shorter than the 1.3 kilometer distance between the test and the well. Accordingly the transport velocities may be slower than that calculated assuming colloid transport alone. The assumption is that 95% of the residual plutonium is incorporated in the melt glass fraction (IAEA, 1998). If this is the case, it is important to resolve whether the plutonium detected at the ER-20-5 well cluster is derived from the 95% fraction resident in the glass or the 5% sited outside the glass. If plutonium outside the glass is indeed implicated as the source, other tests conducted in fractured rock aquifers may also be at similar risk for transport of plutonium at or near ambient groundwater velocities.

Previous Work

Little previous work has been published on the distribution of radionuclides in the sub-surface or the prompt transport of radionuclides associated with underground nuclear tests. This is particularly true of the actinides that pose the greatest long-term health risk. This report concentrates on the underground behavior and transport of refractory radionuclides which are defined as nuclides with high boiling points and low vapor pressures that are largely retained in the melt glass fraction.

The boiling point of elemental plutonium is 3,232 ^{o}C and its melting point is 641^{o}C. The boiling point for elemental uranium is 3,818 ^{o}C and the melting point is 1,132 ^{o}C (CRC, 1990-1991). A study of the radiological distribution of melt glass and explosive rubble from the PILEDRIVER test conducted beneath Rainier Mesa was published in the mid-1970's (Borg, 1975). At most 2 to 3% of the refractory radionuclides –including the actinides - are lost from "good 'puddle' glass samples in which other refractories are equally well-retained" (Borg, 1975). In addition, these same refractory radionuclides show little variation throughout the volume of the melt puddle which is further evidence of their thorough retention in the glass fraction. General experience from the U.S. nuclear testing program based on radiochemical diagnostic data collected from a variety of test matrices suggest that 95 ± 5% of the test-specific inventory of refractory radionuclides are contained in the melt fraction. These estimates were further endorsed

by an international study concerned with the health risks posed by nuclear tests conducted by the French government in the south Pacific (IAEA, 1998). The same study assumes 90% of the uranium and 98% of plutonium post-test inventory resides in the melt glass fraction (IAEA, 1998).

Radionuclides have been transported by prompt processes up to 7 cavity radii from the working point of tests conducted beneath Yucca Flat. Prompt transport has also been observed on Pahute Mesa over distances of approximately 150 m. In all cases, prompt transport – otherwise described as prompt injection - is characterized by localized intervals that 1) are narrow and less than ~ 10 meters in width and 2) that contain a mixture of volatile and refractory radionuclides that are encountered abruptly and anomalously outside of the immediate test cavity and collapse chimney. Prompt transport is also implicated in cases where transport occurs through narrow passages above the water table. As noted by Pawloski (1999) radioactive material can be injected outside the cavity region by hydrofracturing (pressure driven) or spall (opening of layers during stress release of the damaged host rock). Pressure driven radionuclide transport occurs along preferred paths, including the stemming column or structural weaknesses that are in contact with the cavity region.

Specific examples of prompt injection include the detection of ^{90}Sr and ^{137}Cs within an approximately 7 m thick interval adjacent to the edge of the INGOT cavity (Smith et al., 1996). In this case a stratigraphic contact between nonwelded and welded tuff was exploited by the high gas pressures accompanying the detonation. The presence of montmorillonite clays and an increase in formation water content contributed to the zone of weakness. In a different study, Thompson and Gilmore (1991) used Rh isotopes as a unique fingerprint to identify the source of radionuclides in a prompt injection interval was from a neighboring nuclear test approximately 350 m away. Because Rh isotopes are insoluble, their presumed transport mechanism involved dynamic processes associated with the explosion itself and not solute, or colloidal, transport. Until recently, while there was speculation that actinides could be mobilized by hydrofracturing or spall, conclusive evidence from the near-field was lacking. In-situ analyses of radionuclides taken from a 3 m thick zone of radioactivity above the water table at the ER-20-6 #1 well showed the presence of enriched isotope ratios of $^{235}U/^{238}U$ attributed to the BULLION nuclear test (Rose et al., 2001). The enriched uranium isotopes, accompanied by ^{22}Na and ^{137}Cs, were transported more than 350 m from ground zero. Available evidence suggests this feature represents a zone of prompt transport emplaced at the time of the BULLION test because 1) the narrow interval of radioactivity was encountered 37 m above the pre-shot water table, 2) the fracture geometry is consistent with a discrete interval of radioactivity injected along a contact between bedded tuffs and rhyolite lavas, 3) a diverse suite of anthropogenic radionuclides was encountered during spectral gamma logging of the ER-20-6 #1 borehole, and 4) the $^{235}U/^{238}U$ isotope ratio of samples returned from this interval is significantly enriched above natural background. These analyses are the first to detect actinides within a prompt injection interval outside of a nuclear test cavity or chimney.

A Field and Analytical Investigation

The present study targets samples taken from a post-test drill-back into a single nuclear test cavity and chimney at the Nevada Test Site. The drill-back followed standard practices for the return of samples processed to assess device performance. The name of the test is not revealed to avoid disclosing test-specific phenomenology and radiochemical signatures which are classified. This investigation combines a unique suite of post-test debris samples including melt-glass and collapse chimney debris with the ability to measure concentrations and isotope ratios of uranium and plutonium in solid matrices at sub parts-per-billion concentrations using high precision mass spectrometry.

Solid Samples

Samples were collected from a post-shot drilling operation that targeted both the melt glass at the base of the cavity as well as overlying chimney debris. This sampling scheme is atypical because it includes volatile-enriched chimney samples of less diagnostic value. Specific discussions of cavity formation, chimney collapse and radiochemical partitioning in the underground environment have been presented in detail elsewhere and will not be repeated here (e.g., Pawloski, 1999).

The holes selected for solid sampling were first surveyed using a gamma logging tool as is the convention for post-shot drilling operations. Six samples were analyzed from a single test. Sampling was conducted using a Hunt side-wall tool which forces samples into a shoe under the weight of the drill-bit; approximately 120 grams of sample are returned per sampling trip in the hole. Five samples were taken over a slant depth interval of 69m from one borehole (hole 1) and one additional sample of melt glass was taken from a secondary boring (hole 2) drilled into the same test cavity. Samples, relative sampling depths, and sample type (volcanic glass, melt glass or ash) are compiled in Table 1.

Table 1. Solid samples collected from below the water table.

Sample Number	Relative Slant Depth	Sample Type	Hole
1	shallow	ash	1
2		ash	1
3		glass	1
4		volcanic glass	1
5		ash	1
6	deep	glass	2

This test was conducted in Tertiary volcanic tuffs and was detonated below the static water level. All of the above solid samples listed in Table 1 were collected at slant depths below the water table. The samples were also recovered below the level of the device depth-of-burial. Gamma logs and spectral gamma counting of the solid samples revealed the presence of fission products and activation products throughout the

stratigraphic interval that was sampled by the sidewall tool. Refractory radionuclides including ^{60}Co, ^{152}Eu, ^{154}Eu, ^{155}Eu were detected in the lowermost region of the cavity where these radioisotopes were volumetrically incorporated in the melt-glass. In contrast, volatile radionuclides including ^{3}H and ^{125}Sb were detected higher in the collapse chimney at stratigraphic intervals above the melt glass. The volatile radionuclides condensed at lower temperatures and were deposited on mineral and fracture surfaces exposed on the collapse debris.

As noted above, solid samples selected for the analysis of actinides were chosen from holes drilled into both the test cavity and chimney. While only a single representative glass sample was selected from the main hole, a suite of samples were chosen in ascending order from the melt-glass horizon upwards through the collapse zone from the side-track hole. Samples taken from the melt puddle consisted of vitreous, dense samples of dark-colored melt glass, while the samples taken from the collapse region were brecciated samples of light colored ash typical of the in-fall environment. High magnification photos of the melt glass fragments and volcanic ash samples are shown in Figures 1 and 2, respectively. It is noteworthy that both glass and ash samples are interspersed throughout the 69 meter sampling interval within the bottom half of the test cavity. Glass samples occur at the very bottom of the puddle region as well as higher in the hole where they are mixed in with the ash samples. The chaotic juxaposition of glass and lithic materials is a result of the collapse of the standing cavity and creation of the rubble chimney. During this process, glass may get "splashed" or otherwise displaced higher in the cavity region.

Analytical Methods

Analysis of actinides in the solid samples involves the separation of uranium and plutonium from the samples and measurement of isotope ratios and concentrations using isotope dilution with a non-isobarically interfering enriched isotope spike. Magnetic sector inductively coupled mass spectrometry was used for the high-sensitivity, high-precision analyses of uranium and plutonium.

Half-gram samples of the melt glass and debris samples were ground in a mortar and pestle and weighed before 0.3 milliliters of ^{233}U and ^{244}Pu mono-isotope spikes were added to each by weight. Samples were dissolved in concentrated HNO3, HF, and HClO4 acids. Once in solution, the dissolved samples were run through three ion-exchange resin columns to first separate the uranium and plutonium together, next to separate the uranium from the plutonium, and finally to purify the plutonium aliquot. Samples were subsequently diluted to give proper ion counts for the multi-collector mass spectrometer.

The magnetic sector inductively coupled mass spectrometer delivers high sensitivity and precision (~1E+6 atoms detection limit; ±100 ppm) measurements of actinide concentrations and isotope ratios in both solid and liquid matrices. This instrumentation allows for the routine determination of plutonium abundance and high precision isotope ratios at microgram concentrations (1E-6 grams). Isotopic ratios and concentrations of uranium and plutonium were analyzed separately for each of the six samples by this

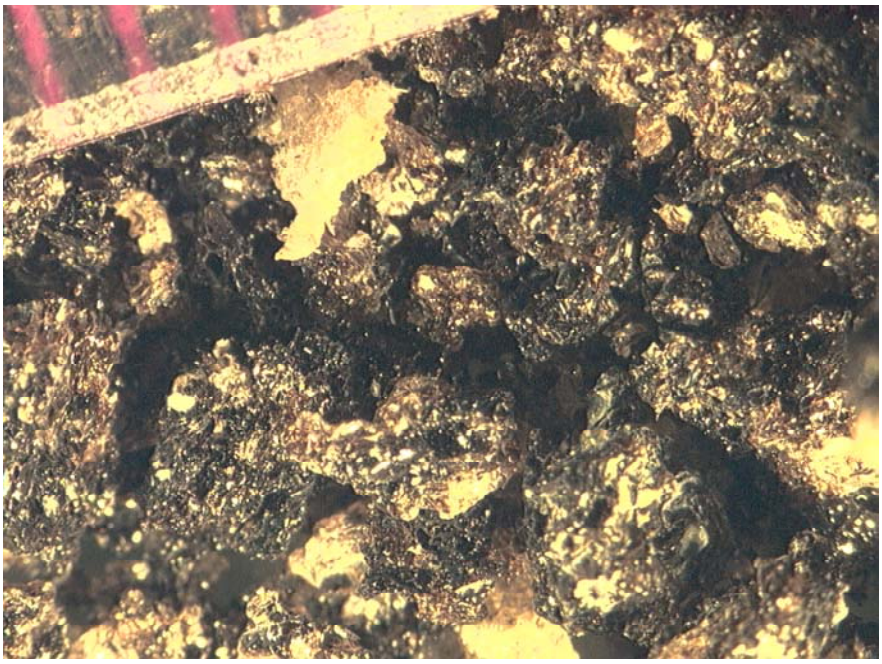

Figure 1. Photomicrograph of Sample #6 of dark melt-glass returned from the base of the cavity and melt-glass puddle. Millimeter scale in red at top of frame.

Figure 2. Photomicrograph of Sample #2 of light colored ash collected higher in the collapse pile. Millimeter scale in red faintly visible at lower right of frame.

technique. One-sigma errors on the isotope ratio measurements for $^{238}U/^{235}U$ averaged 0.0597. Two-sigma errors on the isotope ratio measurements for $^{240}Pu/^{239}Pu$ averaged 0.00101. Both errors are considerably lower than the variations in the measured isotope ratios.

Distribution of Uranium and Plutonium in the Cavity and Collapse Chimney

Uranium and plutonium were detected in each of the samples analyzed. The presence of uranium is expected given that uranium occurs in natural concentrations of several parts-per-million (microgram/gram) in the silicic tuffs and rhyolites of the Nevada Test Site. The presence of plutonium in all the samples is significant because it provides unequivocal evidence that weapons-derived actinides were dispersed above the melt-glass horizon.

Uranium Data

The uranium data is presented in Table 2. The concentrations vary only slightly between 3 and 4 parts per million (ppm) and are consistent with natural uranium abundances in the tuff that comprise the host media for this test. The nuclear test fuses a considerable amount of rock that contains a mixture of natural uranium with uranium from the nuclear device. Assuming 700 metric tons of rock are melted per kiloton of nuclear yield (Olsen, 1967), more than 7000 metric tons of rock are melted in a 10 kiloton yield underground explosion. The amount of natural uranium volumetrically incorporated the resulting body of glass will range between 2.1E+4 (assuming 3 ppm initial concentration) and 2.8E+4 grams (assuming 4 ppm initial concentration).

Anomalies in the $^{235}U/^{238}U$ isotope ratio and $^{234}U/^{238}U$ activity ratio are indicative of the presence of uranium derived from unburned actinide fuels or device parts. The natural $^{235}U/^{238}U$ isotope ratio is 0.007. Corresponding $^{234}U/^{238}U$ activity ratios are 1.0 for samples in secular equilibrium. Two of the six samples show enrichments in ^{235}U isotopic composition and ^{234}U activity that unequivocally demonstrates the incorporation of a bomb fraction. Not unexpectedly these samples correspond to the dark melt-glass samples that partition the actinides. Radiochemical diagnostics associated with the nuclear testing program have long recognized that uranium is slightly volatile in the high temperature underground environment accompanying a nuclear test. A 'volatility correction' is normally applied to arrive at the correct bomb-fraction. We can infer that weapons-derived uranium may have been transported away from the device during detonation and became incorporated in the damage zones or region of chimney collapse. However the large amount of natural uranium in the rock overwhelms any uranium isotopic signature from the device. That other gamma-emitting radionuclides are detected in the debris samples but anthropogenic uranium is not suggests that that the gamma-emitting species are pervasively deposited on fracture and minerals surfaces while the fuel uranium never is concentrated at levels where it can be detected above natural background.

Table 2. Uranium data.

Sample	Relative Slant Depth	Uranium Concentration in μg/g	$^{235}U/^{238}U$ Isotope Ratio	$^{234}U/^{238}U$ Activity Ratio
1	shallow	4.11	0.00727	1.022
2		3.12	0.00735	1.122
3		4.32	0.10110	41.152
4		3.72	0.00733	1.020
5		3.22	0.01397	3.8383
6	deep	3.98	0.03730	13.908

Plutonium Data

Plutonium concentration data is presented in Table 3. Plutonium isotope ratios, while collected, have been omitted for classification purposes. Unlike uranium, plutonium is diagnostic of the test device due to the absence of any naturally–occurring isotopes of this radionuclide. The analytical results show the highest concentrations of plutonium are associated with the melt glass fraction (Sample #3 and Sample #6). Glass Sample #4 contains relatively low concentrations of plutonium and is reddish in color with a flow banded texture that suggests it may represent a volcanic glass. The presence of volcanic glass is confirmed by the corresponding natural uranium isotope and activity ratios. Not only is the melt glass heterogeneously distributed in the collapse cavity, but the plutonium concentrations vary by approximately a factor of three between the two glass samples.

Table 3. Plutonium concentration data.

Sample	Relative Slant Depth	Sample Type	Plutonium Concentration in ng/g
1	shallow	ash	3.02E-2
2		ash	1.03E-1
3		glass	1.58E+2
4		glass	1.23E-1
5		ash	6.86E0
6	deep	glass	4.81E+1

In the context of prompt-injection processes, the most significant results are the observed presence of plutonium in samples taken from the cavity collapse outside of the melt-glass horizon. Plutonium concentrations in the ash samples increase with depth and range from 3.0E-2 to 6.9E0 nanograms/gram. It is unknown how the plutonium is sited on or within these crystalline matrices. Most likely the plutonium is a metal or oxide condensate that was deposited on available surfaces; alternately it could be incorporated as minute pieces of glass or associated with silicates that were displaced in the collapse pile. Because

there is no natural reservoir of plutonium, the plutonium detected in these samples has not been obscured by mixing between natural and anthropogenic sources.

Discussion

The availability of a contiguous suite of samples and the ability to provide reliable measurements of plutonium concentrations and isotope ratios allows for insight into the initial distribution of plutonium within a nuclear test cavity and collapse chimney. There have only been a few studies of the distribution of radionuclides in melt-glass (Borg et al., 1975; Eaton and Smith, 2001) and only one documented case of actinides being transported by prompt injection outside of the immediate cavity and chimney system (Rose et al., 2000). However, the detection of ^{134}Cs, ^{137}Cs, ^{106}Ru, ^{125}Sb and enriched ^{235}U within a 3 meter thick interval in tuff at a distance of 166m southwest and 37 m above the water table of the 1990 BULLION underground test suggests that prompt injection may be responsible moving otherwise relatively insoluble radionuclides – including actinides – away from the working point (Rose et al., 2000). While actinides have been detected in aquifers downgradient from nuclear tests (Kersting et al., 1999), an important question is the specific mechanism by which residual post-test plutonium is transferred to groundwater regime. In particular we would like to determine whether the plutonium found at the ER-20-5 well cluster originated from prompt injection accompanying the BENHAM explosion, movement in groundwater involving glass dissolution and subsequent sorption on colloids, or both. Pawloski (1999) reports that recent recalculation of averaged medium properties (water content, porosity, and grain density) for the BENHAM ground zero suggest that cavity growth was restricted and resulted in unusually high higher internal cavity pressures (~ 500 to 700 bars). The higher cavity pressure may have cracked lava immediately above the BENHAM device permitting radionuclides to be transported outside the cavity region and potentially upwards into the saturated zone.

Using the results of data acquired during this study, we have plotted the distribution of actinides with depth in the lowermost cavity and chimney in Figure 3. Variations in the $^{235}U/^{238}U$ clearly mimic those for plutonium concentrations. Notably there is not a regular enrichment in actinide concentrations with depth but rather a sharp spike in enrichment in residual actinides at mid-level within the cavity-chimney system. This is the result of melt glass that has become incorporated higher in the cavity environment likely due to the chaotic in-fall of overburden accompanying the collapse of the cavity. Glass was displaced and "splashed" upwards as cooler blocks fell into the melt puddle and the melt rapidly cooled in the void space between the chimney rubble. As noted above, the uranium concentrations are relatively uniform due to the high abundance of natural uranium in the rock.

Isotope ratios and concentrations measured in these samples provide new insight into the underground phenomenology, distribution, and transport of plutonium underground. Figure 4 plots the isotope ratio of plutonium verses concentration in parts per billion. For classification purposes, labels for the measured $^{239}Pu/^{240}Pu$ ratios are omitted.

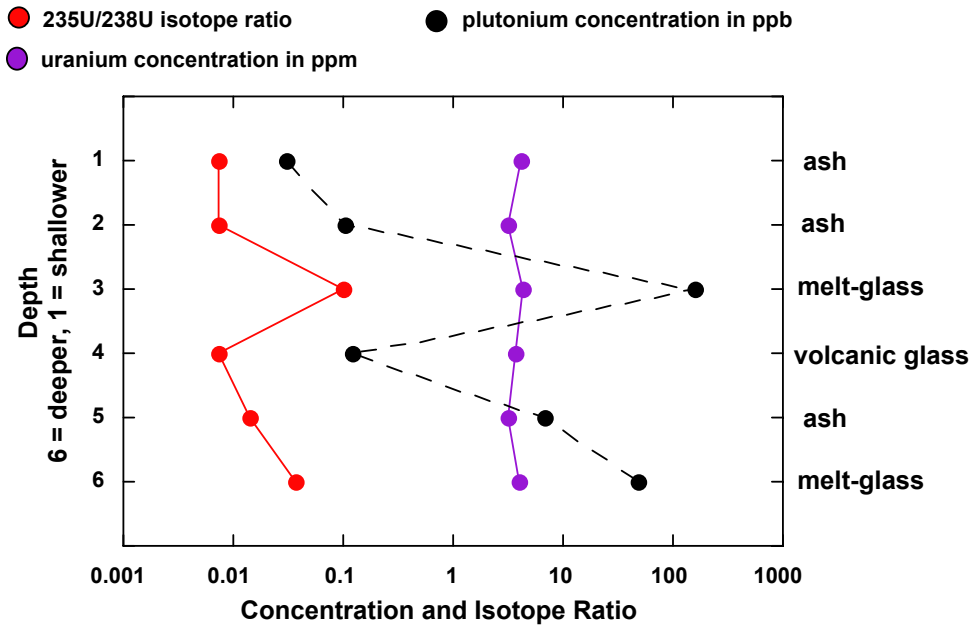

Figure 3. Plot of the distribution of $^{235}U/^{238}U$ isotopes (red), uranium concentrations in ppm (purple), and plutonium concentrations in ppb (black) in sidewall cores taken from the base of the melt puddle (depth = 6) upwards in the collapse chimney (depth = 1). Sample type with depth indicated on right axis.

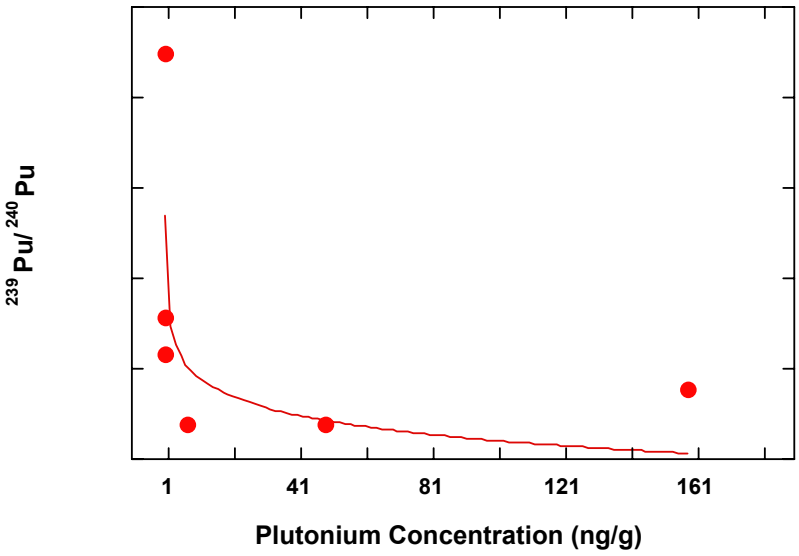

Figure 4. Plot of $^{239}Pu/^{240}Pu$ isotope ratio (the ordinate label is omitted) and plutonium concentration in parts-per-billion. A hyperbolic mixing line joins plutonium enriched melt glass samples with lower $^{239}Pu/^{240}Pu$ isotope ratios to plutonium depleted samples with enriched $^{239}Pu/^{240}Pu$ ratios.

Samples fall along a hyperbolic trend that is indicative of two component mixing. The melt glass end-member has enriched plutonium concentrations but a lower $^{239}Pu/^{240}Pu$ isotope ratios than the end-member samples of ash taken higher in the collapse zone. However the continuum of data along a mixing line suggests that the plutonium behaves systematically as a result of chemical and physical processes at early times in the history of the cavity-chimney system. It is important to note that there is only one initial plutonium isotope ratio associated with the device. The fact that the plutonium data plot on a two-component mixing line demonstrates that the plutonium isotopes were fractionated during volatile transport.

As a check on the mixing relations, a companion plot of plutonium isotope ratios plotted against the inverse of the plutonium concentrations in parts per billion is presented in Figure 5. Again, labels for the plutonium isotopes are omitted to avoid compromising classified information. The inverse concentration plot is linear which is expected of a true mixture.

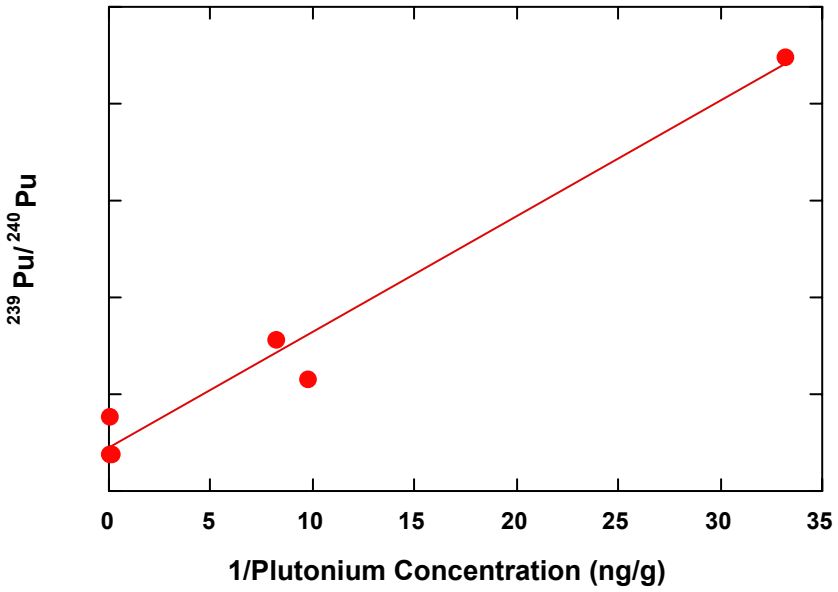

Figure 5. Plot of $^{239}Pu/^{240}Pu$ isotope ratio (the ordinate label is omitted) and the inverse of plutonium concentration in parts-per-billion. A linear mixing line joins isotopically enriched melt glass samples to isotopically depleted breccia samples.

Conclusions

The results of this work clearly indicate the heterogeneous radiochemical environment that exists in the region between the device depth of burial and the bottom of the cavity. Melt glass formed during the detonation coalesces as a puddle on the floor of the standing cavity. The textural and radiochemical profile indicates the glass is subsequently displaced as blocks are chaotically dropped into the melt during cavity collapse. These

results are consistent with photographs and maps produced during the mined re-entry into the base of the RAINIER cavity which first documented the juxtaposition of glass and in-fall debris in the bottom half of the collapse chimney (Wadman and Richards, 1961). The sample with the highest plutonium concentration and strongest enrichment in $^{235}U/^{238}U$ ratio is situated approximately 15 meters above the base of the cavity. These findings are in keeping with other reports on the heterogeneous distribution of tritium, fission, and activation products found in a saturated nuclear test cavity (e.g., Borg, 1975; Mathews et al., 1994; Smith, 1995; Thompson, 1996).

Furthermore, this data unequivocally shows that plutonium may be dispersed throughout the cavity environment at the time immediately following the detonation. This plutonium is associated with fine grained, brecciated, volcanic ash samples that occur within the collapsed region. Mixing diagrams demonstrate that plutonium isotope ratios are fractionated during volatile transport, and suggest that the plutonium sequestered in the melt has mixed with the ash samples. It must be emphasized that the plutonium in the ash is present in extremely low concentrations that are three to four orders of magnitude below those encountered in the melt glass. However due to its prevalence throughout all the debris samples analyzed, low concentrations plutonium are readily available for release to groundwater through surface reactions with the ash. We conclude that for the test under consideration the plutonium that was deposited outside of the melt glass zone is most likely to be transferred to the groundwater regime. In general, transport of plutonium in groundwater likely involves the remobilization of minute amounts of plutonium dispersed throughout the cavity and chimney that subsequently is released to solution. This source may complement release of a larger reservoir of plutonium available through dissolution of melt-glass. The ability of plutonium to be transported pervasively throughout the collapsed cavity and chimney suggests that plutonium may be equally available for movement by prompt-injection outside of this region.

References

Borg, I.Y., 1975, Radioactivity trapped in melt produced by a nuclear explosion, Nuclear Technology, v. 26, p. 88–100.

Borg, I.Y., Stone, R., Levy, H.B., and Ramspott, L.D., 1976, Information pertinent to the migration of radionuclides in ground water at the Nevada Test Site Part 1: review and analysis of existing information, Lawrence Livermore National Laboratory, UCRL-52078 Pt. 1, 216p.

Buddemeier, R.W., Finkel, R.C., Marsh, K.V., Ruggieri, M.R., Rego, J.H., and Silva, R.J., 1991, Hydrology and radionuclide migration at the Nevada Test Site, Radiochimica Acta, v. 52/53, p. 275-282.

CRC Handbook of Chemistry and Physics, 1990-1991, 71st edition, CRC Press.

Eaton, G.F. and Smith, D.K., 2001, Aged nuclear explosive melt glass: radiography and scanning electron microscope analyses documenting radionuclide distribution and glass alteration, J. Radioanalytical and Nuclear Chemistry, v. 248, n. 3, p. 543 – 547.

International Atomic Energy Agency (IAEA), 1998, The radiological situation at the atolls of Mururoa and Fangataufa, Volume 3, Inventory of radionuclides underground at the atolls, IAEA-MFTR-3, 94p.

Kersting, A.B., Efurd, D.W., Finnegan, D.L., Rokop, D.J., Smith, D.K., and Thompson, J.L., 1999, Migration of plutonium in groundwater at the Nevada Test Site, Nature, v. 397, p. 56-59.

Mathews, M., Hahn, K., Thompson, J., Gadeken, L., and Madigan, W., 1994, Subsurface radionuclide investigation of a nuclear test, J. Applied Geophysics, v. 32.

Nimz, G.J. and Thompson, J.L., 1992, Underground radionuclide migration at the Nevada Test Site, U.S. Department of Energy, Nevada Field Office, DOE/NV-346.

Olsen, C.W., 1967, Time history of cavity pressure and temperature following a nuclear detonation in alluvium, Lawrence Livermore National Laboratory, UCRL-70379, Preprint, 11p.

Pawloski, G.A., 1999, Development of phenomenological models of underground nuclear tests on Pahute Mesa, Nevada Test Site – BENHAM and TYBO, Lawrence Livermore National Laboratory, UCRL-ID-136003, in review, 49p.

Rose, T.P., Smith, D.K., and Phinney, D.L., 2000, Secondary ion mass spectrometry measurements of volcanic tuffs containing radionuclides from underground nuclear tests, Radiochimica Acta, v. 88, p. 465-473.

Sawyer, D.A., Thompson, J.L., and Smith, D.K., 1999, The CHESHIRE migration experiment - a summary report, Los Alamos National Laboratory, LA-13555-MS, 32p.

Smith, D.K., Nagle, R.J., and Kenneally, J.M., 1996, Transport of gaseous fission products adjacent to an underground test cavity, Radiochimica Acta, v. 73.

Smith, D.K., 1995, Characterization of nuclear explosive melt debris, Radiochimica Acta, v. 69, p. 157 – 167.

Smith, D.K., 2001, Evaluation of the radiochemistry of near-field water samples at the Nevada Test Site applied to the definition of a hydrologic source term, Lawrence Livermore National Laboratory, unpublished report, 53p.

Thompson, J.L. and Gilmore, J.S., 1991, Migration of fission products at the Nevada Test Site: detection with an isotopic tracer, Radiochimica Acta, v. 52/53, p. 229-231.

Thompson, J.L., 1996, Radionuclide distribution in a nuclear test cavity: the BASEBALL event, Radiochimica Acta, v. 72, p. 157-162.

Tompson, A.F.B., Bruton, C.J., Pawloski, G.A., eds., 1999, Evaluation of the hydrologic source term from underground nuclear tests in Frenchman Flat at the Nevada Test Site: the CAMBRIC test, Lawrence Livermore National Laboratory, UCRL-ID-132300, 319p.

Wadman, R.E. and Richards, W.D., 1961, Postshot geologic studies of excavations below RAINIER ground zero, Lawrence Livermore National Laboratory, UCRL-6586, 27p. with maps and photographs.

Chapter 4

The Redox State of Nuclear Melt Glass

Timothy P. Rose, Erik J. Nelson, Patrick G. Allen,
Frederick J. Ryerson, and Gayle A. Pawloski

Executive Summary

X-ray absorption spectroscopy (XAS) measurements were used to investigate the oxidation states of iron and uranium in three different melt glass samples from underground nuclear test cavities at the Nevada Test Site (NTS). Parallel XAS measurements on four glass reference standards containing iron or uranium in oxidized or reduced states provided constraints on the melt glass redox states. The spectroscopy data indicate that all three nuclear melt glasses contain uranium and iron in mixed valence states (U^{5+}/U^{6+} and Fe^{2+}/Fe^{3+}). The relative proportions of Fe^{2+} and Fe^{3+} in the melt glasses were quantified by modeling the pre-edge feature of the Fe K absorption edge using the method described in Wilke et al. (2001). The melt glass samples were found to contain between 33 and 53 at% Fe^{2+}, implying moderately reducing conditions. The concentrations of plutonium and other transuranic actinides in the melt glass samples are too dilute for the direct measurement of their oxidation states by XAS. However, comparison of the Fe and U results from this study with published redox studies of synthetic glasses suggests that plutonium will be present as Pu^{4+} in the melt glasses. Available data from the literature indicates the oxidation state of the Fe^{2+}/ Fe^{3+} couple in the melt glass will have an important influence on the redox conditions in groundwater during melt glass dissolution.

Introduction

Oxidation-reduction (or "redox") reactions involve the transfer of electrons from one chemical substance to another via the exchange of *valence* electrons, the outermost and most chemically reactive electrons of an atom. If one substance gains electrons (reduction), another substance must lose electrons in the same process (oxidation). A number of elements can exist in more than one oxidation state (also referred to as valence state). For example, four oxidation states of plutonium may coexist in aqueous solution under environmentally relevant conditions: Pu^{3+}, Pu^{4+}, Pu^{5+}, and Pu^{6+} (Allard et al., 1980; Choppin et al., 1997). Pu^{6+} is the most oxidized form, having 'lost' six of its valence electrons, whereas Pu^{3+} is the most reduced form. The redox state of a groundwater is known to have a strong influence on the solubility and transport of multivalent elements in the environment (see Stumm and Morgan, 1996, for review).

In the context of underground nuclear testing environments, the redox state of the melt glass produced by an explosion is also likely to influence the mobility and reactivity of radionuclides in groundwater. This may be particularly true for low permeability

environments, where prolonged interaction of the groundwater with the nuclear test debris may alter the ambient redox state of the fluid. Evidence for strongly reducing groundwater conditions have already been identified in one underground test cavity at the Nevada Test Site (NTS) on the basis of geochemical measurements of fluid samples (Rose et al., 2000).

Very little detailed information currently exists on the redox state of nuclear melt glasses. Borg (1975) reported that the Fe^{2+}/Fe^{3+} ratio of some nuclear melt glasses are as much as a factor of 10 greater than in the unmelted host rock, implying relatively reducing conditions during glass solidification. However, information on the redox state of multivalent actinides in the glass are lacking, and recent efforts to model the release and transport of radionuclides in the near-field environment have relied upon estimated values for many redox-sensitive species (Pawloski et al., 2001).

The objective of this study is to characterize the redox state of melt glass samples from underground nuclear tests at the Nevada Test Site (NTS). Melt glass samples were selected from test program archives and analyzed by X-ray Absorption Spectroscopy (XAS) to determine the redox states of Fe and U in the glasses. Four different reference glass standards containing either oxidized or reduced forms of Fe and U were also analyzed to place constraints on the redox conditions in the melt glasses. Although the concentrations of transuranic actinides such as Pu are too low to measure directly in the melt glass samples, inferences are drawn from literature sources regarding their probable oxidation state using the constraints provided by the Fe and U analyses.

X-Ray Absorption Spectroscopy

X-ray absorption spectroscopy (XAS) is a powerful element-specific technique that is widely used to investigate the chemistry of dilute elements in environmental materials (Brown et al., 1988). The absorption of X-rays by matter has long been used to study the discrete (quantized) energy levels of electrons in atoms and molecules (e.g., Glenn and Dodd, 1968). However, XAS has only been used as a quantitative method of studying molecular structures since the early 1970s, following the development of intense sources of continuous X-rays known as *synchrotron radiation* (Winick and Doniach, 1980). The technique is especially valuable for the analysis of glasses where conventional diffraction methods are not applicable due to the lack of periodicity in the structure (Murata, 1991).

When an incident X-ray is absorbed with energy close to the binding energy of a core-level electron of the absorbing atom, an electron is promoted from the initial core state to an unoccupied valence orbital of the same atom (Figure 1). This process is marked by a sharp increase in X-ray absorption over a narrow range in incident X-ray energies, and is referred to as the *absorption edge*. The excited atom subsequently returns to its ground state through secondary processes such as X-ray emission (fluorescence), which can provide valuable information on bonding and composition. By monitoring the absorption via transmission or fluorescence yield while varying the photon energy through the absorption edge, an X-ray absorption near-edge structure (XANES) spectrum is collected (cf. Bianconi, 1988). This spectrum reflects the unoccupied valence orbitals of the atom,

and therefore is sensitive to both the oxidation state of the atom and its local bonding environment. The energy of the absorption edge differs for cations in different oxidation states, e.g. Fe^{2+} vs. Fe^{3+}, and the XANES spectra of reference materials are often compared to those of the sample to provide "fingerprints" of the local bonding environment.

Sample Descriptions

Nuclear Explosive Melt Debris Samples

Melt glass samples from three different underground nuclear tests were selected for XAS analysis. Two of the tests were conducted below the water table, while the third was detonated in the unsaturated zone. All three tests had working points in tuffaceous volcanic rocks. The glasses exhibit notable differences in color and texture, with sample UGTA-1 being the lightest in color, with a frothy, pumiceous texture. Sample UGTA-2 is also vesicular, but has a smaller mean vesicle diameter than UGTA-1, and is much darker in color. Sample UGTA-3 is a dark brown glass that is similar in appearance to flow-banded obsidian, with sparse, highly flattened vesicles. Brief sample descriptions are given in Table 1.

Table 1. Melt glass descriptions.

Sample I.D.	Test Location	W.P. Lithology	Description
UGTA-1	Pahute Mesa	Rhyolite Tuff; saturated zone	highly vesicular, banded glass, colorless to pale gray color, similar in appearance to pumice; 1-3 mm vesicles, rounded or slightly elongated parallel to banding
UGTA-2	Yucca Flat	Rhyolite Tuff; saturated zone	moderately vesicular, dark brown to gray glass; small, subequant vesicles up to 1 mm size
UGTA-3	Rainier Mesa	Rhyolite Tuff; unsaturated zone	dense, dark brown, banded glass with small reddish-brown inclusions of unmelted volcanic rock; obsidian-like texture; rare vesicles to 1 cm, elongated parallel to banding

Reference Glasses

A simplified Lake County Obsidian (LCO) composition was prepared to provide reference standards for XAS analysis of uranium and iron. Two "doped base glass" compositions were prepared by adding ~1000 ppm of either uranium or iron oxide to 2-gram aliquots of the simplified LCO sintered oxide mix. The redox state of uranium and iron in the glass was controlled by the synthesis conditions. The oxidized glass standards were prepared in air (oxygen fugacity [fO_2] = 0.23 atm). Reduced glass standards were synthesized by re-melting the doped base glass compositions in a one-to-one mixture of flowing CO-CO_2 gas in a vertical tube muffle furnace, at an oxygen fugacity of $10^{-9.1}$ atm. The uranium-doped glass was placed in a small, open Pt crucible

and melted at ~1360˚C. The melt was quenched in water to form a glass. The reduced Fe-doped glasses were more problematic, as iron alloys with Pt at low oxygen fugacity and can be lost from the sample. To minimize this effect, glass starting materials were suspended on Pt wire loops (0.010" Pt wire) and melted at ~1360˚C. The spherical bead was quenched in water at the end of the experiment. A second Fe-doped bead was then prepared using the same Pt wire loop. The wire had an increased Fe content due to contact with the first bead, and hence, was less likely to absorb additional iron from the second glass bead.

Glass Compositions

The melt glass samples were analyzed for their major element compositions on a JEOL 8200 electron microprobe using a 7.5 nA, 15 keV electron beam defocused to a diameter of 30 μm. X-ray intensities were converted to element concentrations using a CITZAF algorithm. Reference standards included a variety of silicate and oxide minerals. Each sample was analyzed at 10 randomly selected spots. Compositional averages are reported in Table 2 as oxide weight percent. The composition of Lake County Obsidian (LCO) is included for comparison. Note that the simplified LCO composition used to prepare the reference standards contained a smaller weight fraction of iron (0.1 wt.%) than the natural composition reported below.

Table 2. Major element compositions of nuclear melt glass and reference glass samples.

	UGTA-1	**UGTA-2**	**UGTA-3**	**LCO**
SiO_2	77.25	75.08	68.69	76.01
TiO_2	0.07	0.17	0.40	0.11
Al_2O_3	12.56	13.17	16.55	13.00
FeO*	0.79	1.61	2.90	0.70
MnO	0.00	0.13	0.29	0.08
MgO	0.08	0.27	1.41	0.09
CaO	0.61	0.94	3.92	0.52
Na_2O	3.25	3.37	1.87	4.81
K_2O	5.22	4.38	2.73	3.65
Total	99.82	99.10	98.74	98.97

*Total Fe is reported as FeO.

The melt glass samples have major element compositions that generally reflect the chemistry of tuffaceous volcanic rocks found at the Nevada Test Site (Broxton et al., 1989). The darker-colored glass samples (UGTA-2 and UGTA-3) have lower SiO_2 and higher FeO contents than the pale-gray UGTA-1 sample, and may contain some iron that was inherited from the device assembly. Schwartz et al. (1984) observed that the iron

content of the melt glass tends to increase near the working point of an underground nuclear test.

Results

X-Ray Absorption Spectroscopy Data

X-ray Absorption Near-Edge Spectra (XANES) data were collected near the U L_{II} (binding energy 20.9 keV) and Fe K (7.1 keV) absorption edges in three nuclear melt glasses (UGTA-1, -2 and -3) at beamline 4-1 of the Stanford Synchrotron Radiation Laboratory (SSRL). The absorption from the dilute levels of uranium (<10 ppm) in these samples were detected using a Ge fluorescence detector, while the absorption from the more concentrated iron was measured by the loss in X-ray transmission through the sample. XANES spectra also were collected from the more concentrated reference glasses containing U or Fe (1000 ppm) prepared under low or high oxygen fugacity conditions (samples UGTA-4 through UGTA-7). To calibrate the energy of the sample absorption edges, the XANES from a UO_2 powder or Fe metal foil placed after the sample were recorded simultaneously by measuring the loss in X-ray transmission. The size of the absorption edge jump was normalized to one after subtracting off the pre-edge background.

The U L_{II} edge XANES spectra from the melt glasses and reference samples are shown in Figure 2. The U L_{II} XANES spectra of the melt glasses (UGTA-1, -2, -3) all have the same leading edge position as the high oxygen fugacity U reference glass (UGTA-4). The difference in noise level is due to the dilute concentrations of uranium in the melt glasses. The leading edge of the spectra for the low oxygen fugacity U reference glass (UGTA-6) is at a lower energy than those from the melt glasses, and agrees with the edge position for the U^{4+} reference compound UO_2. Figure 3 compares the U L_{II} XANES spectra for UGTA-4 to the XANES spectra from the U^{5+} and U^{6+} oxidation states and from the actinyl and uranate bonding environments, as well as from the mixed valence uranium oxide U_3O_8.

In the case of U^{5+} uranyl, which is not easily prepared in solution, the Np L_{III} XANES from aqueous $Np(V)O_2^+$ is scaled relative to the edge energy of NpO_2. The U XANES are correspondingly scaled to the UO_2 edge energy. The comparison of XANES for different oxidation states and environments is the same for U, Np, and Pu, as shown by Allen et al. (1997). Since the leading edge of the reference glass (UGTA-4) XANES is shifted to lower energy than both of the U^{6+} standards, the XANES results are consistent with oxidation of uranium to a mixed U^{5+}/U^{6+} oxidation state within all three nuclear melt glasses and the high oxygen fugacity reference glass. Similar results have been reported in the literature for uranium-bearing silicate glasses prepared under analogous conditions (Calas, 1979; Schreiber, 1983; Farges et al., 1992).

The corresponding Fe K edge XANES spectra are shown in Figure 4. The XANES of the low oxygen fugacity (UGTA-7) and high oxygen fugacity (UGTA-5) iron reference glasses have edge positions at lower and higher energy, respectively, indicating lower and higher oxidation states. The low oxygen fugacity reference glass has an edge position

close to the Fe^{2+} oxidation state, while that for the high oxygen fugacity reference glass is closer to Fe_3O_4 (average oxidation state +2.7). The Fe K edge and iron oxidation state from one of the melt glass samples (UGTA-1) closely matches the high oxygen fugacity reference glass, while the other two melt glasses (UGTA-2 and UGTA-3) have similar XANES spectra with an edge position and iron oxidation state intermediate to the two reference glasses.

To develop a more quantitative determination of the relative populations of Fe^{2+} and Fe^{3+} oxidation states in the melt glasses, we applied the method described in Wilke et al. (2001) and Petit et al. (2001). Using a wide range of Fe-containing minerals, Wilke et al. (2001) found a correspondence between oxidation state, coordination number, and the relative peak energies and intensities of the features in the "pre-edge" region of the Fe K edge (the 7110-7115 eV region in Figure 4). These pre-edge features are related to electronic transitions from the Fe 1s core state to a hybridized Fe 3d/4p valence state, and are sensitive to local oxidation state and Fe-O bonding geometry. The features appear at different energies for the Fe^{2+} and Fe^{3+} oxidation states: 7112.0 and 7113.8 eV respectively (see Figure 5). In addition, the intensity of the peaks increases with increasing oxidation state population as well as with decreasing symmetry of the local bonding environment, i.e. tetrahedral environments exhibit larger pre-edge features than octahedral environments.

In Figure 5, the Fe pre-edge features are fit to two Voigt functions (convoluted Lorentzian and Gaussian peaks). The sloping background of the Fe K edge was subtracted using arctangent and error functions (which are the integral step functions of Lorentzian and Gaussian peaks), and the widths of the two peaks were set equal at a total width of 2.2 eV while the intensities and peak positions were allowed to vary. The total integrated pre-edge intensity of the two peaks is plotted against their centroid (area-weighted average position) in Figure 6, and compared to the pure Fe^{2+} and Fe^{3+} endpoints determined by Wilke et al. (2001). All of the melt glasses, as well as the high and low oxygen fugacity reference glasses, appear on the line between the tetrahedral $^{(4)}Fe^{2+}$ and $^{(4)}Fe^{3+}$ oxidation states, indicating the presence of mixed Fe oxidation state in all of the glasses. Although the data clearly indicate tetrahedral coordination of the Fe in the glasses, octahedral coordination of some of the Fe cannot be ruled out, as the contribution of octahedral Fe to the pre-edge feature is small and would be dominated by the tetrahedral component. From the position of the glass data points relative to the pure Fe^{2+} and Fe^{3+} endpoints, the Fe^{2+} and Fe^{3+} populations in the glasses can be determined. The results are given in Table 3. Of the three nuclear melt glasses, UGTA-1 has a larger Fe^{3+} content (67%), while UGTA-2 and UGTA-3 are similar with nearly equal amounts of Fe^{2+} and Fe^{3+}. In addition, the high and low oxygen fugacity references glasses are not purely Fe^{3+} and Fe^{2+}, respectively, but each contain about 20% of the minority species. These oxidation state results are consistent with those determined from the position of the Fe K edge, and indicate that Fe is in mixed oxidation states within all of the glasses.

Table 3. Fe^{2+} and Fe^{3+} oxidation states in nuclear melt glass and reference glass samples.

Sample	Fe^{2+} population (at %)	Fe^{3+} population (at %)
Nuclear Melt Glasses		
UGTA-1	33%	67%
UGTA-2	53%	47%
UGTA-3	51%	49%
Reference Glasses		
UGTA-5 (high fO_2)	23%	77%
UGTA-5 (high fO_2)	85%	15%

Discussion

Implications for the Oxidation State of Actinides in the Melt Glass

The concentrations of plutonium and other transuranic actinides (Np, Am) in the melt glass samples are too dilute for the direct measurement of their oxidation states by XAS. However, we can make inferences about their oxidation states (valences) by comparing the Fe and U results from this study with published studies of synthetic glasses containing Fe and/or U in combination with other actinides. Most of the literature on this topic pertains to the development of materials for the disposal of spent nuclear reactor fuel.

Karraker (1982) used optical absorption spectroscopy to investigate actinide valence states in borosilicate glasses containing 0.4 to 0.9 wt.% U or Pu. Glass samples prepared in air at 1100°C were found to contain U^{6+} as the uranyl ion, and plutonium as Pu^{4+}. The effect of reducing agents was then explored by adding graphite to the glass in excess of that required for the reaction:

$$UO_3 + C \rightarrow UO_2 + CO.$$

Using an eight-fold graphite excess, the spectra showed that uranium in the glass was reduced to the U^{4+} and U^{5+} valence states. However, an attempt to reduce plutonium under similar conditions showed little change in the spectral data, indicating that little, if any, of the Pu^{4+} was reduced to Pu^{3+}. It is notable that the high fO_2 samples prepared by Karraker (1982) appear to be slightly more oxidized (mostly U^{6+}) than the NTS melt glass samples, whereas the low fO_2 samples are clearly more reduced (containing mostly U^{4+}). Hence, these data nicely bracket the melt glass XAS results, and suggests that plutonium is likely to be in the Pu^{4+} oxidation state in the melt glass samples.

Several other studies appear to support this conclusion. For example, Eller et al. (1985) used electronic absorption spectroscopy (not the same technique as XAS) to determine the valences of U, Np, Pu, and Am in borosilicate glass prepared in air at 1000°C. Only

the U^{6+}, Np^{4+}, Pu^{4+}, and Am^{3+} valence states were observed, and these conditions did not change after aging the samples for one year.

In another study, Hess et al. (1998) performed XAS measurements on borosilicate glass samples containing several different multivalent cations, including 1 wt.% PuO_2. The samples were aged for 15 years prior to analysis. From measurements of the absorption edge energies, the oxidation states of the metal cations in the glass samples were determined to be Mn^{2+}, Fe^{3+}, and Pu^{4+}. The XANES spectra also showed the presence U^{6+} in the form of uranyl ions, but the absorption edge was shifted to lower energies than would be expected if only U^{6+} were present, implying that uranium was present in multiple oxidation states. This is similar to the XANES results for the NTS melt glass samples and the high fO_2 U reference glass (sample UGTA-4; see Figure 3).

Finally, Morss et al. (2000) recently prepared glass-bonded sodalite ceramic waste forms under an inert atmosphere (low fO_2 conditions) containing either U or Pu in combination with rare-earth elements. XAS measurements taken near the Pu L absorption edges showed essentially the same spectra as that of a reference PuO_2, indicating that only Pu^{4+} was present. Uranium-bearing glass-bonded sodalite prepared under the same conditions contained only U^{4+} (as UO_2).

Although synthetic glasses and ceramics are not compositionally the same as the aluminosilicate glasses that comprise nuclear melt debris, they are structurally similar. For example, B^{3+}-linkages in borosilicate glasses are analogous to the Al^{3+}-linkages in aluminosilicate glasses (e.g. Tossell and Sághi-Szabó, 1997). Hence, we would expect actinide cations to occupy similar positions within either of these structures. The redox state depends primarily on the fO_2 conditions at the time the glass is formed, but is also influenced by alkali oxide content. For most redox sensitive elements, increasing the alkali content (e.g. Na and K) tends to favor more oxidizing conditions (e.g. Paul, 1990; Duffy, 1999). The glasses used in nuclear waste containment studies usually have higher alkali contents than 'natural' aluminosilicate glasses (as much as 25 wt.% in some borosilicate glasses, compared to <10 wt.% in the melt glass samples from this study). This implies the actinide redox data from the waste glass literature may reflect somewhat more oxidizing conditions than in the aluminosilicate glasses in this study. Nevertheless, the waste glass data are still broadly applicable to interpreting actinide redox conditions in the melt glasses since the range in experimental redox conditions are much broader than the natural redox variations observed in the melt glasses.

The results of synthetic glass studies suggest that Pu^{4+} is stable over a wide range of oxygen fugacity conditions in silicate glasses. Pu^{4+} is the dominant valence state under both oxidizing (atmospheric) conditions that favor the stability of U^{6+} and Fe^{3+}, as well as reducing conditions that favor the development of U^{4+}. Measured reduction potentials of silicate melts show that iron will be present as Fe^{2+} in glasses that contain uranium predominantly in the U^{4+} valence state (Schreiber, 1983). Since the measured NTS melt glass samples contain both Fe and U in mixed redox states, we can conclude that Pu^{4+} is probably the dominant form of plutonium in the melt glasses.

Data are lacking regarding Np and Am oxidation states in silicate glasses over a range of redox conditions. Np^{4+} and Am^{3+} were reported in borosilicate glasses prepared under high fO_2 conditions (Eller et al., 1985), but a literature search failed to turn up additional information. The oxidation states reported by Eller et al. (1985) are consistent with those predicted for redox equilibrium with U^{6+} and Pu^{4+} in an aqueous solution at pH = 7, (Silva and Nitsche, 1995), although Np^{5+} is generally more stable than Np^{4+} under normal oxidizing conditions (Kim, 1986; Dozol and Hagemann, 1993).

Implications for Redox Conditions During Melt Glass Dissolution

Previous studies of silicate glass systems suggest that iron acts as an internal buffer of the redox conditions in silicate melts (e.g. Bonnin-Mosbah et al., 2001). Under moderately reducing conditions, such as those found in some NTS melt glass samples, the Fe^{2+}/Fe^{3+} redox couple stabilizes the U^{5+}/U^{6+} couple from other oxidizing and reducing agents because: (1) Fe^{2+} is easier to oxidize than U^{5+}, (2) Fe^{3+} is easier to reduce than U^{5+}, and (3) the concentration of iron is usually greater than all other redox-sensitive species in the glass (Schreiber et al., 1985). The iron may therefore be considered to act as a buffer for other redox couples as well.

In groundwater systems, the redox balance is generally determined by the availability of dissolved atmospheric oxygen, organic carbon, and iron minerals. In groundwater systems with low organic carbon content, like those at the NTS, the initial oxygen content in the water may be rapidly reduced by interaction with Fe^{2+}-bearing phases, resulting in the formation of $Fe(OH)_3$ (e.g. Grenthe et al., 1992). Chemical analyses of reduced groundwaters have confirmed that that the Fe^{2+}/Fe^{3+} couple controls the oxidation potential in solution (Jantzen and Bibler, 1985). In a nuclear test cavity environment, the iron redox state of the melt glass is therefore likely to have an important influence on the redox conditions in solution. The melt glass samples from this study were found to contain 33 to 53 at% Fe^{2+}, although values as high as 83 at% Fe^{2+} were reported by Borg (1975), suggesting that groundwater in contact with the glass will likely evolve toward more reducing conditions.

The results of glass leaching experiments show that the *solubility* of actinide species (particularly Np) decreases in the presence of iron due to the locally reducing redox potentials imposed by Fe^{2+} (Apted et al., 1986; Bodoglio et al., 1988; Inagaki et al., 1998). However, these same studies suggest that the presence of iron enhances the formation of colloids, particularly Pu-bearing colloids. These observations show it is difficult to predict the transport characteristics of actinides in solution using only redox potentials; complexation reactions, hydrolysis, and colloid generation must also be considered (Kim, 1986). We can nevertheless conclude that the redox state of the Fe^{2+}/Fe^{3+} couple is likely to be the dominant factor controlling oxidation potentials during melt glass dissolution.

Conclusions

The principal conclusions of this study are as follows:

(1) X-ray absorption spectroscopy measurements were used to determine the redox state of Fe and U in three nuclear melt glass samples from the NTS. The data indicate that Fe and U are present in mixed valence states (Fe^{2+}/Fe^{3+} and U^{5+}/U^{6+}) in all three samples.

(2) The relative proportions of Fe^{2+} and Fe^{3+} in the glasses were quantified by modeling the pre-edge feature of the Fe K absorption edge. The melt glass samples were found to contain between 33 and 53 at% Fe^{2+}, implying moderately reducing conditions.

(3) A comparison of the Fe and U redox states in the NTS melt glasses with published redox studies of synthetic glasses suggests that plutonium is in the Pu^{4+} oxidation state in the melt glasses.

(4) Available data from the literature indicates the oxidation state of the Fe^{2+}/Fe^{3+} couple in the melt glass will have a major influence on the redox conditions in groundwater during melt glass dissolution.

Acknowledgments

Funding for this investigation was provided by the Environmental Restoration Division's Underground Test Area Project at the National Nuclear Security Administration, Nevada Operations Office. This work was performed under the auspices of the U.S. Department of Energy by Lawrence Livermore National Laboratory under contract number W-7405-Eng-48.

References

Allard, B., Kipatsi, H., Liljenzin, J.O. (1980) Expected species of uranium, neptunium and plutonium in neutral aqueous solutions. J. Inorg. Nucl. Chem., v. 42, pp 1015-1027.

Allen, P.G., Bucher, J.J., Shuh, D.K., Edelstein, N.M., and Reich, T. (1997) Investigation of the Aquo and Chloro Complexes of UO_2^{2+}, NpO_2^{+}, Np^{4+}, and Pu^{3+} by X-ray Absorption Fine Structure Spectroscopy. Inorg. Chem., v. 36, pp 4676-4683.

Apted, M.J., McVay, G.L., and Wald, J.W. (1986) Release of actinides from defense waste glass under simulated repository conditions. Nuclear Technology, v. 73, pp 165-178.

Bianconi, A. (1988) XANES spectroscopy. In: D.C. Koningsberger and R. Prins (eds.), *X-Ray Absorption: Principles, Applications, Techniques of EXAFS, SEXAFS and XANES*. Chemical Analysis v. 92, Wiley, New York, pp 573-662.

Bodoglio, G., Offermann, P, DePlano, A., and Lazzari, G.P. (1988) Influence of groundwater composition on glass leaching and actinide speciation. In: M.J. Apted

and R.E. Westerman (eds.), *Scientific Basis for Nuclear Waste Management XI*. Mat. Res. Soc. Symp. Proc. v. 112, pp 621-630.

Bonnin-Mosbah, M., Simionovici, A.S., Metrich, N., Duraud, J.P., Massare, D., and Dillmann, P. (2001) Iron oxidation states in silicate glass fragments and glass inclusions with a XANES micro-probe. J. Non-Crystal. Solids, v. 288, pp 103-113.

Borg, I.Y. (1975) Radioactivity trapped in melt produced by a nuclear explosion. Nuclear Technology, v. 26, pp 88-100.

Brown, G.E., Jr., Calas, G., Waychunas, G.A., and Petiau, J. (1988) X-ray absorption spectroscopy and its applications in mineralogy and geochemistry. In: F.C. Hawthorne (ed.), *Spectroscopic Methods in Mineralogy and Geology*. Mineralogical Society of America, Reviews in Mineralogy v. 18, pp 431-512.

Broxton, D.E., Warren, R.G., Byers, F.M., and Scott, R.B. (1989) Chemical and mineralogic trends within the Timber Mountain–Oasis Valley caldera complex, Nevada: Evidence for multiple cycles of chemical evolution in a long-lived silicic magma system. J. Geophys. Res., v. 94, pp 5961-5985.

Calas, G. (1979) Etude expérimentale du comportement de l'uranium dans les magmas: états d'oxydation et coordinance. Geochim. Cosmochim. Acta, v. 43, pp 1521-1531.

Choppin, G.R., Bond, A.H., and Hromadka, P.M. (1997) Redox speciation of plutonium. J. Radioanal. Nucl. Chem., v. 219, pp 203-210.

Dozol, M., and Hagemann, R. (1993) Radionuclide migration in groundwaters: Review of the behavior of actinides. Pure & Appl. Chem., v. 65, pp 1081-1102.

Duffy, J.A. (1999) Stability of metal ions in molten glass: The definition of reduction and oxidation. Phys. Chem. Glasses, v. 40, pp 54-56.

Eller, P.G., Jarvinen, G.D., Purson, J.D., Penneman, R.A., Ryan, R.R., Lytle, F.W., and Greegor, R.B. (1985) Actinide valences in borosilicate glass. Radiochim. Acta, v. 39, pp 17-22.

Farges, F., Ponader, C.W., Calas, G., and Brown, G.E., Jr. (1992) Structural environments of incompatible elements in silicate glass / melt systems: II. U^{IV}, U^{V}, and U^{VI}. Geochim. Cosmochim. Acta, v. 56, pp 4205-4220.

Glenn, G.L., and Dodd, C.G. (1968) Use of molecular orbital theory to interpret x-ray K-absorption spectral data. J. Appl. Phys., v. 39, pp 5372-5377.

Grenthe, I., Stumm, W., Laaksuharju, M., Nilsson, A.C., and Wikberg, P. (1992) Redox potentials and redox reactions in deep groundwater systems. Chemical Geology, v. 98, pp 131-150.

Hess, N.J., Weber, W.J., and Conradson, S.D. (1998) X-ray absorption fine structure of aged, Pu-doped glass and ceramic waste forms. J. Nuclear Materials, v. 254, pp 175-184.

Inagaki, Y., Sakata, H., Furuya, H., Idemitsu, K., Arima, T., Banba, T., Maeda, S., Matsumoto, Y., Tamura, Y., and Kikkawa, S. (1998) Effects of water redox conditions and presence of magnetite on leaching of Pu and Np from HLW glass. In: I.G. McKinley and C. McCombie (eds.), *Scientific Basis for Nuclear Waste Management XXI*. Mat. Res. Soc. Symp. Proc. v. 506, pp 177-184.

Jantzen, C.M., and Bibler, N.E. (1985) The role of groundwater oxidation potential and radiolysis on waste glass performance in crystalline repository environments. In: L.O. Werme (ed.), *Scientific Basis for Nuclear Waste Management IX*. Mat. Res. Soc. Symp. Proc. v. 50, pp 219-229.

Karraker, D.G. (1982) Actinide valences in borosilicate glass. J. Amer. Ceramic Soc., v. 65, pp 53-55.

Kim, J.I. (1986) Chemical behavior of transuranic elements in natural aquatic systems. In: A.J. Freeman and C. Keller (eds.), *Handbook on the Physics and Chemistry of the Actinides*, vol. 4. Elsevier, Amsterdam, pp 413-455.

Morss, L.R., Lewis, M.A., Richmann, M.K., and Lexa, D. (2000) Cerium, uranium, and plutonium behavior in glass-bonded sodalite, a ceramic nuclear waste form. J. Alloys Compounds, v. 303, pp42-48.

Murata, T. (1991) Synchrotron radiation for structure analysis – EXAFS and XANES. Mikrochim. Acta, v. 2, pp 435-444.

Paul, A. (1990) Oxidation-reduction equilibrium in glass. J. Non-Crystal. Solids, v. 123, pp 354-362.

Pawloski, G.A., Tompson, A.F.B., and Carle, S.F. (2001) Evaluation of the hydrologic source term from underground nuclear tests on Pahute Mesa at the Nevada Test Site: The Cheshire test. Lawrence Livermore National Laboratory report, in preparation.

Petit, P.E., Farges, F., Wilke, M., and Sole, V.A. (2001) Determination of the iron oxidation state in earth materials using XANES pre-edge information. J. Synchrotron Radiation, v. 8, pp 952-954.

Rose, T.P., Pawloski, G.A., and Smith, D.K. (2000) Environmentally closed nuclear test cavity-chimney systems: Evidence and controlling factors. Lawrence Livermore National Laboratory, unpublished report prepared for the U.S. Department of Energy, Nevada Operations Office, Environmental Restoration Division, September 2000, 31 p.

Schreiber, H.D. (1983) The chemistry of uranium in glass-forming aluminosilicate melts. J. Less-Common Metals, v. 91, pp 129-147.

Schreiber, H.D., Carpenter, B.E., Eckenrode, J.P., and Balazs, G.B. (1985) The chemistry of uranium in borosilicate glasses. Part 5. The ferric-ferrous couple as a redox buffer for the uranium redox state distribution against reducing agents in a borosilicate melt. Phys. Chem. Glasses, v. 26, pp 24-30.

Schwartz, L., Piwinskii, A., Ryerson, F., Tewes, H., and Beiriger, W. (1984) Glass produced by underground nuclear explosions. J. Non-Crystal. Solids, v. 67, pp 559-591.

Silva, R.J., and Nitsche, H. (1995) Actinide environmental chemistry. Radiochim. Acta, v. 70/71, pp 377-396.

Stumm, W., and Morgan, J.J. (1996) *Aquatic Chemistry, Third Edition*. Wiley, New York, 1022 p.

Tossell, J.A., and Sághi-Szabó, G. (1997) Aluminosilicate and borosilicate single 4-rings: Effects of counterions and water on structure, stability, and spectra. Geochim. Cosmochim. Acta, 61, pp 1171-1179.

Wilke, M., Farges, F., Petit, P.E., Brown, G.E., Jr., and Martin, F. (2001) Oxidation state and coordination of Fe in minerals: An Fe *K*-XANES spectroscopic study. Amer. Mineral., v. 86, pp 714-730.

Winick, H. and Doniach, S. (1980) *Synchrotron Radiation Research*. Plenum Press, New York, 680 p.

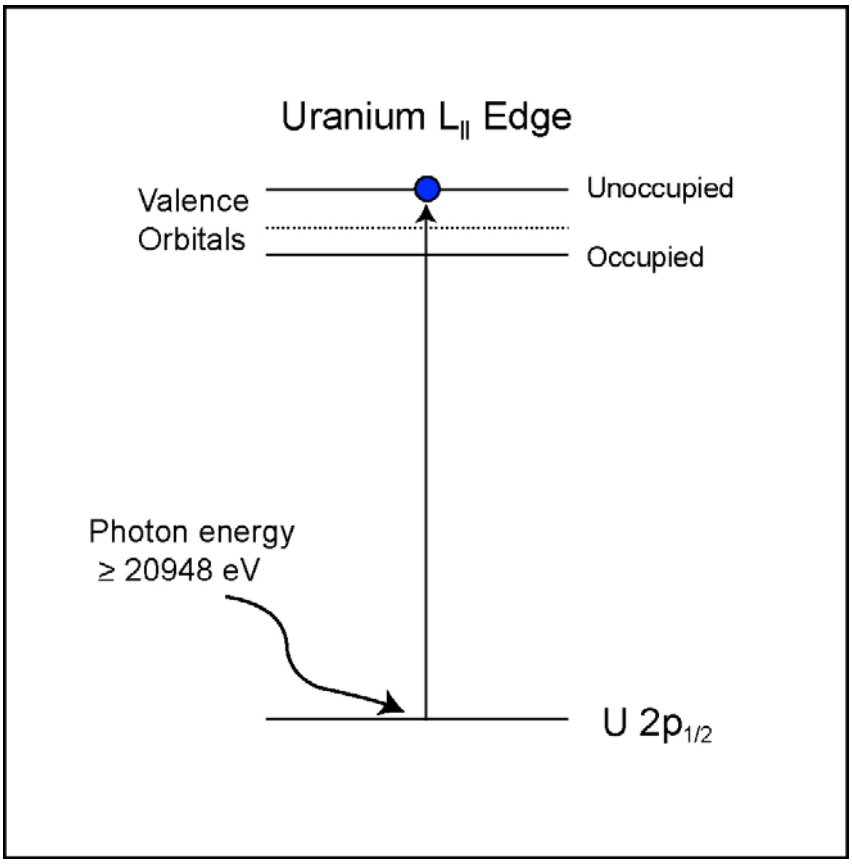

Figure 1. Energy-level diagram of the X-ray absorption process. Near the absorption threshold, a core-level (U $2p_{1/2}$ or Fe 1s) electron absorbs the energy from an incoming X-ray and is promoted to an unoccupied valence orbital of the same atom. By varying the incoming X-ray photon energy, unoccupied states of differing energy can be probed and an X-ray absorption near-edge structure (XANES) spectrum is collected. The unoccupied states, and the XANES spectrum, are sensitive to the oxidation state and local bonding environment of the absorbing atom.

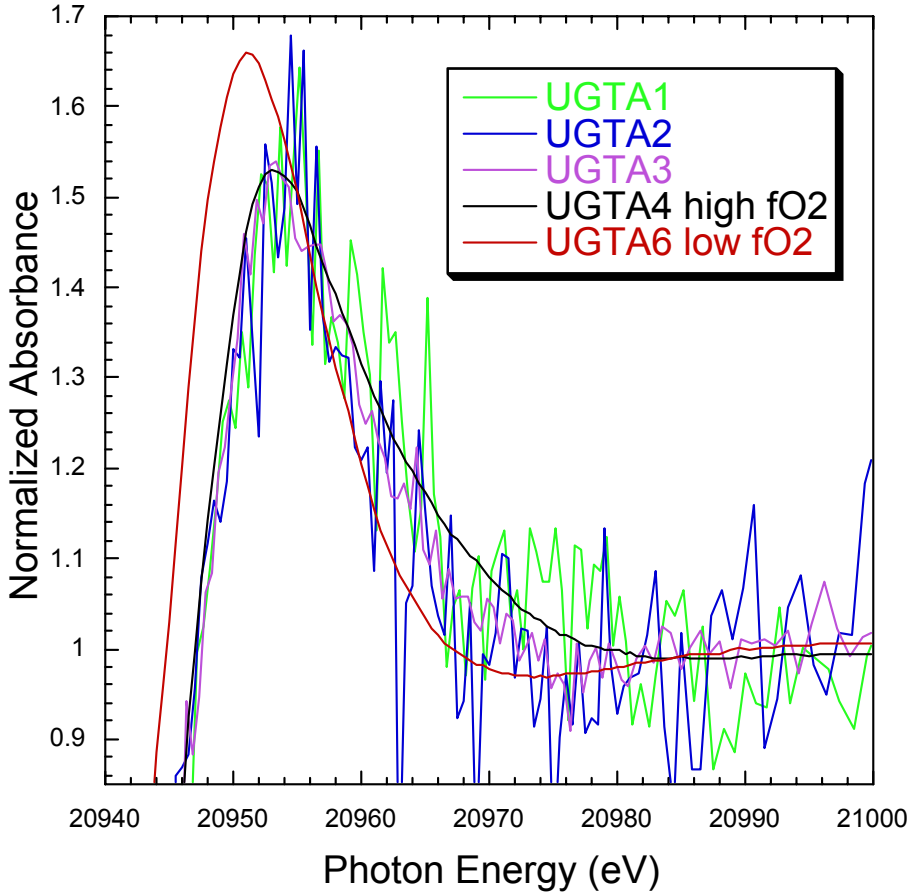

Figure 2. U L_{II} XANES spectra for three nuclear melt glasses (UGTA1-UGTA3) and high and low oxygen fugacity reference glasses (UGTA4 and UGTA6 respectively). The absorption edges of all three melt glasses match the high oxygen fugacity glass. The low oxygen fugacity glass is in the U^{4+} oxidation state.

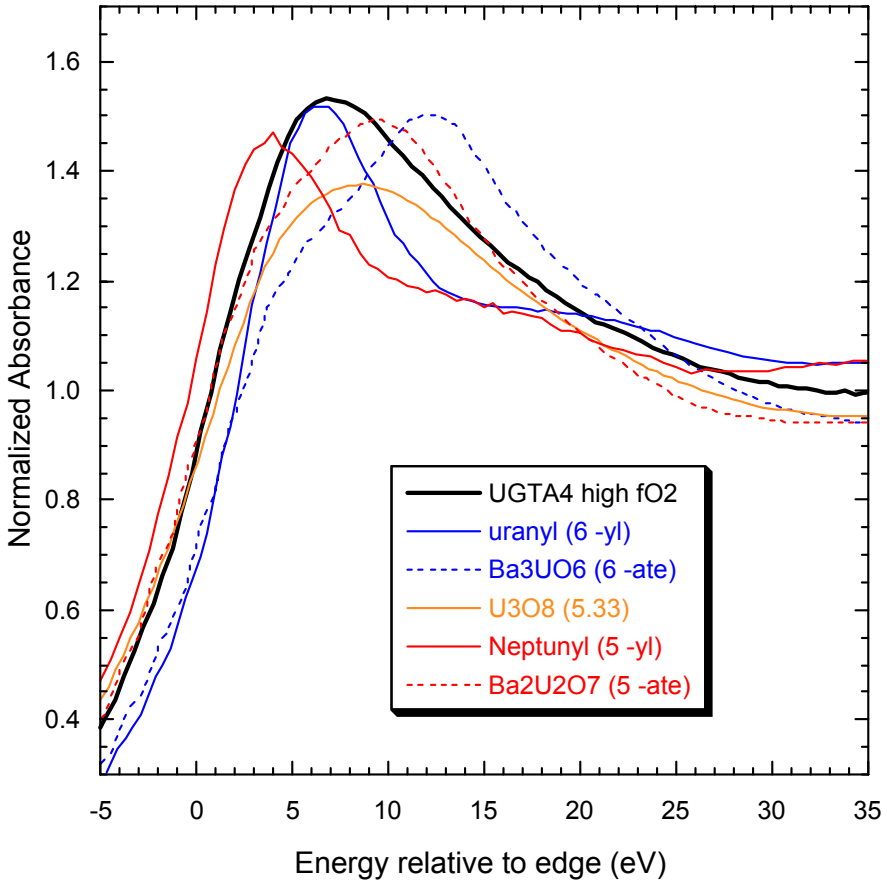

Figure 3. XANES spectra for the high oxygen fugacity reference glass (UGTA4) compared to uranium in the U^{5+} and U^{6+} oxidation states and different coordination geometries. The actinyl(V) standard was taken from a NpO_2^+(aq) solution. All XANES are referenced to the edge position for their corresponding dioxide (UO_2 or NpO_2). The XANES spectra for the nuclear melt glasses (UGTA1-UGTA3) match that of the reference glass (UGTA4), but have been omitted for clarity. The shift of the leading edge of the reference glass XANES to the left of both U^{6+} standards indicates a U^{5+}/U^{6+} oxidation state mixture in the nuclear melt glasses and high oxygen fugacity reference glass.

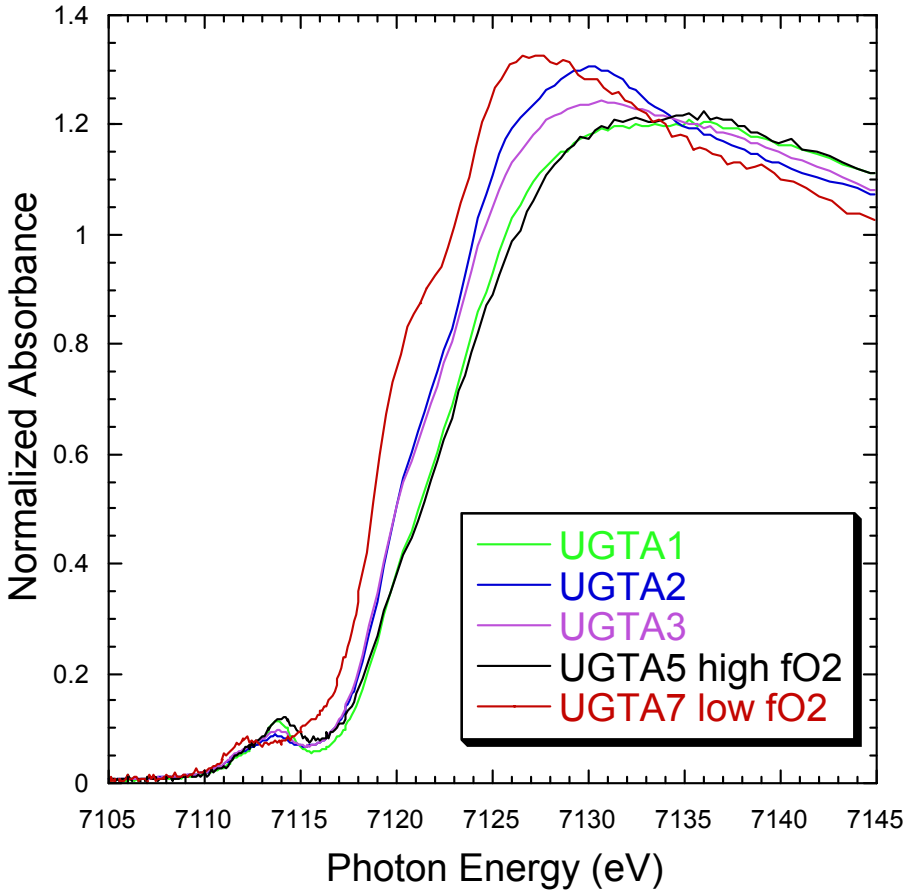

Figure 4. Fe K edge XANES spectra for three nuclear melt glasses (UGTA1-UGTA3) and high and low oxygen fugacity reference glasses (UGTA5 and UGTA7 respectively). The high fugacity reference glass has an oxidation state close to that of Fe_3O_4 (+2.7) while the low fugacity reference glass is close to the Fe^{2+} oxidation state. The iron oxidation state of each melt glass is between those of the reference glasses and scales with the absorption edge energy.

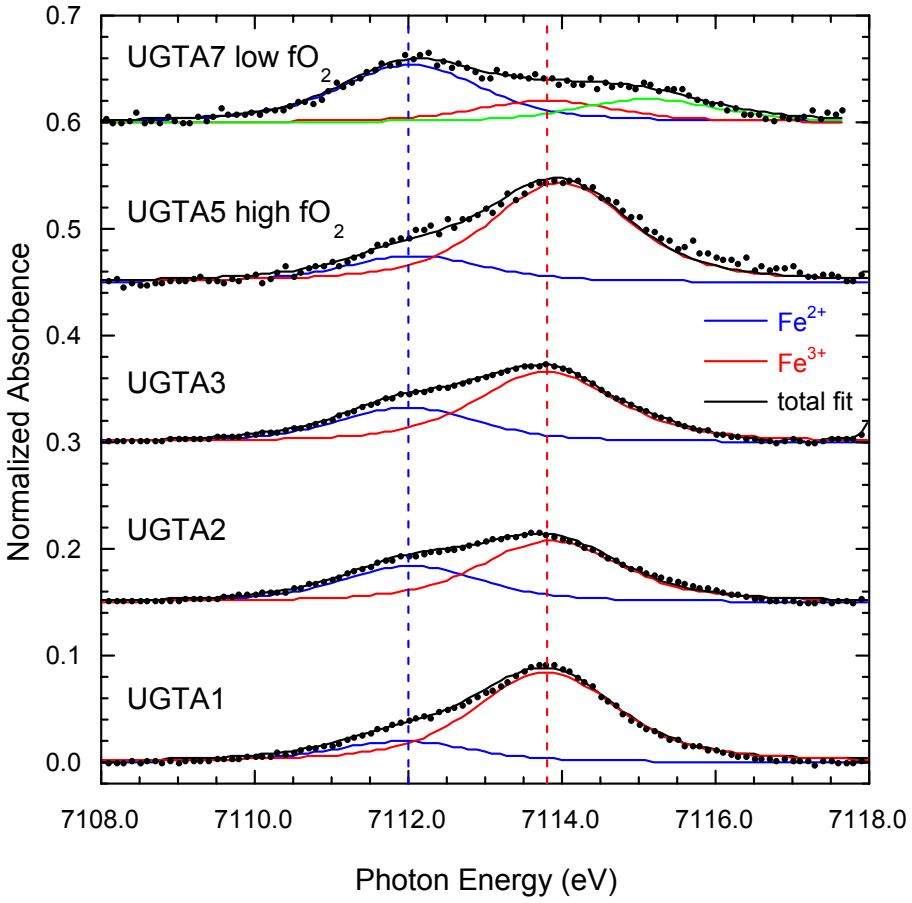

Figure 5. Fits to the pre-edge region of the Fe K edge data for the three nuclear melt glasses (UGTA1-UGTA3) and high and low oxygen fugacity reference glasses (UGTA5 and UGTA7 respectively). The pre-edge background was subtracted using a sum of arctangent and error functions, and the two peaks are Voigt functions of total width 2.2 eV. The peaks at 7112.0 eV and 7113.8 eV correspond to Fe in the Fe^{2+} and Fe^{3+} oxidation states, respectively.

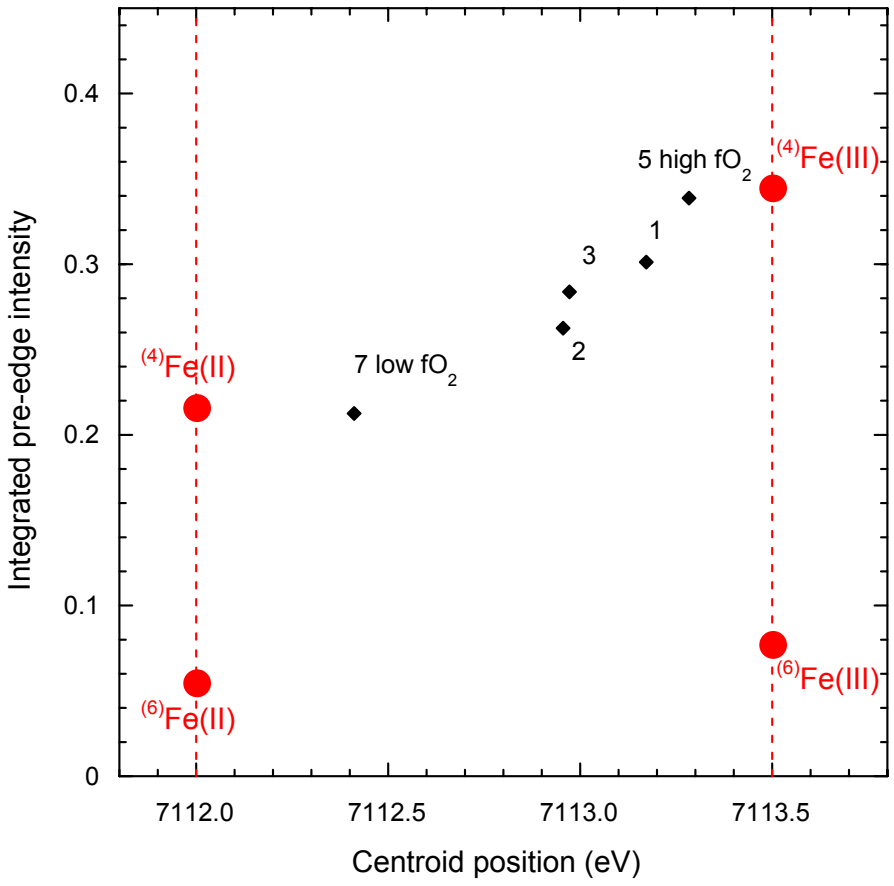

Figure 6. Integrated pre-edge intensity versus centroid (area-weighted average energy position) of the two peaks in the pre-edge feature of the Fe K edge, for the three nuclear melt glasses (UGTA1-UGTA3) and high and low oxygen fugacity reference glasses (UGTA5 and UGTA7 respectively). Also plotted are the tetrahedral and octahedral Fe^{2+} and Fe^{3+} endpoints as determined by Wilke et al. (2001). All glasses appear on the line between tetrahedral $^{(4)}Fe^{2+}$ and tetrahedral $^{(4)}Fe^{3+}$. From the relative positions of the glasses' data points along this line, the Fe^{2+} and Fe^{3+} populations in the glasses are determined.

Chapter 5

α-Autoradiography: A Simple Method to Monitor the Migration of α-Emitters in the Environment

Carola A. Laue and David K. Smith

Abstract

Environments contaminated with α-emitters (mostly actinides) represent a serious hazards to humans and nature. Current technologies to monitor and remediate areas contaminated with α-emitters are often hindered by our limited understanding of the actinide fate and transport behavior in those environments. Here we demonstrate how the well-established simple technique of α-autoradiography can be deployed in a field setting to enhance our understanding of actinide transport, to determine the spatial distribution of actinides in soils, and to help identify the morphology of the association of actinides with soil constituents. Preliminary conclusions are drawn relative to controls that govern the fate and transport of actinides that were deposited more than 40 years ago in the semi-arid soils of the Nevada Test Site. Our experimental data clearly indicate that actinides move through desert soils. This observation contradicts previous assumptions that actinides are relatively immobile and remain within the very top soil layer. We were able to demonstrate that the designed tool can be applied for screening in monitoring and remediation efforts.

Introduction

The existence of α-emitters in our natural environment is a result of both natural and of anthropogenic factors. Of major concern to the public are the lower actinide elements such as uranium, plutonium and americium, all of which can be found as low-level background throughout the world today. This background distribution of actinide elements has several anthropogenic sources including global and local fallout from atmospheric weapons testing, reentry of space equipment powered by plutonium heat sources, accidental releases from fuel production and reprocessing, nuclear power generation and other military applications.

The Fate and Transport of Actinide

The fate and transport of the actinide elements has become a major concern at contaminated U.S. Department of Energy nSite, the Hanford Reservation, and at the Nevada Test Site (NTS). Reasons for increased concern are motivated by path-to-closure remediation efforts of DOE complexes and originate in the toxicity and radioactivity of actinides. Although the toxic properties are comparable to other heavy metals including lead and mercury, the tissue damaging properties of their radioactivity, distinguish the actinides from heavy metals. Actinide-bearing aerosols pose serious health risks (Shinn &

Homan, 1985), as they can be directly inhaled or be deposited on food plants. Equally hazardous is the transport of actinides through the soil, creating a pathway to either enter water sources or to accumulate in food plants. Those concerns were already recognized in the mid-1970s by the Nevada Applied Ecology Group (NAEG). Extensive studies (White & Dunaway, 1975; White et al., 1977; Hanson, 1980) have been performed investigating the resuspension of actinide and fission products and their potential pathways to human ingestion. Results from studies on the distribution of actinide in soils yielded the controversial conclusion that actinides are relatively immobile. The NAEG results showed that after an initial fast movement of the actinide within the top layer of the soil, the infiltration of the actinides stopped and did not change over the course of 20 years (Essington et al, 1976; Shinn et al., 1993). Recent studies (Kersting, et al., 1999) of an aquifer at the NTS, which is in contact with a test cavity indicate that plutonium can move in a saturated groundwater system. In a nuclear test cavity the actinides were thought to be incorporated in the melt glass formed after a nuclear detonation, and thereby, to be immobilized. Aside from the geology and weathering that occurs in the environment, the chemical nature of the contamination source strongly affects the fate and transport of the contaminant. One of our objectives was to investigate geochemical controls on actinide movement in desert soils. To accomplish this goal, a technique had to be devised that would allow us to study in-situ the range of actinide transport, the spatial distribution of the actinides in soils, and the morphology of the actinide association to soil constituents.

α-Autoradiography

α-Autoradiography, our technique of choice, relies on the actinide decay properties to visualize their spatial distribution. This simple and proven technique has been known for as long as radioactivity itself. The radiation creates latent tracks through its damaging interaction with the detector material, which is treated chemically to reveal the tracks after the exposure. In fact, Becquerel discovered simultaneously radioactivity and radiography by accidentally misplacing his photographic plates on a uranium mineral (Bequerel, 1896). Kinoshita (1910) observed the first α-particle tracks induced in commercial photographic emulsion in 1910. Nuclear emulsions are now widely used in the nuclear chemistry and physics (Fleisher, et al., 1975). After the discovery of tracks in dielectric solids, solid state nuclear track detectors (SSNTD) soon outcompeted emulsions for reasons including: ease of handling, transportability into remote and/or difficult to access areas, independence of any electronic equipment, speed of obtaining results, visualization of the results, possibility to automate track analysis, and their low cost. Common SSNTD materials are glass, mica, and several plastic materials. The most widely used plastic is CR-39, a polymer of polyallyl diglycol carbonate, which was also utilized in our study. CR-39 (Cartwright, et al., 1978) responds uniform with less than 1% variation; a high sensitivity toward 1 MeV protons, 6 MeV alphas, and minimum-ionizing iron; and a superb optical quality making CR-39 ideal for identification of mass and charge of nuclear particles. Several studies (Vapirev, et all, 1990; Akopova, et al., 1993) have investigated the distribution of radioactive contaminants and transport mechanism of radioactive particulates in the environment using radiographic methods,

but only one study (Espinosa & Silva, 1995) applied radiography for in-situ soil characterization.

Nevada Test Site and Pertinent NAEG Results

The NTS is a 3,561 km^2 vast desert area 105 kilometers north west of Las Vegas (see Figure 2). Atmospheric tests and safety experiment tests (SET) with non-critical or partial yield of nuclear weapons were performed at NTS. SETs involving a detonation of nuclear weapons by conventional explosives also have been done to assess the impacts of such terror attacts. As a result, extensive surfacial actinide contamination occurred, which was thoroughly characterized immediately after testing; during the NAEG program in the 1970's (White & Dunaway, 1975, Essington, et al., 1976; White, et al, 1977; Hanson, 1980; Shinn & Homan, 1985; Shinn, et al., 1993); and through ongoing efforts of the long-term stewardship program. In addition, the geological, hydrological, and weathering characteristics of the semi-arid environment at the NTS was well studied as part of U.S. nuclear testing efforts (Borg, et al., 1976). Partial data from extensive NAEG studies pertaining to our investigation are summarized in Table 1. The areas selected hosted SETs conducted at the surface resulting in dispersal of actinide material.

The NAEG investigations document that in locations where the safety tests had a slight nuclear yield, the particles bearing the majority of the actinides are a silicate based material and are so large as to not be susceptible to resuspension. In locations where the

Table 1. Summary NAEG investigation results documenting actinide occurrence in NTS surficial soils (Gilbert, et al., 1988).

	Area 18 NS 201	**Area 18 NS 219**	**Area 13**	**Area 11**
Type of test	Safety w/ slight nuclear yield	Safety w/ slight nuclear yield	Safety	Safety
Documented type of actinide occurrence	Spherical glass or glass coated	Sponge-like highly porous, very fragile silicate glass	High density oxide particle	*
Particle size fraction w/ highest actinide conc.	0.1 to 2 mm	2-50 mm	20-50μm	*
Resuspendable particle fraction bearing actinides (% of particles < 0.1 mm in Ø)	5	13	98	*
Depth with majority of actinide load in cm	top 5	top 5	top 2.5	top 2.5

* No information available

safety tests had no nuclear yield, the hot particles are extremely small, highly sintered actinide oxide particles. These differences result in variations in resuspension and migration behavior. The actinide contamination, which was measured directly after the safety tests, was found to be in the uppermost soil layer in the Areas 11 and 13. Twenty years later, NAEG studies determined that the actinides were mostly concentrated at a soil depth of 2.5 cm, but also found measurable amounts at depths of 25 cm. The vertical profile of the actinide contamination in Area 18, however, did not change with time indicating a strong correlation between source properties and transport behavior.

The objective of our investigation was to design and deploy a simple in-situ screening tool for α-emitting contaminants in soils. The spatial distribution of actinides in soils was of particular interest because actinide depth profiling allows us to evaluate the actinide fate and transport in desert environments. This in-situ technique was also developed due to its potential to support remedial actions that may be required in the future.

Experimental Work

Design of the in-situ soil exposure of CR-39 detectors to α-emitters

The design of the tool used to expose CR-39 track detectors to the soil column in the field was critical for our work. Features to minimize the soil disturbances, to avoid the cross contamination by transporting radioactive particulates downward while inserting the tool, and to protect the CR-39 from scratches that significantly decrease detector sensitivity, were incorporated into the design.

A schematic of the in-situ exposure tool is provided in Figure 1. The actual dimensions of the tool are: 1 cm thick steel backing, 74 cm long, and 6 cm wide. As Figure 1 shows, the tool was constructed with a track to fix the detectors in place and to hold a removable shield in front of the detectors to avoid scratches during the emplacement in the ground.

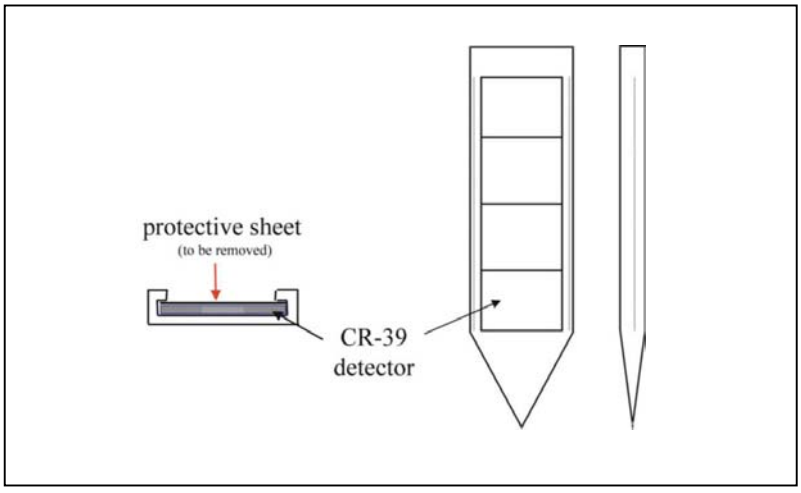

Figure 1. Schematic drawing of the exposure tool, designed and employed. Drawing is not to scale.

The CR-39 is a high quality SSNTD (TASTRAK™) obtained from Track Analysis System, Ltd. in Bristol, UK, 50x50x1 mm in dimension, each plate having a unique ID number engraved. The actual detector area exposed to the soil column is 46 mm wide and a maximum of 60 cm deep. The detectors were placed in sequential order and fixed in place by double sided tape.

CR-39 etching and evaluation procedure

Based on conventional etching procedures (Bondarenko, et al., 1996; Laue, 1996), a 6 mol/L sodium hydroxide etch solution was heated and kept constant at 73°C in a water bath. During the etch process of 6 hours, the etch solution was stirred. The detectors, removed from exposure tool and transported from field site to our lab, were placed in the etch solution in a holder that spaced them vertically 1 cm apart. The etch process was stopped by rinsing the detectors several times with distilled water. An optical microscope equipped with a digital camera was used to examine the radiographic detectors.

Field Site: Plutonium Valley, NTS

Plutonium Valley in Area 11 of the NTS was the location of four SETs in the mid-1950's, which contaminated the surface soils with uranium, plutonium and americium. Site D in Area 11 was selected in our study because the site had been previously studied by the NAEG. Area 11 offers the benefit of being secured and secluded (see its location in Figure 2) with disturbances to the desert soil limited to natural weathering processes and native animal activities subsequent to the last recorded soil suspension studies (Shinn & Homan, 1985) and contamination surveys (Gilbert, 1977; DOE, 1991; Hendricks & Riedhauer, 1999). Although actinide particulate partitioning had not been investigated here as for Area 13 and 18, substantial information regarding the contaminants exists (White & Dunaway, 1975; Essington, et al., 1976; Gilbert, 1977; White, et al., 1977, Hanson, 1980; Shinn & Homan, 1985; Gilbert, et al., 1988; Shinn et al., 1989; DOE, 1991; Shinn, et al, 1993; Hendricks & Riedhauer, 1999). The references detail locations of those earlier studies, which enabled us to avoid areas with disturbed soil profiles. Shinn et al. (Shinn, et al., 1989; Shinn, et al., 1993) published data based on NAEG studies on the vertical distribution of ^{239}Pu at Site D in 1993: in 1973, 99% of ^{239}Pu was located in the top 1.25 cm, while in 1981, 98.4% of the ^{239}Pu was in the top 7.5 cm of soil, and 1% was detected between 7.5 to 15 cm. However, the data from 1973 are based on chemical measurements, while the data from 1981 are based on γ-spectrometry, measuring ^{241}Am, and determining ^{239}Pu by a fixed ratio of ^{241}Am to ^{239}Pu of 1 to 7 (Romney, et al., 1976; Shinn, et al., 1989). Results described in (Essington, et al., 1976) question the reliability of the fixed ^{241}Am to ^{239}Pu ratio to determine plutonium in soils as applied be measurements via the americium γ-activity. Americium, a trivalent cation, was observed to behave differently in soils than plutonium, which occurs as oxide, tetravalent cation or pentavalent plutonyl ion, and hence, obeys a different chemistry than americium. Earlier contamination surveys and later demarcation efforts (Hendricks & Riedhauer, 1999) provided valuable information on the levels of contamination such as obtained by the 1994 aerial radiation survey measuring the ^{241}Am count rate per second for Plutonium Valley as shown in Figure 3, with Site D enlarged.

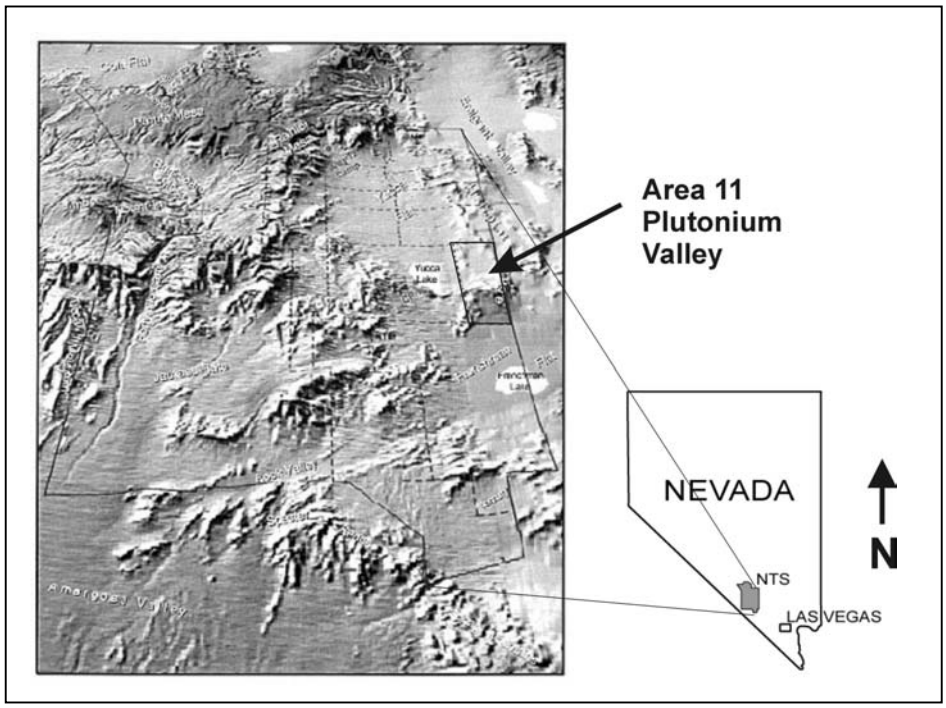

Figure 2. Topographic Map of NTS with superimposed area grid, Area 11 highlighted, showing NTSs location in Nevada. U.S. DOE Photograph (Townsend & Grossman, 2000).

Field Exposure Experiments

Two in-situ exposure experiments were performed in October and December 2001. The exposure locations are labeled 1 through 5 in Figure 3C. After inserting the in-situ detector device into the ground using a field hammer, the detector protector sheet was carefully removed to avoid moving soil particulates up with the protector sheet. The in-situ detector device was covered to prevent rainwater from channeling down the surface of the detectors during the exposure. The exposure (St #1) in October lasted for 35 days. The analysis of the first set of detectors indicated that the ambient activity levels might result in overexposure.

Hence, in December, the second set of in-situ experiments (St #2-5) were exposed to the soils for only two weeks. Table 2 summarizes the experimental parameters for each in-situ exposure. The distances of the exposure locations to ground zero of Site D range from 70 to 200 m. A manual survey with a fidler (NaI) gamma-ray probe provided an indication of the surface contamination at each location. “Characteristics” describes the susceptibility to wind erosion or to trapping of suspended particles, as observed in areas sheltered by rooted sage brush. The retrieval of the exposure tool was performed in a manner that avoided scratching of the detector material.

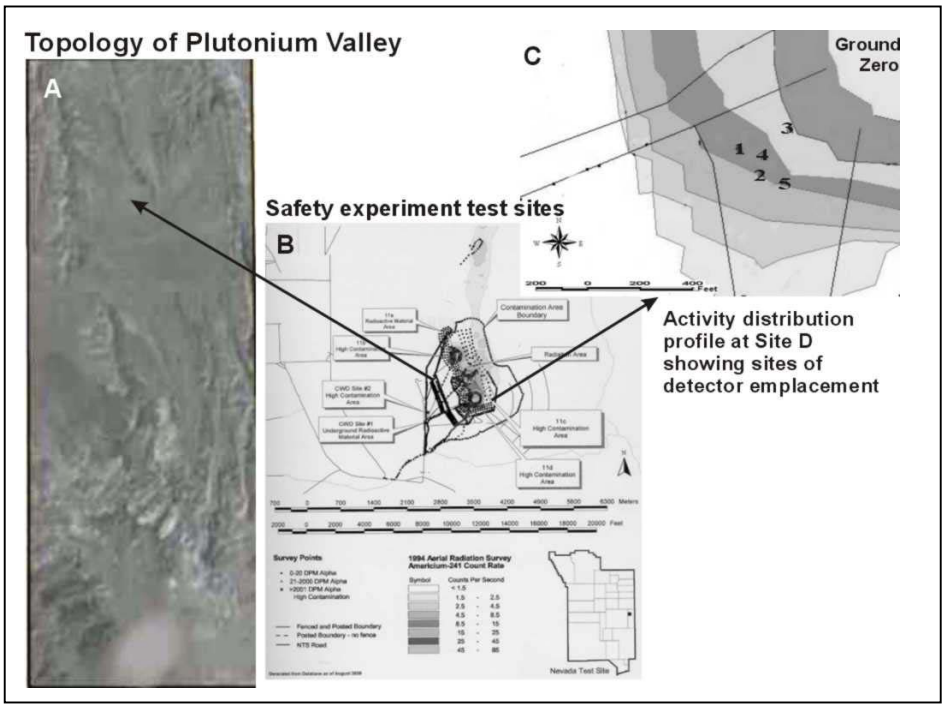

Figure 3. Plutonium Valley detailed: A) a topographical map identifying the SET sites;B) an activity level map of the SET sites as determined by 1994 arial gamma-ray survey (Hendricks & Riedhauer, 1999); and C) our experimental site, Site D, indicating activity levels and detector deployment sites (White & Dunaway, 1975; Essington, et al., 1976; White, et al., 1977; Hanson, 1980; Shinn & Homan, 1985).

Table 2. Experimental parameter of in-situ exposures of CR-39 detectors to soils in Plutonium Valley at the NTS, NV performed in 2001.

ID	Duration	Exposure Depth	Experiment Location GPS coordinates	Fidler (NaI) reading, Dpm	Characteristics of Location
St #1	35 days	39 cm	N36°58'233" W115°57'409"	10^5	among sage brush, rain had wetted soil 15 cm deep
St #2	14 days	37.5 cm	N36°58'222" W115°57'395"	3×10^4	desert pavement
St #3	14 days	24 cm	N36°58'244" W115°57'376"	5×10^4	among sage brush
St #4	14 days	17.75 cm	N36°58'230" W115°57'393"	8×10^3	desert pavement water exposure
St #5	14 days	23 cm	N36°58'216" W115°57'380"	2×10^4	among sage brush

Observations and Discussion

Photographs of the etched CR-39 detectors as shown in Figures 4, 5, and 6 illustrate the distribution of the α-contamination in the soils studied. Points of concentrated α-activity (hereafter called 'hot spots') can be seen as white spots in the photographs of the detector plates in Figures 5 and 6. Evenly distributed α-tracks, random in their orientation, indicate evenly distributed α-emitters, which are observed but can only be seen using optical magnification. Hot spots are distinguishable by their generated α-tracks arrangement. In Figure 4, a schematic and several examples for the structure of hot spots as observed are shown. The center of a hot spot has perfect circular tracks but if the track density is too high the structure is erased. With increasing radial distance from the center, the tracks become more ellipsoidal with a larger diameter at the center side caused by the decreasing impact angle of the α–particle hitting the detector. The center size of a star-like structure is directly related to the size of the particle creating the hot spot, as snhown in the schematic in Figure 4. The track density observed is directly proportional to the activity and could be used as a measure for the in-situ radioactivity.

An observation, noted for all 5 exposures, is particularly conspicuous in experiment St #5: some very small hot spots have a high track density that erases the center structure and have nearly no surrounding ellipsoidal tracks (Fig.4c). Determining the size and nature of the particulates generating such small hot spots is speculative. However, such small hot spots with such high tracks density indicate the presense of particles that carry much higher activities than the larger particles generating the common star picture as shown in Figure 4a.

The composite picture of figure 5 shows clearly that α-emitting contamination has reached depths of at least 39 cm. The left and right column are photographs of the detector plates pasted together to resemble the actual arrangement during the in-situ exposure. Stake #1, left, reached a depth of 39 cm and Stake #2 a depth of 37.5 cm.

White spots are particularily frequent and visible in the 2^{nd} and 3^{rd} detector plates. The white spots are the previously described hot spots that are large enough to be seen by the human eye without magnification. The observed band of hot particles on the 2^{nd} and 3^{rd} detector, which can also be seen in the stakes shown in Figure 6, illustrates the region (4 to 20 cm) where currently most of the α-contamination exists. The photographs in the center section of Figure 5 show several examples of hot spots optically magnified and, for comparison, a section of the detector plate that was not exposed to the soil. Aside from the background photo, three photographs of hot spots from the major α-contamination zone are shown. The lower four photographs are magnifications of hot spots found at depth as low as 38 cm. The density of the randomly orientated tracks varies significantly for the different locations as well as for the different depths.

The detector plates of two other exposure experiments reveal a surprising activity distribution pattern. As in Figure 5, Figures 6 shows in the left and right columns the detector plates of the in-situ exposures for St #3 and St #5, as reference for the magnified

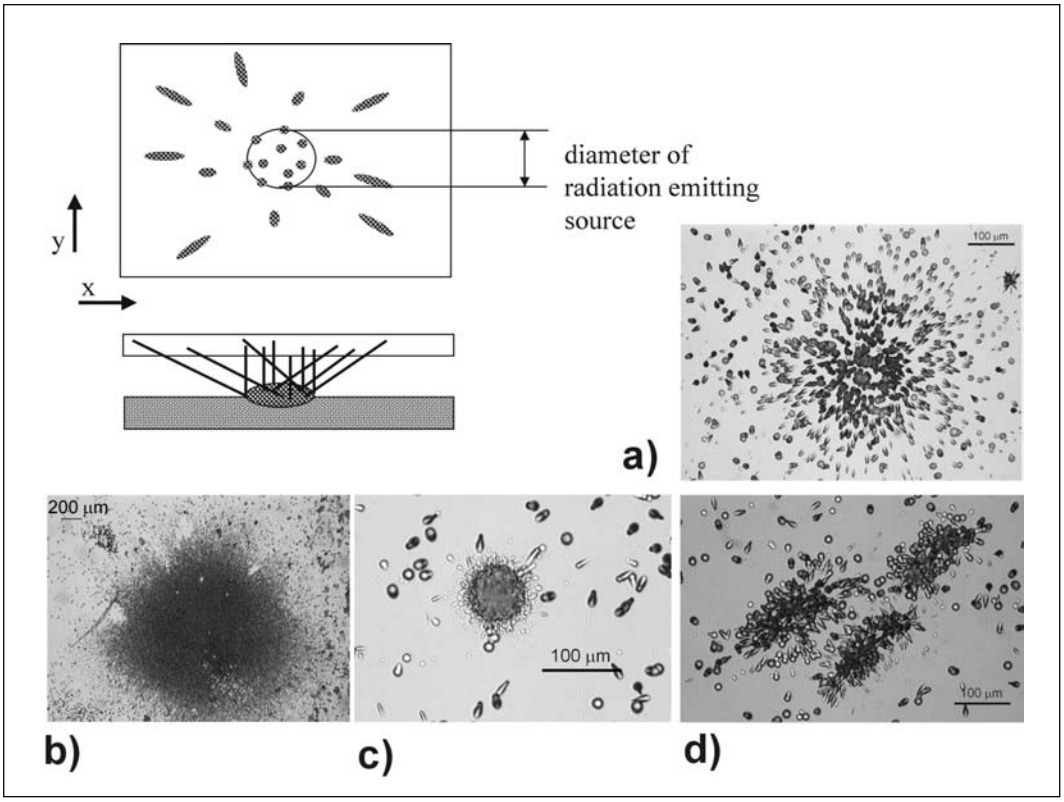

Figure 4. Schematic drawing of the radiographic process and photographic example images obtained in our experiments. a) Picture of a typical star-like structure generated by particles emitting α-radiation - circular tracks in the center that become more ellipsoidal with increasing distance to the center. b) Same star-like appearance, but the particle emitting the α's is much larger and has a much higher activity level (its location is indicated by a (*) in Fig. 6). c) Gun-shot like, very high track density that erases the center structure, no surrounding ellipsoidal tracks indicate a very small particle with exceedingly high activity. d) Rod shaped center surrounded by star-like ellipsoidal tracks is a newly observed accumulation of α-activity in soils (more detail in Fig. 6).

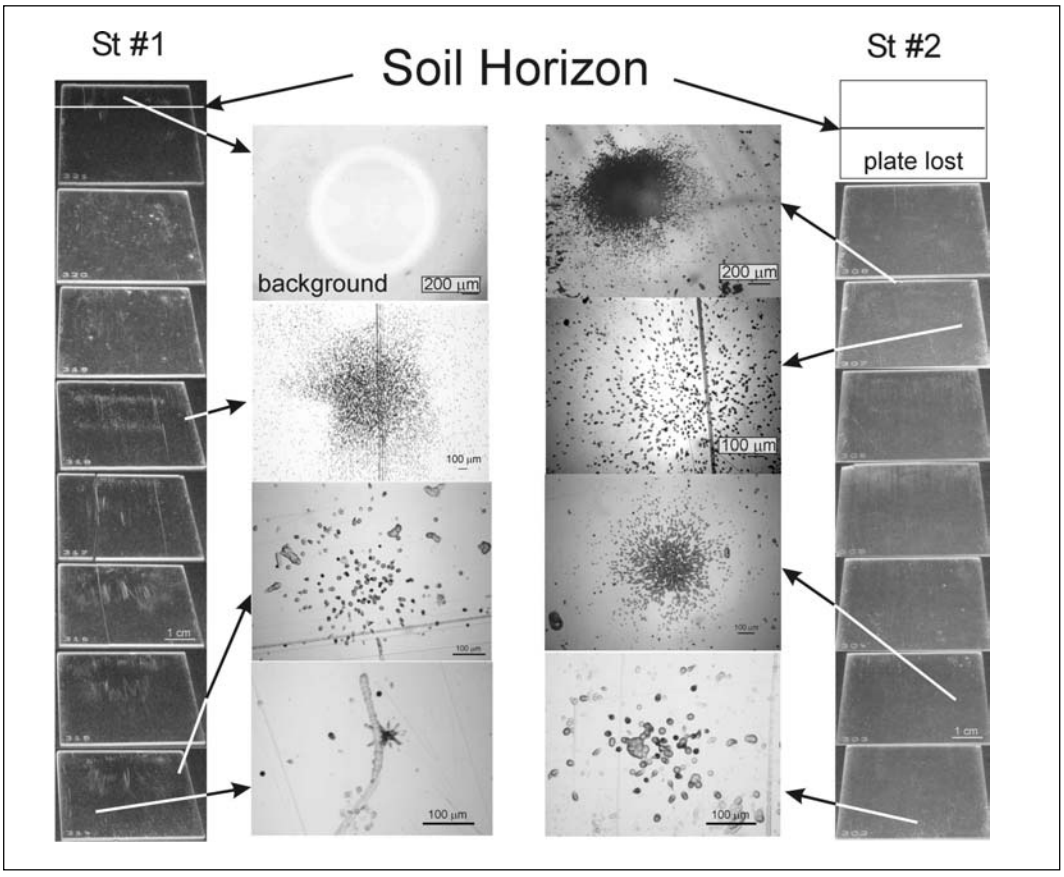

Figure 5. Left and right columns show photopgraphs of detector plates as emplaced in-situ. St #1 reached a depth of 39 cm and St #2, 37.75 cm. The white circular spots on the plates are hot spots large enough to be visible to the eye, but most are too small so that optical magnification is necessary for identification. Examples for α-active particulates detected at greater depths are provided. (the perpenticular streaks are due to handling)

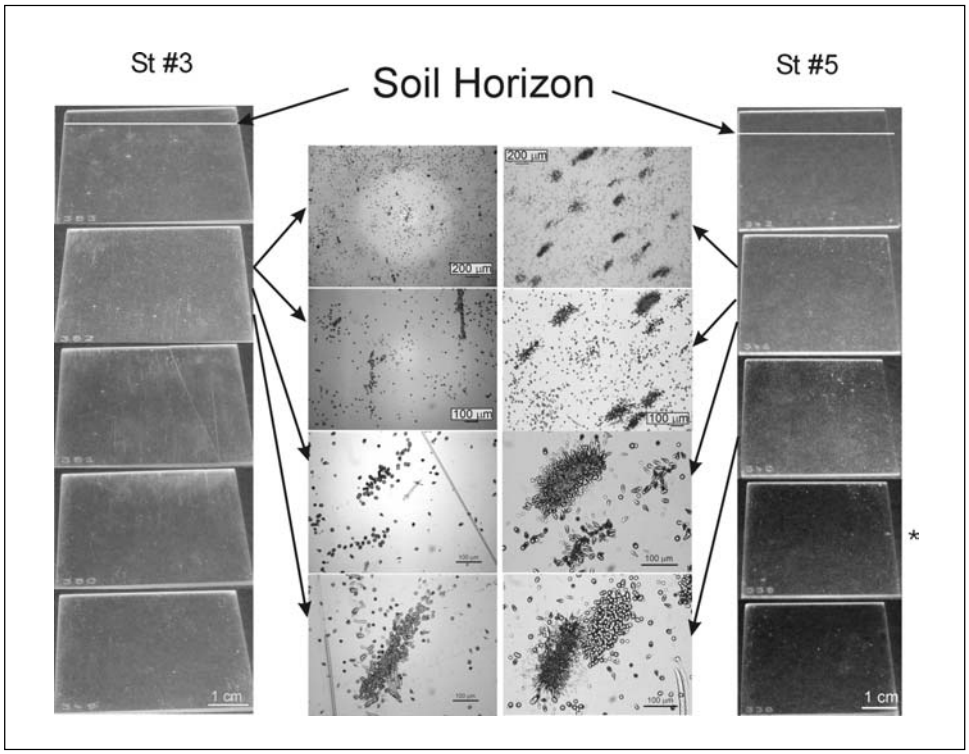

Figure 6. The left and right columns show photographs of St #3 & #5 detector plates, with maximum exposed depth of 24 and 23 cm, resp., both were in close proximity to sage brush. At depths below 5 cm an unsual but repetitive pattern of rod shape structures made of α-induced tracks is observed. Examples are pictured in appropriate magification in the center. The asterisk (*) indicates the particle that is magnified in Fig. 4.

photographs in the center. Although, as illustrated by the photos, the pattern is much more dominant in Stake #5, the same pattern is still observed in Stake #3. The obvious pattern is characterized by rod shaped structures that all seemed to be aligned, and have a center that is not circular but rather an oval that is surrounded by star-like tracks beams. The lengths and thicknesses of those apparent ovals vary. The shape could resemble that of a microbe, however, the size exceedes microbial dimensions. Another, more reasonable explanation for such a rod shape with inherent orientation is offered by the presence of very fine root hairs of the sagebrush that is native to the field site. Fine root hairs were noticed during our experiments at the field site and were also found in soil samples taken after the exposure tools were removed. The detectors of the experiments (St #3 & #5) had been placed between sagebrush, approximated 40 cm from the sagebrush stem.

This observation poses the question, whether sagebrush roots adsorb or even take up α-active nuclides? Which nuclides are adsorbed, and furthermore, if those nuclides are accumulated by the plant? This question has to be posed since α-radiography can not easily distinguish between different α-emitters, such as ^{241}Am and ^{239}Pu mostly of concern here. Another possibility could be that the plant and its root system behave as a

conduit for facilitating rapid transport of actinides and water. So far actinide uptake by plant material has been neglected due to the belief that the actinides ionic size, high valency, and oxy-ion structure make the actinides unfavorable for uptake in plant processes.

The 1994 aerial radiation survey, shown in Figure 3B, provides a valuable assessment tool of macroscopic scale, however, the survey does not and cannot reflect the microscopic vertical α-emitter profiling studied in the present investigation. The aerial contamination survey indicates a gradual decrease in contamination with increasing distance from the detonation center. In the enlarged section of Site D in Figure 3C our experimental locations are specified, demonstrating that in-situ exposures were performed in areas of different surface contamination according to the survey. The aerial survey accounts for the activity found on the surface only, while our technique can be used for determining the activity at the surface and also for depth profiling providing an additional dimension. Although we have not quantified our observations, we do observe that the macroscopic aerial survey is consistent with our microscopic screening assessment when we take only the top 5 mm of the exposed soils into account. At location #3 we find a much higher frequency of hotspots and overall track density (both measures of the activity) in the top 5mm of the soil than in any other location, as shown in the left and right columns of Figures 5 and 6, demonstrating the heterogeneity of the α-activity with depth. While for St #3 white spots are visible at the soil horizon, this is not the case for all other profiles. Noteworthy is the observation that in St #1 and St #5 a sudden apperance of hot spots with similar intensity as for St #3 is visible at ~4.5 cm and ~3 cm, respectively. Such observations were made by earlier NAEG studies, too, and where attributed to sand mound accumulation on top of the original soil surface among sagebrushes due to wind erosion. This shift in soil horizon could explain the sudden hot spot onset for the exposures St #1 and #5. This observation also illustrates the impact of the erosion processes on the depth profiling of the α-emitters.

Summary

By choosing a previously well-characterized field site, we were able to compare the vertical distribution of the actinides in the soil horizon with similar earlier investigations and draw conclusions on possible controls affecting the fate and transport of actinides in semi-arid desert environments. While large-scale surface survey maps are valuable assessment tools, the heterogeneities in the actinide distribution in the underlying surface profiles are not assessed by those surveys, and hence, yielding potentially incomplete contamination profiles. This techniques adds the third dimension to our understanding of actinide transport. In our field-deployed experiments, we found that α-emitting nuclides have moved to at least 39 cm in depth, far deeper than previously expected. We suggest that the α-active particulates found at that depth were transported by either, 1) the adsorption of the α-emitter to plant roots, which might be transported via translocation, 2) the plant-root systems that represents a conduit for facilitating the rapid transport of the α-active particulate, or 3) transport by successive sorption-desorption processes of the α-emitter on soil constitutents through rain water infiltration.

We observe different types of hot spots structures: star-like, rod-shaped, and gunshot-like hot spots without any structures. While the star-like structures are known, the other two were novel observations. The variety of observed hot spot structures can be explained through several formation modes of the particles that generate the hot spots. The larger, less active particles that generate the star-like structures are probably formed by adsorbing α-active nuclides, which can be mobilized by weathering processes, facilitating an actinide movement through soil by successive sorption-desorption steps. The rod-shaped structures are attributed to sorption of α-emitter to the surface of root hairs of the native sage brush. The very small and highly active particles are inducing gunshot-like structures, and are most likely finely dispersed plutonium metal or oxide particulates, that resulted from the weapon detonation initiated by conventional explosives. Possible pathways for moving those small highly active particles deeper in the soil are water induced channeling through cracks in the dry, hydrophobic desert soils, through translocation by the plant root systems, or animal activities. Those particle-size and adsorption specific processes as described explain the movement observed for the α-active contaminants to deeper layers as previously observed.

Our results not only demonstrate the utility of α-radiography to investigate the controls of the movement of actinides in desert soil, but also that this technique is simple, field-deployable, and can be applied for rapid, in-situ screening of α-contamination in upper soil layers. When comparing the efforts, the detector exposure time necessary and the subsequent etching procedure require less time than obtaining, processing, and analyzing numerous soil samples essential to achieve the same results by traditional wet chemical methods. Furthermore, this technique does not require transport and handling of radioactive material, and does not generate radioactive waste and minimizes human exposure due to soil disturbance. Field technicians can easily deploy and retrieve a network of detectors. Hence, we believe that this technique can be advantageously deployed, where α-activity contamination has to be rapidly assessed as part of an environmental remedial investigation or characterization.

Current and Future Work

Currently, we are analyzing the soil samples to establish a relationship between α-activity concentration, particle size, and composition of the α-activity bearing particles. The primary objective is to continue to identify the key factors that control the fate and transport of the actinides in semi-arid soils.

Acknowledgement

This work was performed under the auspices of the U. S. Department of Energy by the University of California, Lawrence Livermore National Laboratory under Contract No. W-7405-Eng-48, and funded by the Hydrologic Resources Management Resource Program of U.S. Department of Energy / National Nuclear Security Administration - Nevada Operations Office. We would have not been able to perform this work without the help of many colleagues at the Nevada Test Site: Jeff Haeberlin, Billy Hyatt, Don Felske, and CP Williams. Radiological control support in the field from Colleen Corlett and Ken Corville of Bechtel-Nevada was invaluable. Earl Kelly of LLNL's Engineering

Directorate facilitated the design and timely production of the field-deployable exposure tool.

References

Akopova, A.B., Viktorova, N.V., Krishchian, V.M., Magradze, N.V., Ovnanian, K. M., Tumanian, K.I.., and Chalabian, T.S. (1993) Nucl. Tracks Radiat. Meas. v. 21, pp 323-328.

Becquerel, H. (1896) Cmpt. Rend. v. 122, pp 501-503.

Bondarenko, O.A.; Salmon, P.L.; Henshaw, D.L.; Fews, A.P.; Ross, A.N. (1996) Alpha-particle spectroscopy with TASTRAK (CR-39 type) plastic, and its application to the measurement of hot particles. Nuclear Instruments and Methods in Physics Research Section A, v. 369, 582-587.

Borg, I.Y., Stone R., Levy H.B., and Ramspott L.D. (1976) Information pertinent to the migration of radionuclides in ground water at the Nevada Test Site, Part I: Review and analysis of existing information. Lawrence Livermore National Laboratory internal report, UCRL-52078, 216 p.

Cartwright, B.G., Shirk, E.K., and Price, P.B. (1978) Nuclear Instruments and Methods in Physics. v. 153, pp 457-460.

Espinosa, G., Silva, R., (1995) J. Radioanal. Nucl. Chem. Art. v. 194, pp 207-212.

Essington, E.H., Fowler, E.B., Gilbert, R.O., and Eberhardt, L.L. (1976) *in* Transuranium Nuclides in the Environment, Proceeding Series, IAEA, Vienna, pp 157-172.

Fleischer R.L., Price, P.B., and Walker, R.M., *Eds*. (1975) Nuclear Tracks in Solids. University of California Press: Berkeley, CA, 605 p.

Gilbert, R. O. (1977) *in* Transuranics in Desert Ecosystems, White, M.G., Dunaway, P. B., and Wireman, D.L., *eds*. U.S, Department of Energy, Nevada Operations Office, Las Vegas, NV, NVO-181, pp 423-429.

Gilbert, R.O., Shinn, J.H., Essington, E.H., Tamura, T., Romney, E.M., Moor, K.S., and O'Farrell, T.P. (1988) Health Phys. v. 55, pp 869-887.

Hanson, W.C., *eds*. (1980) Transuranic Elements in the Environment. TIC/U.S. Department of Energy: Springfield, VA.

Hendricks, T.J., and Riedhauer, S.R., (1999) An Arial Radiological Survey of the Nevada Test Site. DOE/NV/11718-324; Bechtel Nevada: Las Vegas, NV.

Kersting, A.B., Efurd, D.W., Finnegan, D.L., Rokop, D. J., Smith, D.K., and Thompson, J.L. (1999) Migration of plutonium in ground water at the Nevada Test Site. Nature, v**.** 397, n. 6714, pp 56-59.

Kinoshita, S. (1910) Proceedings of the Royal Society. v. 83, pp 432-453.

Laue, C.A. (1996) α-Strahler und Korrosionsprodukte in den Kühlmedien von Leichtwasserreaktoren. Verlag Görich & Weiershäuser GmbH: Marburg, Germany, Ph.D Thesis, Philips University Marburg.

Romney, E.M., Wallace, A., and Gilbert, R.O. Kinnear, J.J. (1976) *in* Transuranium Nuclides in the Environment, Proceeding Series, IAEA, Vienna, pp 479-491.

Shinn, J.H., Essington, E.H., Gouveia, F.J., Patton, S.E., and Romney, E.M. (1993) Predicting depth profiles of fallout plutonium contamination in soil at the Nevada Test site: statistical similarity of five sites. Lawrence Livermore National Laboratory internal report, UCRL-JC-115992, 13 p.

Shinn, J.H., Essington, E.H., Miller, F.L., O'Farrell, T.P., Orcutt, J.A., Romney, E.M., Shugart, J.W., and Sorom, E.R.(1989) Health Phys. v. 57, pp 771-779.

Shinn, J.H., and Homan, D.N. (1985) Plutonium-aerosol emission rates and potential inhalation exposure during cleanup and treatment tests at Area 11, Nevada Test Site. Lawrence Livermore Internal Report, UCID-20514, 13 p.

Townsend, Y.E., and Grossman, R.F., *eds.* (2000) Annual Site Environmental Report for Calendar Year 1999, DOE/NV/11718 – 463; Bechtel Nevada: Las Vegas, NV, pp 2-8.

US Department of Energy (1991) Radionuclides in Surface Soil at the Nevada Test Site. DOE/NV 10845 – 02, Desert Research Institute: Las Vegas, NV.

Vapirev, E.I., Kamenova, T., Mandjoukov, I.G., and Mandjoukova, B. (1990) Radiat. Prot. Dos. v. 30, pp 121-124.

White, M.G., and Dunaway, P.B. *eds.* (1975) The radioecology of plutonium and other transuranics in desert environments. U.S, Energy Research & Development Administration, Nevada Operations Office, Las Vegas, NV, internal report, NVO-153.

White, M.G., Dunaway, P.B., and Wireman, D.L., *eds*. (1977) Transuranics in Desert Ecosystems. U.S, Energy Research & Development Administration, Nevada Operations Office, Las Vegas, NV, internal report, NVO-181.

Chapter 6

^{241}Am Analyses by Multi-Collector Inductively Coupled Plasma Mass Spectrometry

Ross W. Williams

Introduction

The UGTA and HRMP programs have a long vested interest in improving our ability to measure radionuclides of interest. LLNL has successfully developed the ability to measure environmental levels of ^{241}Am by multi-collector inductively coupled plasma mass spectrometry. The method detection limit of 0.017 pCi/L is about two times lower than the best analyses possible by alpha spectrometry. The ability to measure trace quantities of ^{241}Am improves our ability to understand the fate and transport of this and other important actinides that have been and will be needed in future NNSA missions at the Nevada Test Site.

Method Overview

Femtogram quantities of americium-241 can be detected by multi-collector inductively coupled plasma mass spectrometry (MC-ICPMS) and quantified by isotope dilution analysis using a ^{243}Am spike. The MC-ICPMS at LLNL is a Micromass IsoProbe and the sensitivity for Am is equivalent to that observed for uranium and plutonium and other actinides. The analytical parameters are given in the following table and a procedure developed for the analysis of ^{241}Am in water or solid samples is given below.

Mass Spectrometry / LLNL IsoProbe Parameters

The specific activity of ^{241}Am (t ½ = 432 years) is 0.127 Becquerel per picogram (Bq/pg) or 3.43 picoCurie per picogram (pCi/pg). Using the practical quantification limit of 5 fg, this corresponds to an ^{241}Am activity of 0.017 pCi/L or pCi/g for a 1 liter water sample or a 1 gram solid sample. This limit is about two times lower than the best analyses possible by alpha spectrometry.

As for alpha spectrometry, ^{243}Am (t ½ = 7370 years) is used as the isotope dilution spike. The ^{243}Am tracer used for MC-ICPMS analyses is NIST SRM 4332D. Also, as for alpha spectrometry, there are interferences from Pu that must be eliminated during purification. In alpha spectrometry, the interference is from ^{238}Pu that has a similar alpha energy. In mass spectrometry, the interference is the isobaric ^{241}Pu. The following procedure was developed for americium separation and purification to specifically minimize the Pu contamination.

Table 1. IsoProbe Parameters

Sample introduction	Aridus desolvating system. Nebulizer uptake at 40 uL/min. Sample in 2% HNO_3.
Torch and plasma parameters	Cool gas 14 L/min. Intermediate gas 1.0 L/min. RF power 1350 watts.
Collision (hexapole) gas	Argon at 1.2 mL/min.
Ion extraction and accelerating potential	Hard extraction (negative bias) at 20% of maximum (ca. -120V). HV = - 6 kV.
^{241}Am sensitivity	12,500 cps/ppt (counts per second / part per trillion) or 12,500 cps/pg ^{241}Am in 1 mL.
Background and ion detection	200 cps on the Axial Daly pulse counter
Minimum Detectable Level	0.003 ppt or 3 ppq (parts per quadrillion: fg/mL)
Practical Quantification Limit	Ca. 10 ppq or 5 femtograms in 0.5 mL

Purification of Americium for ^{241}Am Analysis by Multi-collector Inductively Coupled Plasma Mass Spectrometry (MC-ICPMS)

Purpose

The purpose of this procedure is to separate and purify americium of major and minor elements for quantification of ^{241}Am by MC-ICPMS. Although some trace contamination in the final sample can be tolerated, a relatively pure Am fraction is required to eliminate potential isobaric interferences and plasma loading effects.

Application

This procedure is applicable to any environmental sample that may be dissolved in 8 M HNO_3. It is necessary to decompose and digest complex solid materials using suitable methods prior to this procedure. These methods may include wet or dry ashing to eliminate organics, hydrofluoric acid based digestions or flux-assisted fusions to open-out silicate rich samples, or aqua-regia dissolutions for metallic samples. Preparation of water samples is specifically provided for herein. Whatever digestion method is used, the sample should be converted to nitrates by repeated drying with concentrated HNO_3 before using this procedure.

Interferences

Iron is a known interference that affects the instrumental mass bias. The mass bias is the deviation of the measured isotopic composition from the true, and is determined by analyses of standard reference materials. This procedure should reduce Fe to less than 10

ppm, at which level there is no effect. ^{241}Pu, a direct interference, is substantially reduced, but this procedure is designed to be rapid and adequately specific for americium in environmental samples. Where plutonium at greater than 10 nanogram is expected, additional purification steps should be done. To address the possibility of significant Pu in the Am fraction, Step 7 is included as an option.

Sample Preparation

^{243}Am spike should be added at an appropriate level to solid samples before they are digested and dissolved. Digestion techniques for solids may vary, as mentioned above, and care should be taken to avoid preferential sample or spike loss prior to equilibration. For water samples, a measured aliquot should be spiked with ^{243}Am, acidified with HNO_3, and heated for several hours on a hotplate. Total evaporation of the water sample is the preferred technique, but Am may also be scavenged by co-precipitation with Fe-hydroxide carrier. For total evaporation, as volume is reduced the sample should be transferred to a Teflon beaker or jar and 2 mL of concentrated hydrofluoric acid plus 0.2 mL of perchloric acid should be added. The sample should be dried completely on a hotplate, with heat-lamp assistance to eliminate the perchloric fumes, and then dried again with a few mL of concentrated HNO_3.

Purification

(1) Prepare a 2 mL resin bed with AG-1X8, 100-200 mesh, chloride form anion exchange resin in a suitable column with about a 10 mL reservoir capacity. A disposable polyethylene Bio-Rad Poly-Prep column is an example. Condition the resin bed by passing 10 mL of deionized water (DI H_2O at 18 MOhm-cm) followed by 12 mL of 8 M HNO_3. Use of ultra-pure sub-boiling distilled HNO_3 and the elimination of all glassware from this step onward is recommended.

(2) Dissolve the sample in a minimum volume of 8 M HNO_3 (preferably less than 5 mL). Warm the sample on a hotplate to help it to dissolve then add 0.04 mL of saturated sodium nitrite solution per mL of acid. Place the sample in an ultrasonic bath and allow it to agitate while cooling.

(3) Place a teflon vial or beaker large enough to contain the sample and rinses under the column. Load the sample on the conditioned resin bed and allow it to pass by gravity. Rinse the column with 6 mL of 8 M HNO_3 loaded as 2 mL, 2 mL and 2 mL, using a gradient technique to rinse through Fe and other major and trace elements. Am passes with the bulk of the salts, including the lanthanides, while Pu, Th and most of the U are retained on the resin. Take the sample to dryness on a hotplate.

(4) Prepare a 1 mL resin bed with Eichrom TRU resin in a suitable column and condition it with a few mL of DI H_2O and then with 4 mL of 3 M HNO_3.

(5) Dissolve the sample in a minimum volume of 3 M HNO_3 and load on the resin bed._Am adsorbs and the contaminating salts pass through. Rinse the column with 6 mL of 3 M HNO_3 loaded in 2 mL increments using a gradient

technique. Catch and retain the column effluent in a suitable container or transfer it to waste as desired.

(6) Place a vial for the Am fraction under the column and wash the Am from the TRU resin by adding 2 mL of 9 M HCl followed by 6 mL of 4 M HCl. Dry this fraction on a hotplate. Add a few drops of concentrated HNO_3 and dry again. Repeat.

(7) This step is optional and can be used to reduce the potential isobaric interference from ^{241}Pu on ^{241}Am. Prepare a 1 mL resin bed with AG-1X8 as in Step 1. Condition the resin by passing 5 mL of DI H_2O followed by 6 mL of 8 M HNO_3. Dissolve the sample from Step 6 in 1 mL of 8 M HNO_3 + 0.04 mL of saturated sodium nitrite. Place a vial under the column to catch the Am fraction and load the sample on the resin bed. Rinse the column with 5 mL of 8 M HNO_3 loaded as 1 mL, 2 mL and 2 mL using a gradient technique. Take the Am fraction to dryness.

(8) Submit the sample for MC-ICPMS analysis of americium.

Chapter 7

A Chlorine-36 Study of Vertical Groundwater Transport in Frenchman Flat, Nevada Test Site

Timothy P. Rose, Jean E. Moran, and Lennox J. Harris

Executive Summary

Chlorine-36 data were used to evaluate vertical groundwater transport processes and flow rates in Frenchman Flat. Groundwater samples from the Cenozoic alluvial and volcanic aquifers tend to have high $^{36}Cl/Cl$ ratios (greater than 5×10^{-13}) and low Cl concentrations (less than 23 mg/L) that generally indicate low levels of water-rock interaction. The high $^{36}Cl/Cl$ ratios of these samples are consistent with recharge during the late Pleistocene (10 to 20 kyr ago) when atmospheric ^{36}Cl production rates were greater. Carbonate aquifer groundwaters generally have lower $^{36}Cl/Cl$ ratios (less than 4.25×10^{-13}) and higher Cl concentrations (24 to 44 mg/L) than the Cenozoic aquifer waters, reflecting water-rock interaction with the carbonate host rock.

Groundwater from well ER-5-3 #2 is enriched in $^{36}Cl/Cl$ relative to other nearby wells completed in the lower carbonate aquifer (e.g. WW-C1). This enrichment is consistent with a mixing process related to the vertical transport of groundwater through the overlying Cenozoic units. $^{36}Cl/Cl$ mixing models suggest that between 25 and 44% of the water in ER-5-3 #2 originated from the semi-perched volcanic and alluvial aquifers. On the basis of hydrologic mass balance calculations and observed $^{36}Cl/Cl$ mixing relationships, the vertical transport fluxes in Frenchman Flat are estimated to be between 330 and 585 ac-ft/yr. Assuming vertical crossflow through a 180 km^2 area with an effective interstitial porosity of 10%, this flux corresponds to an average vertical velocity of 0.02 to 0.04 m/yr. This implies a mean travel time of 20,000 to 34,000 yrs for a water particle moving vertically through the 790 m volcanic section in ER-5-3 #2. These results suggest that transport of soluble, non-sorbing radionuclides will be extremely slow in Frenchman Flat.

Chloride leaching experiments were performed on twelve rock samples from the ER-5-3 #2 borehole. The highest concentrations of leachable chloride were obtained from carbonate rocks and one sample of alluvium. Volcanic rocks tended to yield lower concentrations of leachable chloride. $^{36}Cl/Cl$ ratios measured on chloride leachates were consistently lower than the $^{36}Cl/Cl$ ratios of groundwater from similar hydrostratigraphic intervals. This suggests that the ^{36}Cl in the rock is not in equilibrium with the ^{36}Cl in the surrounding groundwater, and implies the rate of water-rock exchange is very slow, particularly in the alluvial and volcanic aquifers.

Introduction

Frenchman Flat is a topographically closed intermontane basin located in the southeastern part of the Nevada Test Site (NTS). Between 1965 and 1971, ten underground nuclear tests were conducted at depths up to ~300 m within the alluvial and volcanic deposits that underlie the basin (DOE/NV, 1999; 2000). Several of the tests were detonated near or below the water table, resulting in localized groundwater contamination. Conceptual hydrogeologic models suggest that groundwater within the basin is transported vertically through the alluvial and volcanic aquifers to the underlying regional carbonate aquifer, where it then moves laterally toward the southwest (Winograd and Thordarson, 1975; Laczniak et al., 1996). Flow models predict that contaminants reaching the lower carbonate aquifer may be transported beyond the boundaries of the NTS in as little as 200 years (DOE/NV, 1997). Hence, understanding the vertical transport rates through the alluvial and volcanic aquifers is essential to defining the contaminant boundary for this part of the NTS.

The objective of this study is to use chlorine-36 (^{36}Cl) data to evaluate vertical transport processes in Frenchman Flat, and to develop data interpretations that will assist in verifying CAU-scale flow and transport model predictions for the Underground Test Area (UGTA) project. Chlorine-36 is a highly conservative tracer that can provide insight into groundwater flow paths, transport rates, residence times, and mixing processes, particularly when coupled with other chemical and isotopic data. It is well suited for evaluating conservative radionuclide transport, since it is a major activation product of nuclear detonations (although our focus will be on naturally-occurring ^{36}Cl). In a previous report, we evaluated ^{36}Cl variations in groundwater samples collected throughout southern Nevada, and identified end-member compositions for both initial (recharge) and chemically evolved components (Moran and Rose, 2000). In this study, new data are analyzed for groundwater samples and for chloride extracted from rock samples from boreholes in Frenchman Flat. A series of new wells drilled and completed during FY 2000 and FY 2001 were particularly important to this investigation because they provided samples from relatively deep parts of the basin.

Background

Regional Hydrogeologic Setting

The Nevada Test Site (NTS) is located within the 15,800 mi^2 Death Valley regional flow system in the southern Basin and Range province (Harrill et al., 1988; Laczniak et al., 1996). The principal aquifers in the region consist of basin-fill deposits and fractured carbonate rocks, although volcanic rocks also form locally important aquifers (Winograd and Thordarson, 1975; Thomas et al., 1996). Much of the region is underlain by a thick sequence of Paleozoic carbonate rocks through which groundwater is transported along deep regional flowpaths that transcend local topographic boundaries (Dettinger et al., 1995). Mesozoic thrust faulting and Cenozoic normal faulting have locally juxtaposed rocks of different ages and lithologies, compartmentalizing the flow system. For this reason, regional hydraulic gradients tend to be step-like rather than smooth (Winograd and Thordarson, 1975). The hydrogeology and geochemical characteristics of the

regional carbonate aquifer are described in Winograd and Thordarson (1975), Mifflin and Hess (1979), and Thomas et al. (1996). Recharge to the regional flow system occurs in high elevation areas in central Nevada, and in the Spring Mountains and Sheep Range in southern Nevada (e.g. Davisson et al., 1999). Major discharge areas occur at Ash Meadows and Death Valley.

Hydrogeology of Frenchman Flat

The hydrogeologic characteristics of Frenchman Flat are summarized in Winograd and Thordarson (1975), Laczniak et al. (1996), and in various UGTA project documents (e.g. IT Corporation, 1999; DOE/NV 1999). Major hydrostratigraphic units underlying the basin include a shallow basin fill alluvial aquifer, a volcanic sequence at intermediate depth, and a deep carbonate rock aquifer. The volcanic sequence consists of rhyolitic tuffs and lavas that are broadly subdivided into an upper tuff aquifer and a lower tuff aquitard. The lateral extent of the tuff-confining unit beneath Frenchman Flat is poorly defined, but it appears to be present in areas where underground testing was conducted (Laczniak et al., 1996).

The depth to the water table in Frenchman Flat ranges from ~700 ft near the center of the basin to ~1100 ft near its margins (Table 1). Most wells perforate Cenozoic age alluvial and/or volcanic aquifers. Water levels in wells tapping the lower carbonate aquifer are as much as 30 feet lower than levels in the Cenozoic units. This head difference implies that the Cenozoic strata are semi-perched relative to the lower carbonate aquifer (Winograd and Thordarson, 1975, p. 60). The only pathway by which the semi-perched water leaves Frenchman Flat is by downward leakage into the underlying carbonate aquifer. The downward flux is estimated to be small (70 ac-ft/yr) due to the relatively impermeable nature of the tuff aquitard (Winograd and Thordarson, 1975). Slow vertical leakage through the tuff aquitard is the probably the main rate-limiting step in the transport of radionuclides out of Frenchman Flat.

Lateral movement of groundwater through Frenchman Flat is restricted to the lower carbonate aquifer, and is controlled by the structural position of the lower clastic confining unit and the Belted Range thrust system (DOE/NV, 1997; p. 6-22). Regional flow within the lower carbonate aquifer likely originates as a west-verging component of the White River flow system from the vicinity of Pahranagat Valley (Winograd and Friedman, 1972; Thomas et al., 1996). The regional flow system passes beneath Frenchman Flat, and continues to the southwest toward discharge areas at Ash Meadows, Alkali Flat and Death Valley (Winograd and Thordarson, 1975; Laczniak et al., 1996). Regional flow from Pahranagat Valley also enters southern Yucca Flat, but is then diverted southward into Frenchman Flat by the low permeability Belted Range thrust system (Winograd and Thordarson, 1975). The relatively flat hydraulic gradient between Yucca Flat and Ash Meadows (<1 ft/mile) suggests a high degree of hydraulic continuity within the aquifer, and probably reflects high fracture permeability (Laczniak et al., 1996).

Chlorine-36 as a Tracer in Hydrologic Systems

• ***Natural production and variation in initial ratios***

Chlorine has one long-lived radioactive isotope, ^{36}Cl, with a half-life of 301,000 years. Natural production of ^{36}Cl occurs in three ways: (1) cosmic-ray spallation of ^{40}Ar and neutron activation of ^{36}Ar in the atmosphere; (2) cosmic-ray spallation of K and Ca on and near the earth's surface; and (3) neutron activation of ^{35}Cl (from U-Th series decay) at depth over long periods of time. In addition, neutron activation of ^{35}Cl in seawater during atmospheric nuclear testing raised $^{36}Cl/Cl$ ratios in the atmosphere by more than two orders of magnitude in the 1950s and early 1960s (Bentley et al., 1982). However, the high concentration of chloride in seawater effectively dilutes the $^{36}Cl/Cl$ ratios in the ocean to below the detection limit (1×10^{-15}) of accelerator mass spectrometry (AMS).

Seaspray-derived chloride in meteoric water causes $^{36}Cl/Cl$ ratios in precipitation to vary with distance from the ocean. The lowest ratios are recorded along coastal regions (15×10^{-15}) and the highest ratios are found in the continental interior (up to 1000×10^{-15} for the continental U.S.; Bentley et al., 1986). Recent studies suggest that the 'initial value' for the decay of ^{36}Cl in hydrologic systems is poorly constrained in many hydrologic settings (Davis et al., 1998). This may be in part because ^{36}Cl from nuclear weapons testing is still cycling in the atmosphere (Cornett et al., 1997). Furthermore, chloride sources in groundwater may be mixed even near the recharge area, and seasonal recharge may not reflect average annual ^{36}Cl concentrations.

In the southwestern United States, published estimates of the initial $^{36}Cl/Cl$ ratio range from 400 to 880×10^{-15} (Bentley and Davis, 1982; Hainsworth et al., 1994; Davis et al., 1998). Moran and Rose (2000) reported $^{36}Cl/Cl$ ratios of 522 and 590×10^{-15} for two different springs from the Spring Mountains near Las Vegas, Nevada. Both springs contain bomb-pulse tritium. Groundwater collected from a mountain spring located near Pahranagat Valley (150 km N of Las Vegas) had a $^{36}Cl/Cl$ ratio of 716×10^{-15}, whereas a meteoric water sample collected over a six-month period near Austin, Nevada (400 km NW of Las Vegas) had a $^{36}Cl/Cl$ ratio of 910×10^{-15} (Moran and Rose, 2000).

Tyler et al. (1996) examined variations in $^{36}Cl/Cl$ ratios with depth in soil water samples taken from the PW-1, PW-2 and PW-3 boreholes in northern Frenchman Flat. Measured ratios as high as $\sim 950 \times 10^{-15}$ were observed at 10 m depth, and elevated ratios persisted at much greater depths (e.g. $^{36}Cl/Cl = 700 \times 10^{-15}$ at 213 m depth in PW-1). The $^{36}Cl/Cl$ ratios in all three boreholes are significantly higher than the estimated modern ratio of $\sim 500 \times 10^{-15}$ measured in the soil zone at Yucca Mountain (Fabryka-Martin et al., 1993). Tyler et al. (1996) notes that the elevated ratios are consistent with predicted increases in atmospheric ^{36}Cl production during late Pleistocene time, corresponding to periods of significantly reduced strength in the earth's magnetic field (Mazaud et al., 1991). Atmospheric ^{36}Cl production rates 20,000 years ago were estimated to be a factor of 1.6 higher than the modern value, implying an initial ratio of 800×10^{-15} in southern Nevada at that time. Hence, the $^{36}Cl/Cl$ variations at depth in the PW boreholes probably reflect groundwater recharge during the last pluvial period, when the climate in southern Nevada was notably less arid relative to current conditions (e.g. Mifflin and Wheat, 1979; Spaulding, 1985; Quade et al., 1995).

• ***Chlorine-36 in groundwater***

Chloride is a highly mobile, non-reactive anion in groundwater systems. The $^{36}Cl/Cl$ ratio may be modified along a flow path due to ^{36}Cl decay, subsurface ^{36}Cl production, groundwater mixing, and water-rock interaction. Radioactive decay probably has a negligible influence on observed $^{36}Cl/Cl$ ratios in southern Nevada since estimated groundwater residence times are much less than the half-life of ^{36}Cl (cf. Thomas et al., 1996; Davisson et al., 1999).

The secular equilibrium $^{36}Cl/Cl$ ratios resulting from the subsurface production of ^{36}Cl in low-chlorinity waters are $\sim 30 \times 10^{-15}$ for granite and $\sim 10 \times 10^{-15}$ for limestone (Bentley and Davis, 1982). In comparison, the $^{36}Cl/Cl$ ratios measured for more than 50 groundwater samples from southern Nevada were all $>100 \times 10^{-15}$, with the lowest values occurring in carbonate aquifer groundwaters (Moran and Rose, 2000). In general, subsurface production ratios are at least an order of magnitude lower than the groundwater $^{36}Cl/Cl$ ratios in the volcanic and carbonate aquifers at the NTS, implying that subsurface production should not have a major impact on measured ratios.

Evapotranspiration at the earth's surface can modify dissolved chloride concentrations, but will not affect the $^{36}Cl/Cl$ ratio. In contrast, rock leaching and/or mineral dissolution processes can alter both the chloride concentration and the $^{36}Cl/Cl$ ratio of a groundwater. Mixing of groundwaters with different $^{36}Cl/Cl$ ratio will yield intermediate compositions that can be delineated on a plot of $^{36}Cl/Cl$ vs. 1/Cl.

Sampling and Analytical Methods

Groundwater Samples

Groundwater samples were collected for $^{36}Cl/Cl$ analysis from 16 wells located in or near Frenchman Flat (Figure 1). Samples were obtained during two separate field operations, one in 1993 (10 samples) and the other during 2000-2001 (6 samples). These include seven samples from the alluvial aquifer, two from wells completed in both the alluvial and volcanic aquifers, three samples from volcanic units, and four from the lower carbonate aquifer (although only one carbonate aquifer sample is from a well located within the Frenchman Flat basin). Well locations, depths, production intervals, and hydrostratigraphic intervals are given in Table 1. Also included are available data for two additional wells in Frenchman Flat where ^{36}Cl data were not obtained.

All water samples collected for ^{36}Cl analysis were stored in plastic bottles with no preservative. Waters were processed using the standard technique for preparation of AgCl targets for analysis on an accelerator mass spectrometer (Elmore et al., 1979). Sulfur species (which have an isobar at mass 36) were removed by precipitation of $BaSO_4$ with $Ba(NO_3)_2$. The chloride was then precipitated as AgCl using $AgNO_3$. Procedural and reagent blanks were processed using halite from a Silurian formation in Michigan, which has ^{36}Cl levels below the AMS detection limit.

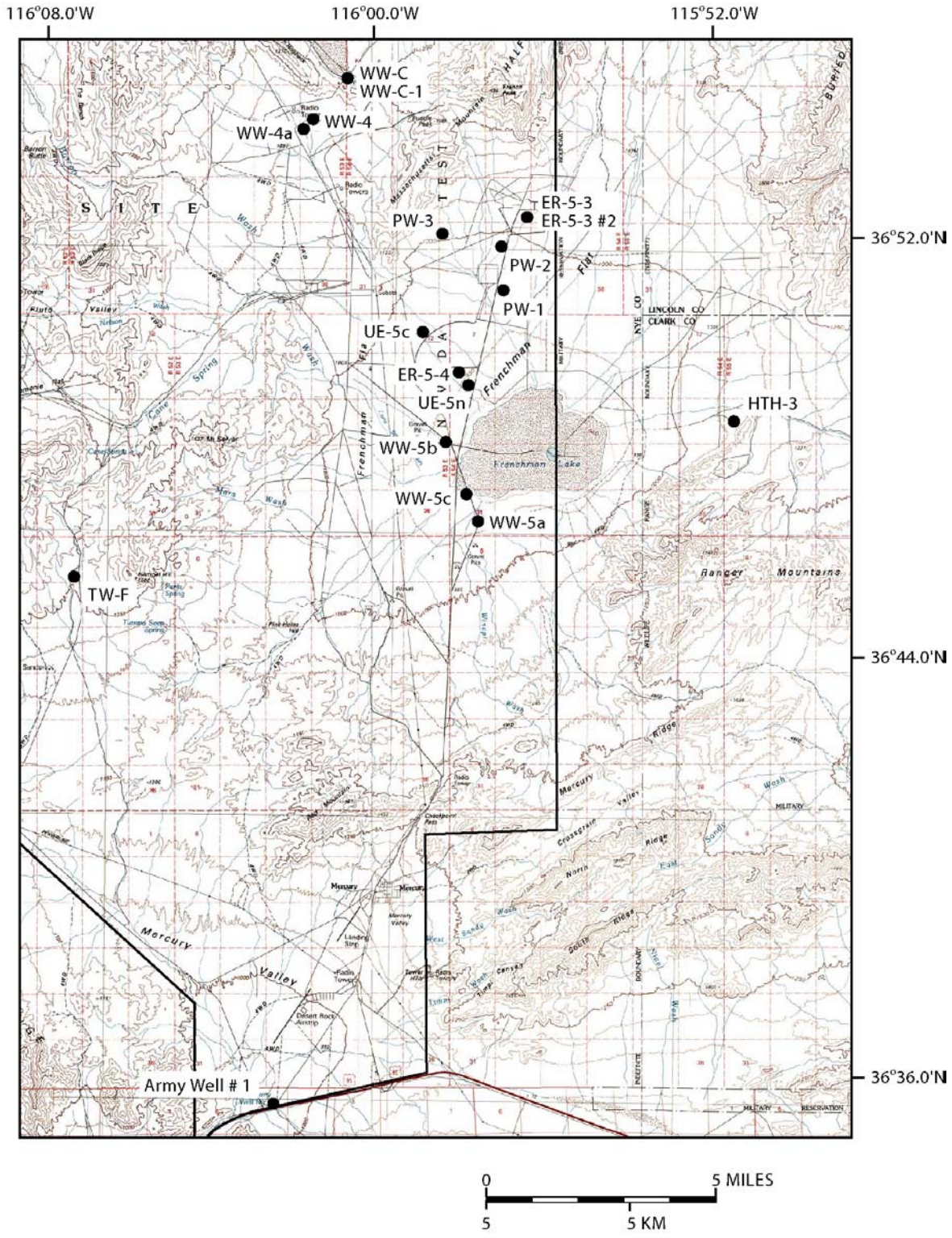

Figure 1. Map of the southeastern Nevada Test Site showing well locations discussed in this report. Base map is from U.S. Geological Survey 1:100,000-scale metric topographic maps of Beatty and Indian Springs 30 × 60 minute quadrangles.

Table 1. Site information for selected wells located in Frenchman Flat and vicinity.

Sample	Latitude (d m s)	Longitude (d m s)	Surface Elevation (ft asl)	Total Depth (ft bgs)	EOI (ft bgs)	Depth to SWL (ft bgs)	SWL Elevation (ft asl)	Primary HSU
Army Well #1	36 35 30	116 02 14	3154	1953	800-1946	786	2368	LCA
TW-F	36 45 34	116 06 59	4143	3400	3150-3400	1751	2392	LCA
Water Well 5a	36 46 35	115 57 29	3092	910	642-877	695	2397	AA
Water Well 5c	36 47 08	115 57 44	3081	1200	887-1187	689	2392	AA
Water Well 5b	36 48 05	115 58 08	3093	900	700-900	683	2410	AA
HTH-3	36 48 30	115 51 26	3484	1853	1193-1853	1103	2381	LCA
UE-5n	36 49 15	115 57 41	3112	1690	720-1687	705	2407	AA
ER-5-4	36 49 28	115 57 48	3127	3732	1770-2113; 3136-3350	726	2401	AA
UE-5c WW	36 50 11	115 58 47	3216	2682	1100-2682	806	2410	AA; WVCU
UE-5 PW-1	36 51 05	115 56 58	3178	839	772-839	771	2407	AA
UE-5 PW-2	36 51 52	115 56 57	3246	920	841-920	840	2406	AA
UE-5 PW-3	36 52 01	115 58 16	3297	955	891-955	891	2406	TMA
ER-5-3	36 52 23	115 56 17	3334	2606	1480-1737; 2420-2549	927	2410	AA; TMA
ER-5-3 #2	36 52 23	115 56 18	3334	5683	4674-4868	952	2382	LCA
Water Well 4a	36 54 12	116 01 39	3604	1517	944-1502	835	2769	TMA
Water Well 4	36 54 18	116 01 26	3602	1479	942-1435	833	2769	TMA
Water Well C-1	36 55 07	116 00 34	3924	1707	1540-1650	1544	2380	LCA
Water Well C	36 55 08	116 00 35	3924	1701		1542	2382	LCA

Data Sources

DOE/NV (1997)

IT Corporation (1999; 2000a; 2001a,b)

Key to primary hydrostratigraphic units (HSU)

AA = Alluvial Aquifer

TMA = Timber Mountain Aquifer

WVCU = Wahmonie Volcanic Confining Unit

LCA = Lower Carbonate Aquifer

Lithologic Samples

Analysis of groundwater samples provides insight into $^{36}Cl/Cl$ variations within the different hydrostratigraphic intervals in Frenchman Flat, but does not permit a *systematic* evaluation of $^{36}Cl/Cl$ as a function of depth through the stratigraphic sequence. To determine the variation with depth, samples are needed at discrete intervals from one geographic location. One possible approach is to examine the $^{36}Cl/Cl$ ratios of leachable chloride extracted from lithologic samples. However, there are some clear limitations to this approach. For instance, leaching experiments performed over a period of a few days in a laboratory cannot replicate natural water-rock interactions that take place over thousands of years. Moreover, crushing the rock samples can expose a number of surfaces that previously had no direct contact with circulating groundwater, thereby releasing chloride that might otherwise have very slow exchange rates. The extent to which the leachable ^{36}Cl in the rock is in equilibrium with the ^{36}Cl in the groundwater is also uncertain, and must be estimated by comparing water and leachate $^{36}Cl/Cl$ values from similar depth intervals. The equilibrium condition is most likely to be satisfied by leaching only loosely bound chloride using deionized water.

Leaching experiments were performed on lithologic samples from well ER-5-3 #2, located in northern Frenchman Flat (Figure 1). ER-5-3 #2 was drilled to a total depth of 5,683 ft (1,732 m), and perforates the entire alluvial and volcanic section in this part of the basin. Paleozoic carbonate rocks were encountered at a depth of 4,678 ft (1,426 m) below the surface (IT Corporation, 2000a). Composite drill cuttings were collected every 10 ft during drilling, and are archived at the U.S. Geological Survey Geologic Data Center and Core Library in Mercury, Nevada. Approximately 100 g of cuttings were selected from 12 different intervals in ER-5-3 #2, with each interval spanning 30 to 50 ft of section within a particular lithologic unit. These include 2 alluvium samples, 8 volcanic rock samples, and 2 carbonate rock samples. Lithologic descriptions of these samples are found in Appendix A.

Previously measured leachable chloride concentrations in volcanic rocks range from ~0.1 to 2 ppm per gram of rock (ppm by weight, or ppmw), whereas leachable chloride in carbonate rocks commonly exceeds 10 ppmw (Kenneally, 1995; Moran and Rose, 2000). A potential concern is that the ER-5-3 #2 cuttings may have been contaminated with chloride during drilling. However, a LiBr tracer was added to the drilling fluid (~21 mg/L; IT Corporation, 2000a), and the residue can be detected by measuring the bromide concentration of the leachate. To test for the presence of bromide, 3 g of unwashed cuttings were placed in an acid-rinsed HDPE container with 3 mL of water, and then loaded on a shaker-table for 1 hour @ 100 rpm. Concentrations of dissolved chloride and bromide were then measured by ion chromatography. This experiment was performed on five different samples, yielding leachable chloride concentrations ranging from 1.6 to 8.2 ppmw (see Table 2, "initial rinse"). Bromide was present in two samples at concentrations just above the detection limit, but in each case the bromide level was

Table 2. Chloride concentration from leaching experiments.

Depth Interval (ft bgs)	Lithologic Unit	Initial Rinse		Leaching Expt # 1		Leaching Expt # 2	
		Chloride (ppm by wt)	Bromide (ppm by wt)	size fraction (μm)	Chloride (ppm by wt)	size fraction (μm)	Chloride (ppm by wt)
940-990'	Alluvium (Qta)	2.76	n.d.	88 - 295	16.23	< 88 - 295	3.13
				< 88	22.33		
1330-1360'	Alluvium (Qta)	---	---	< 88	2.02	---	---
2110-2150'	Ammonia Tanks Tuff (Tma)	1.64	n.d.	150 - 295	1.54	< 88 - 295	0.60
				88 - 150	2.85		
				< 88	4.15		
2310-2340'	Ammonia Tanks Tuff (Tma)	---	---	< 88	3.01	---	---
2520-2560'	Rainier Mesa Tuff (Tmr)	---	---	150 - 295	4.77	< 88 - 295	0.42
				88 - 150	6.82		
				< 88	11.72		
2830-2860'	Tuff of Holmes Road (Tmrh)	---	---	< 88	4.76	---	---
2920-2960'	Topopah Spring Tuff (Tpt)	8.17	n.d.	150 - 295	2.80	< 88 - 295	1.77
3250-3280'	Wahmonie Formation (Tw)	---	---	150 - 295	3.54	< 88 - 295	0.59
				88 - 150	8.40		
				< 88	7.83		
3720-3760'	Tunnel Formation (Tn)	3.04	0.24	88 - 295	2.06	< 88 - 295	0.69
				< 88	5.29		
4150-4190'	Bullfrog Tuff (Tcb)	---	---	< 88	4.38	---	---
4780-4820'	Sevy Dolomite (Dss)	---	---	< 88 - 295	22.55	< 88 - 295	5.31
5350-5390'	Laketown Dolomite (Sl)	4.24	0.23	< 88 - 295	9.92	< 88 - 295	1.67

n.d. = not detected

~2 orders of magnitude below the concentration of LiBr in the drilling fluid. This suggests that very little residual drilling fluid is present in the samples.

As a precaution, all of the rock cuttings were rinsed with deionized water prior to beginning the leaching experiments in order to remove possible surface contamination. This involved placing hand picked cuttings in an acid-rinsed HDPE container, adding deionized water at a 3:1 water-rock ratio for ~3 minutes, and then decanting off the liquid and oven drying the samples at 70°C. The cuttings were then crushed using a mortar and pestle and passed through a sieve nest to obtain 50-100 mesh, 100-170 mesh, and <170 mesh size fractions (295-150 μm, 150-88 μm, and <88 μm grain sizes, respectively).

Crushed rock samples were loaded into 150 mL HDPE bottles in approximately a 1:1 ratio with deionized (milli-Q) water and tumbled @ 200 rpm for 3 days. The liquid was separated from the residual solids using a centrifuge, and the supernatant was filtered (0.45 μm) to remove fine-grained particulates. Chloride concentrations in the leachate solutions were measured by ion chromatography, with a detection limit of 0.1 mg/L and a typical relative standard deviation of 1 to 4%. A number of leaching experiments were performed to determine the relative amounts of chloride released as a function of grain size, and to compare chloride yields during sequential leaching trials (see discussion below). The leachate used for ^{36}Cl analysis was taken from the smallest grain fraction (where the chloride yield was highest), or from a combination of size fractions. AgCl targets were prepared for ^{36}Cl analysis following the standard technique described in the preceding section. ^{36}Cl/Cl ratios were measured at the Center for Accelerator Mass Spectrometry at Lawrence Livermore National Laboratory, with an analytical detection limit of ~5×10^{-15} and a typical relative standard deviation of 5%.

Results

^{36}Cl/Cl Variations in Frenchman Flat Groundwater

Chemical and isotopic data for groundwater samples collected in and near Frenchman Flat are summarized in Tables 3 and 4. Figure 2 shows a graph of Cl concentrations vs. ^{36}Cl/Cl ratios for Frenchman Flat groundwaters, illustrating compositional variations within the different hydrostratigraphic units. The pattern is similar to that shown in Moran and Rose (2000) for a larger set of samples collected throughout southern Nevada. Groundwater from the lower carbonate aquifer has relatively high Cl values (24 to 44 mg/L) and low ^{36}Cl/Cl ratios (1.66 to 4.23×10^{-13}) reflecting significant water-rock interaction with chloride-rich carbonate rocks. Army Well #1 has the highest ^{36}Cl/Cl ratio among the carbonate aquifer samples, and is interpreted to represent a mixture of regional underflow beneath Frenchman Flat with groundwater originating from the Spring Mountains.

Samples from the volcanic aquifer have lower Cl concentrations (10 to 16 mg/L) and higher ^{36}Cl/Cl ratios (6.13 to 8.42×10^{-13}) compared to the carbonate aquifer samples, and plot in a fairly tight group with the exception of the sample from ER-5-3, which is a mixture of alluvial and volcanic aquifer waters. The chloride content of the bulk volcanic rocks is probably sufficiently low that it should not have a major impact on the ^{36}Cl/Cl

Table 3. Water chemistry data for selected wells located in Frenchman Flat and vicinity.

Sample	Sample Date	Temp (°C)	Cond (mS/cm)	pH	TDIC (mg/L HCO_3)	F (mg/L)	Cl (mg/L)	SO_4 (mg/L)	Na (mg/L)	K (mg/L)	Ca (mg/L)	Mg (mg/L)	Data Source
Army Well #1	5/12/1993	29.3	625	7.5	207	1.1	24.0	54.7	40	5	43.5	20.0	1
TW-F	3/12/1980	64.0	625	7.3	244	3	20	75	64	9.7	44	16	3
Water Well 5a	8/14/2000	22.3	600	8.9	313	1.1	11.1	28.5	147	5.8	2.2	0.9	2
Water Well 5c	5/20/1993	25.4	603	8.8	256	1.0	12.3	29.6	130	6	13.5	0.8	1
Water Well 5c	8/7/2000	28.2	601	8.7	306	1.0	11.3	29.3	149	7.3	2.2	0.8	2
Water Well 5b	8/7/2000	24.6	512	8.5	171	0.7	23.4	55.0	101	12.4	8.2	2.6	2
HTH-3	6/16/1990	34.5	---	7.4	323	---	23.2	66.8	79.6	9.2	48.8	19.7	4
UE-5n	5/24/1993	26.0	427	8.8	163	0.8	14.6	27.2	78	8	6.5	1.3	1
UE-5n	9/9/1999	26.5	453	8.7	183	0.8	12.0	31.8	86	8	7.5	2.0	2
ER-5-4	7/5/2001	30.2	885	8.7	---	6.2	26.8	120	124	7.1	2.2	0.2	2
UE-5c WW	5/13/1993	26.3	452	8.0	160	1.8	14.1	45.6	83	6	8.0	2.2	1
UE-5c WW	8/8/2000	25.8	463	8.5	179	1.8	12.8	43.7	100	7.0	7.1	1.9	2
UE-5 PW-1	5/26/1993	22.5	377	8.3	145	1.3	12.0	34.3	57	6	14.9	4.8	1
UE-5 PW-2	5/26/1993	23.3	368	8.4	173	1.1	15.2	26.6	56	6	19.2	4.9	1
UE-5 PW-3	5/26/1993	24.1	361	8.5	111	1.2	10.1	28.9	60	7	14.5	3.8	1
UE-5 PW-3	8/9/2000	21.5	371	8.3	153	0.9	9.4	31.8	61.8	5.2	16.5	6.5	2
ER-5-3	3/28/2001	30.0	445	8.3	169	2.5	15.5	40.0	78.9	4.0	14.3	3.9	2
ER-5-3 #2	5/17/2001	33.8	1158	6.7	797	1.3	38.0	64.0	145	15.8	86.1	32.6	2
Water Well 4a	8/8/2000	26.5	409	7.9	157	1.2	13.2	39.8	57.3	5.9	26.3	8.1	2
Water Well 4	5/20/1993	25.3	415	7.4	148	0.9	15.2	41.7	48	5	23	5.9	1
Water Well C-1	5/19/1993	32.7	1131	6.5	580	1.1	43.6	67.1	118	13	71.1	25.7	1
Water Well C	5/19/1993	35.2	1135	6.9	564	1.1	43.5	65.1	119	13	79	26.5	1

Data Sources

1. Rose et al. (1997)
2. LLNL unpublished data
3. IT Corporation (2000b)
4. Lyles et al. (1991)

Table 4. Isotopic data for groundwater samples from selected wells located in Frenchman Flat and vicinity.

Sample	Sample Date	δD (‰ SMOW)	$\delta^{18}O$ (‰ SMOW)	$\delta^{13}C$ (‰ PDB)	^{14}C (pmc)	^{14}C age (years)	^{3}H (pCi/L)	$^{36}Cl/Cl$ (x 10^{-13})
Army Well #1	5/12/1993	-100	-13.4	-6.1	4.9	24900	<1.5	4.23
TW-F	3/12/1980	---	---	---	---	---	---	---
Water Well 5a	8/14/2000	-110	-13.8	-4.8	2.6	30300	1.5	8.43
Water Well 5c	5/20/1993	-105	-14.1	-6.0	3.1	28720	< 1.5	6.96
Water Well 5c	8/7/2000	-110.5	-14.0	-6.0	3.4	28050	< 1.5	---
Water Well 5b	8/7/2000	-108	-13.1	-9.5	13.1	16830	< 1.5	7.83
HTH-3	6/16/1990	-104	-14.2	-10.8	36.9	8240	<10	---
UE-5n	5/24/1993	-110	-13.5	---	---	---	9.85E+03	423
UE-5n	9/9/1999	-106	-13.4	-8.3	18.8	13820	1.33E+05	6010
ER-5-4	7/5/2001	-109	-13.6	---	---	---	---	3.94
UE-5c WW	5/13/1993	-105	-13.8	-7.5	6.7	22350	< 1.5	6.13
UE-5c WW	8/8/2000	-106.5	-13.7	-7.2	6.5	22620	< 1.5	---
UE-5 PW-1	5/26/1993	-107	-13.8	-7.9	16.7	14800	< 1.5	8.42
UE-5 PW-2	5/26/1993	-106	-13.8	-8.1	33.8	8970	< 1.5	5.27
UE-5 PW-3	5/26/1993	-102	-13.5	-8.5	21.0	12900	3.8	6.78
UE-5 PW-3	8/9/2000	-105.5	-13.5	-7.5	16.0	15160	< 1.5	---
ER-5-3	3/28/2001	-108.5	-14.1	-8.0	8.5	20380	---	8.42
ER-5-3 #2	5/17/2001	-110	-14.1	-4.3	1.6	34080	---	2.29
Water Well 4a	8/8/2000	-101	-12.8	-8.4	18.3	14050	< 1.5	6.47
Water Well 4	5/20/1993	---	-12.5	-10.9	18.2	14080	<1.5	6.16
Water Well C-1	5/19/1993	-110	-14.0	-3.1	1.0	38070	---	1.66
Water Well C	5/19/1993	-106	-13.9	-4.2	0.6	42300	3.6	1.76

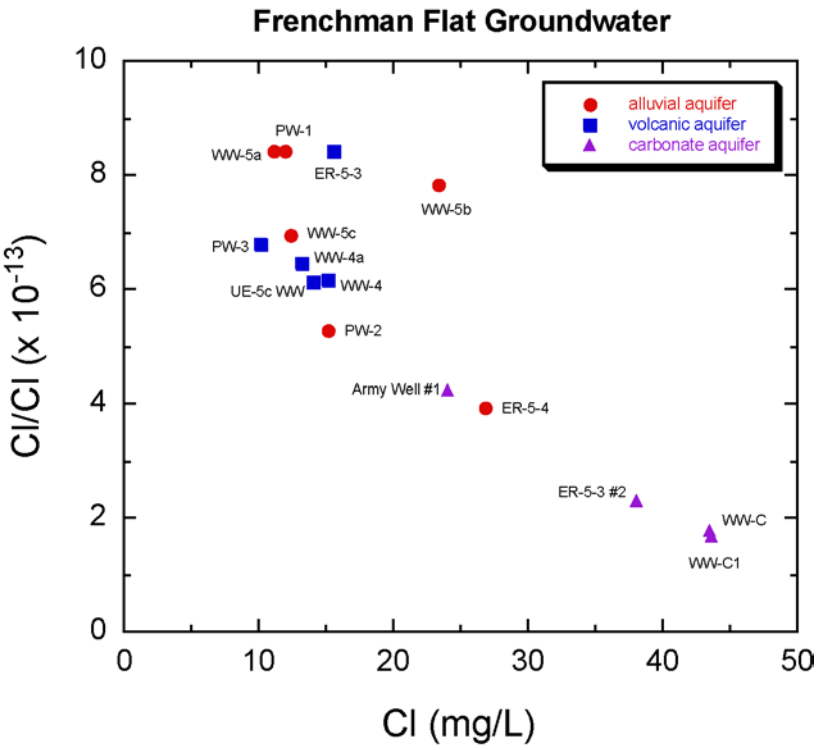

Figure 2. Plot of $^{36}Cl/Cl$ ratios (x 10^{-13}) vs. chloride concentrations (in mg/L) for groundwater samples from Frenchman Flat and vicinity. Red circles = alluvial aquifer samples; blue squares = volcanic aquifer samples; purple triangles = carbonate aquifer samples.

ratio of the groundwater. Moreover, the groundwater residence time is likely to be too short for the ^{36}Cl content to have been affected by either radioactive decay or subsurface production. Reaction with secondary calcite along fractures may alter the $^{36}Cl/Cl$ ratio of groundwater within the volcanic section, although there is little evidence for this in the samples from this study.

Compared to the volcanic aquifer samples, groundwater from the alluvial aquifer shows a broad range in both Cl concentrations (11 to 27 mg/L) and $^{36}Cl/Cl$ ratios (3.94 to 8.43×10^{-13}). The data from well ER-5-4 are particularly notable, both because of their high chloride and low $^{36}Cl/Cl$ values, and because they plot along the same evolutionary trend as the carbonate aquifer samples in Figure 2. The latter observation implies that ER-5-4 groundwater has partially equilibrated with carbonate rock clasts in the alluvium, which originate from the weathering of Paleozoic rocks in the mountains south and east of Frenchman Flat. The extent of water-rock reaction may be flow path dependent since the abundance of carbonate clasts will vary with distance from the source area – hence, the wide-range of $^{36}Cl/Cl$ ratios among the alluvial groundwaters. The key point is that the ER-5-4 data show that $^{36}Cl/Cl$ ratios may be substantially modified by water-rock reactions occurring *outside* of the carbonate aquifer.

A number of samples from both the alluvial and volcanic aquifers have $^{36}Cl/Cl$ ratios above the modern atmospheric ratio (~5.0 to 6.0×10^{-13}). Elevated $^{36}Cl/Cl$ ratios can result from the presence of modern "bomb-pulse" ^{36}Cl in the samples. For instance, groundwater from UE-5n contains very high levels of ^{36}Cl due to the local re-infiltration of water pumped from a nearby underground nuclear test cavity (Bryant, 1992; Smith, 2001). However, the lack of elevated tritium levels in most Frenchman Flat samples (Table 4) implies a general absence of test-derived radionuclides. Although bomb-pulse ^{36}Cl from fallout deposited in Frenchman Flat could be re-mobilized to the water table during large rainfall or snowmelt events, precipitation rates are quite low in Frenchman Flat, averaging only 5.0 in/yr at a gauging station located at WW-5b (19 year record; French, 1985). Recharge events that infiltrate through the 700+ ft thick unsaturated zone are probably very rare.

Tyler et al. (1996) interpreted the high $^{36}Cl/Cl$ ratios in the vadose zone of Frenchman Flat as evidence for recharge during the late Pleistocene, when atmospheric ^{36}Cl production rates were higher. This "paleo-recharge" hypothesis probably accounts for the elevated $^{36}Cl/Cl$ ratios in some Frenchman Flat groundwaters, particularly given the lack of evidence for significant modern recharge in the basin.

Comparison with Oxygen Isotope Data

Stable isotope ratios of oxygen and hydrogen are highly conservative groundwater tracers that are useful in determining the origin and pathways of groundwater flow. Stable isotope data compliment the $^{36}Cl/Cl$ results by providing an independent means of evaluating groundwater sources and mixing processes. We will focus on interpreting oxygen isotope ($^{18}O/^{16}O$) data, although similar conclusions can be drawn from hydrogen isotope data.

Modern precipitation in Frenchman Flat has a weighted mean $\delta^{18}O$ value of -9.5‰ (Ingraham et al., 1991), whereas groundwater from the alluvial and volcanic aquifers has $\delta^{18}O$ values ranging from -12.5 to -14.1‰ (Table 4). The significant difference in precipitation vs. groundwater $\delta^{18}O$ values, and the relatively low precipitation rates in Frenchman Flat suggest a general lack of modern recharge. In contrast, cooler and wetter climate conditions during the last pluvial period would have caused a significant shift toward lower $\delta^{18}O$ values in southern Nevada precipitation, and would have enhanced local recharge rates (e.g. Claassen, 1986). Hence, the $\delta^{18}O$ data tend to support the idea that groundwater in the alluvial and volcanic aquifers beneath Frenchman Flat was primarily recharged during the late Pleistocene.

On a plot of $^{36}Cl/Cl$ vs. $\delta^{18}O$, groundwater from the carbonate aquifer generally exhibits relatively low $\delta^{18}O$ values (-13.9 to -14.1‰; see Figure 3). Mixing with recharge from the Spring Mountains has enriched the Army Well #1 composition (-13.4‰), and HTH-3 groundwater has a $\delta^{18}O$ value of -14.2‰ (Table 4), but lacks a $^{36}Cl/Cl$ analysis. In comparison, samples from the alluvial and volcanic aquifers are more heterogeneous with respect to $\delta^{18}O$, and lack an obvious pattern in Figure 3. The combined $\delta^{18}O$-δD values for WW-4a and WW-5b suggest evaporative enrichment, and WW-4 groundwater may also be evaporated, although it is lacking a δD analysis. The range in $\delta^{18}O$ among the

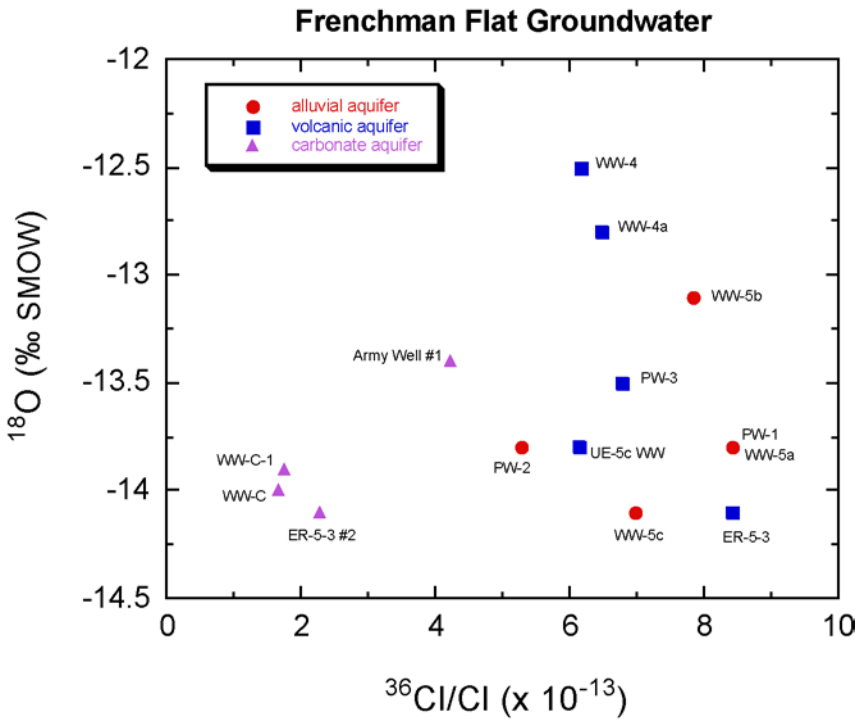

Figure 3. Plot of $\delta^{18}O$ (‰ SMOW) vs. $^{36}Cl/Cl$ ratios (x 10^{-13}) for groundwater samples from Frenchman Flat and vicinity.

seven remaining alluvial and volcanic aquifer samples (-13.5 to -14.1‰) may reflect differences in the isotopic composition of groundwater recharge over time. It is notable that the lowest (most negative) $\delta^{18}O$ values in the alluvial and volcanic aquifers actually overlap with the lowest values in the carbonate aquifer.

For example, groundwater samples from the ER-5-3 and ER-5-3 #2 wells both have $\delta^{18}O$ values of -14.1‰. These wells are located ~100 ft apart in northern Frenchman Flat, but are completed at different depth intervals in the alluvial/volcanic and carbonate aquifers, respectively (Table 1). Despite their similarities in $\delta^{18}O$, they have distinctly different $^{36}Cl/Cl$ ratios (Figure 3) that reflect different histories of water-rock interaction. Groundwater from ER-5-3 #2 contains 5 times more dissolved HCO_3^- and 2.5 times more Cl^- than ER-5-3, reflecting extensive interaction with the carbonate aquifer. Differences in Na^+ and SO_4^{2-} concentrations are more modest, and could suggest a local downward flux of groundwater from the volcanic to the carbonate aquifer.

Winograd and Thordarson (1975) noted the likelihood of vertical leakage from the alluvial and volcanic aquifers to the carbonate aquifer due to differences in hydraulic head. They further noted the carbonate groundwater beneath the eastern NTS was enriched in Na^+ and SO_4^{2-} relative to other carbonate groundwaters in southern Nevada, and proposed that vertical leakage from the tuff aquitard could account for this enrichment. Oxygen isotope data are generally consistent with the vertical leakage hypothesis.

As previously noted, groundwater in the carbonate aquifer beneath Frenchman Flat is inferred to originate from the White River flow system via Pahranagat Valley (Winograd and Friedman, 1972). Both $\delta^{18}O$ and $^{36}Cl/Cl$ data indicate that the groundwater evolves geochemically along this flowpath. Large carbonate springs in Pahranagat Valley have $\delta^{18}O$ values near -14.4‰, whereas carbonate groundwater beneath Frenchman Flat has $\delta^{18}O$ values between -13.9‰ and -14.2‰. The small $\delta^{18}O$ increase between Pahranagat Valley and Frenchman Flat suggests mixing with isotopically heavier (less negative) water. One possible origin of this mixing component is from the overlying Cenozoic aquifers, although mixing due to vertical leakage may occur along the *entire* flowpath from Pahranagat Valley, as opposed to only within the Frenchman Flat basin. The carbonate springs in Pahranagat Valley also exhibit much higher $^{36}Cl/Cl$ ratios (6.1 to 6.5 $\times 10^{-13}$) compared to carbonate groundwater in Frenchman Flat (1.7 to 2.3 $\times 10^{-13}$), reflecting significant water-rock reaction along the flowpath.

Comparison with Radiocarbon Data

A comparison of $^{36}Cl/Cl$ and dissolved inorganic ^{14}C data further illustrates the chemical evolution of groundwater due to water-rock interaction processes. Carbonate aquifer groundwaters inherit their high chloride concentrations and low $^{36}Cl/Cl$ ratios from the dissolution of carbonate rock. The same process causes the groundwater to evolve toward very low ^{14}C values. On a plot of $^{36}Cl/Cl$ vs. ^{14}C (Figure 4), the carbonate groundwaters show a pattern of evolution toward zero values for both parameters due to a near absence of ^{36}Cl and ^{14}C within the Paleozoic carbonate rock matrix.

Groundwater from the alluvial and volcanic aquifers shows more dispersion in ^{14}C, and includes samples with low ^{14}C values but high $^{36}Cl/Cl$ ratios. In the latter case, the groundwater may have evolved toward lower ^{14}C values by dissolution/exchange reactions on secondary calcite, which occurs along grain interstices or as fracture-linings. Secondary calcite may contain less chloride than the Paleozoic carbonate rocks because it was precipitated from fresh water as opposed to a marine environment. Conversely, direct reaction with detrital carbonate clasts in the alluvium will tend to increase chloride concentrations and decrease both $^{36}Cl/Cl$ ratios and ^{14}C values.

Chloride Leaching Experiments on ER-5-3 #2 Drill Cuttings

- ***Chloride concentration data***

Water leaching experiments were performed to extract the chloride in rock samples from various depth intervals in the ER-5-3 #2 borehole. Analytical results are shown in Table 2. The column titled "Leaching Expt #1" summarizes chloride concentration data (in ppm leachable Cl by weight, or ppmw) for twelve different samples that were crushed and sieved to various size fractions, and leached for three days in deionized water. For all samples, the concentration of leachable chloride tends to increase with decreasing grain size, reflecting the higher surface area to volume ratio of the finer-grained samples.

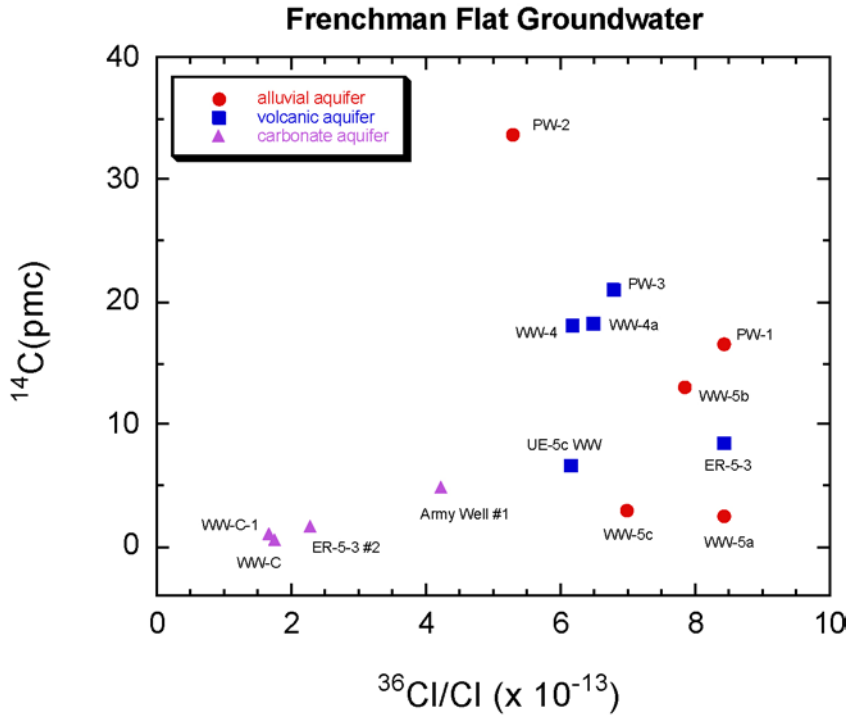

Figure 4. Plot of ^{14}C (percent modern carbon) vs. $^{36}Cl/Cl$ ratios (x 10^{-13}) for groundwater samples from Frenchman Flat and vicinity.

Leachable chloride is plotted as a function of depth in Figure 5 using Cl data from the smallest grain size fraction of each sample. The ER-5-3 #2 stratigraphic column (from IT Corporation, 2000a) is included for comparison. The highest Cl concentrations were extracted from the 940-990 ft interval (alluvium) and the 4780-4820 ft interval (carbonate), each yielding more than 20 ppmw. Surprisingly, one of the lowest measured Cl concentrations was also in an alluvium sample, from 1330-1360 ft depth (2.0 ppmw). This implies an extremely heterogeneous chloride distribution within the alluvial matrix. It should be noted that coarse sand and pebble sized lithic fragments were separated from the fine-grained matrix during sieving to avoid incorporating carbonate clasts that would skew the results. Leaching of the tuffaceous volcanic rocks yielded chloride concentrations between 3.0 and 11.7 ppmw on the smallest size fraction, with a median value of 4.6 (n = 8). The two carbonate rock samples yielded chloride concentrations of 22.6 and 9.9 ppmw.

A sequential leaching experiment (Leaching Expt #2) was performed on several samples that were previously leached in experiment #1, although in this case the different size fractions were combined. The objective was to determine how much additional chloride could be extracted after the samples had already been leached. In each case, a measurable amount of additional chloride was released, but concentrations were typically <25% of the highest value obtained in the first experiment.

In general, the concentration of chloride leached from the rock tends to be much lower than the chloride concentration in groundwater from the corresponding hydrostratigraphic interval. This suggests that the bulk leachable chloride in the rock generally is *not* in equilibrium with chloride in the groundwater. Neglecting mineral dissolution effects, the concentration gradient between the groundwater and the rock will tend to favor diffusion of chloride *into* the rock matrix.

• ***Chlorine-36 in leachate samples***

Chlorine-36 targets were prepared for all twelve rock samples discussed in the preceding section. However, several factors impeded efforts to obtain $^{36}Cl/Cl$ data. A subset of samples was lost when the sample vessels cracked in a centrifuge. The remaining (unleached) drill cuttings were used to prepare a second batch of samples, but the chloride yield was generally small, and the resulting beam current was in some cases too low to produce a reliable measurement on the accelerator mass spectrometer. Six samples produced $^{36}Cl/Cl$ results – but four of the six had unusually high $^{36}Cl/Cl$ ratios, implying contamination with "bomb pulse" chloride that was likely picked up during target preparation. In the end, only two analyses gave reasonable and reliable results. These data are reported below, along with data from two previous chloride leaching experiments (Moran and Rose, 2000).

The most notable aspect of the $^{36}Cl/Cl$ results in Table 5 is that they are consistently lower than the $^{36}Cl/Cl$ ratios of groundwater from similar hydrostratigraphic intervals. For example, alluvial aquifer groundwater has a mean $^{36}Cl/Cl$ ratio of $(756 \pm 126) \times 10^{-15}$ (n = 6) compared with a rock leachate ratio of $(250 \pm 50) \times 10^{-15}$ measured on ER-5-3 #2 alluvium. Mean ratios for volcanic and carbonate aquifer groundwaters are $(639 \pm 30) \times 10^{-15}$ and $(249 \pm 120) \times 10^{-15}$ respectively (n = 4 in each case), whereas rock leachate ratios are more than an order of magnitude lower. These results support the interpretation that the ^{36}Cl in the rock is not in equilibrium with the ^{36}Cl in the surrounding groundwater, and suggest the primary source of the Cl and ^{36}Cl is not from rock leaching. This is particularly true of groundwater from the alluvial and volcanic aquifers.

Table 5. $^{36}Cl/Cl$ results from rock leaching experiments

Sample	Depth Interval (ft bgs)	Lithology	Leachable Cl (ppmw)	$^{36}Cl/Cl$ ($\times 10^{-15}$)
ER-5-3 #2	940-990	Alluvium (Qta)	22.3	250 ± 50
ER-5-3 #2	4150-4200	Tuff (Tcb)	4.4	56 ± 8
UE-7f	2063	Tuff (Tn)	0.7	48 ± 36
Army Well #1	1134	Limestone (Cb)	76.5	11 ± 6

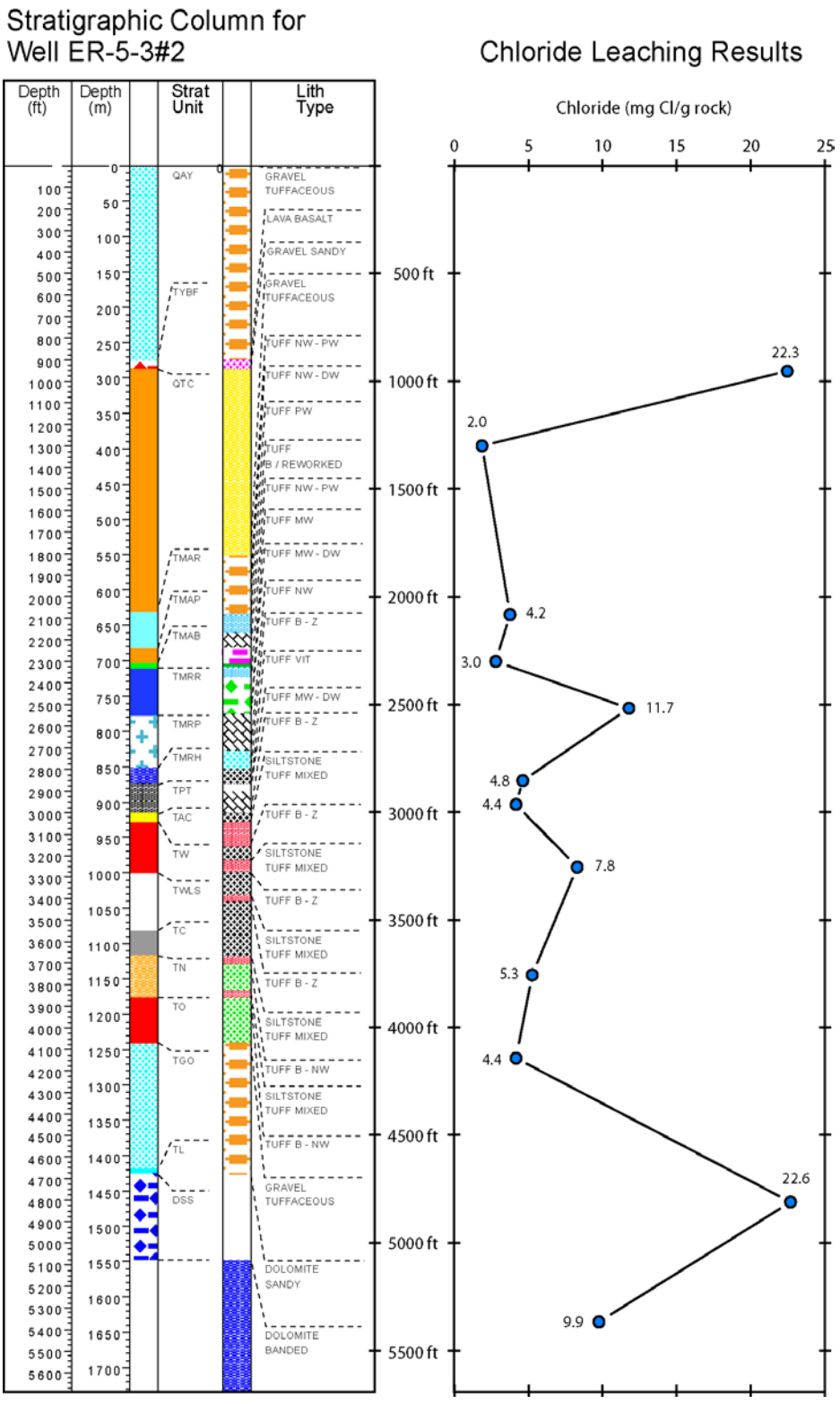

Figure 5. Plot of leachable chloride (ppm by wt) as a function of depth for chloride leached from the smallest grain size fraction of lithologic samples from ER-5-3 #2. The stratigraphic column for ER-5-3 #2 is included for comparison (from IT Corporation, 2000a).

The measured leachate $^{36}Cl/Cl$ ratios in Table 5 are probably similar to the ratios in the bulk rock. For instance, the very low $^{36}Cl/Cl$ ratio of leachable chloride in Army Well #1 limestone is consistent with the fact that the rock should be almost devoid of ^{36}Cl due to its extreme age. The low U and Th concentrations in carbonate rocks result in decreased secular equilibrium $^{36}Cl/Cl$ ratios relative to volcanic rocks. Hence, the carbonate rock leachate has a $^{36}Cl/Cl$ ratio of approximately 10×10^{-15} while the two volcanic tuff leachates have slightly higher ratios of 48×10^{-15} and 56×10^{-15} (Table 5). Given that the low $^{36}Cl/Cl$ ratios in the carbonate groundwaters are inherited from dissolution of the rock matrix, the extent to which the carbonate waters exhibit "non-zero" values largely reflects their remnant initial ratios (inherited during recharge) plus ^{36}Cl acquired during mixing with groundwater of different origin.

In general, the lack of equilibrium between the rock and groundwater ^{36}Cl implies the rate of exchange between these two ^{36}Cl "reservoirs" is relatively slow. In the alluvial and volcanic aquifers, many groundwater samples still have $^{36}Cl/Cl$ ratios above the modern initial value, reflecting recharge conditions from 10 to 20 thousand years ago. However, we also see at least one case where reaction with carbonate detrital material in the alluvium has substantially decreased the $^{36}Cl/Cl$ ratio of the groundwater (ER-5-4). We can conclude that the Paleozoic carbonate rock represents the most reactive matrix in both the lower carbonate and the alluvial aquifers. In the alluvial aquifer, the extent of water-rock reaction is likely determined by the relative abundance of Paleozoic carbonate detritus that a groundwater encounters along its flowpath.

Discussion

Vertical transport and mixing processes in Frenchman Flat

Since we are unable to use the results of the chloride leaching experiments to constrain vertical transport rates, we must rely on interpretations of the groundwater data. Examination of $^{36}Cl/Cl$ mixing relationships provides insight into the relative volume of vertical flux from the volcanic aquifer to the carbonate aquifer. Figure 6 is a plot of $^{36}Cl/Cl$ vs. 1/Cl for Frenchman Flat groundwater samples. Simple mixing processes are linear on this plot. The plot includes the end-member composition for groundwater in equilibrium with carbonate rock (shown as a black triangle), which is represented by the rock leachate data for Army Well #1 limestone (Table 5). The chloride concentration of this end-member may vary somewhat, but will be close to the value represented here.

A hypothetical mixing line is shown in Figure 6 extending from the ER-5-3 data point (alluvial/volcanic groundwater) to the carbonate water/rock end member. This line passes through the data points for the carbonate aquifer samples (WW-C, WW-C1, ER-5-3 #2, and Army Well #1) and is consistent with mixing of groundwater from the Cenozoic aquifers with the underlying carbonate aquifer (i.e. vertical leakage). Note that the carbonate groundwater from well ER-5-3 #2 shows an apparent enrichment in its $^{36}Cl/Cl$ ratio compared to WW-C and WW-C1, implying it contains a larger fraction of groundwater from the Cenozoic aquifers. We can estimate the amount of Cenozoic water in ER-5-3 #2 assuming a two component mixing process.

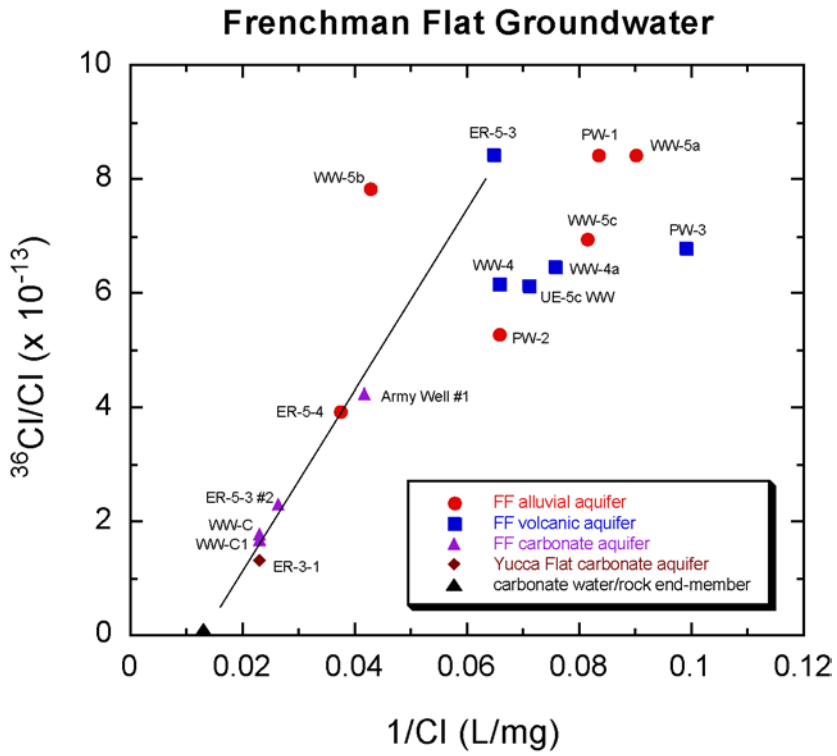

Figure 6. Plot of $^{36}Cl/Cl$ ratios (x 10^{-13}) vs. 1/Cl (in L/mg) for groundwater samples from Frenchman Flat and vicinity. The end-member composition for groundwater in equilibrium with carbonate rock (black triangle) is represented by rock leachate data for Army Well #1 limestone. Mixing trends are linear on this plot. A hypothetical mixing line is shown extending from the ER-5-3 data point (alluvial/volcanic groundwater) to the carbonate water/rock end member, passing through the data points for carbonate aquifer samples. This trend is consistent with mixing of groundwater from the Cenozoic aquifers with the underlying carbonate aquifer (i.e. vertical leakage).

We know that prior to mixing, the carbonate groundwater was not fully evolved to the carbonate water/rock end-member, so we must assume a pre-mixing end-member. WW-C1 has the lowest $^{36}Cl/Cl$ ratio (1.66×10^{-13}) of the carbonate groundwater samples in this study (Table 4). A slightly lower ratio was measured at well ER-3-1 (1.32×10^{-13}) which is located just east of Yucca Flat, ~20 km north of Frenchman Flat. ER-3-1 groundwater presumably originated along a flowpath similar to that of the carbonate groundwater beneath Frenchman Flat, and plots near the mixing line in Figure 6, so it may be reasonable to use as a limiting condition in the mixing equation. We will assume for now that the Cenozoic groundwater end-member is represented by well ER-5-3 ($^{36}Cl/Cl = 8.42 \times 10^{-13}$). The mixing equation is:

$$X_m R_m C_m = X_1 R_1 C_1 + X_2 R_2 C_2$$

where X is the fractional amount of each component, R is the $^{36}Cl/Cl$ ratio, C is the chloride concentration, and the subscripts refer to the mixed water [m], the carbonate

aquifer end-member [1] and the Cenozoic aquifer end-member [2]. Since we are dealing with a two component system, $X_m = X_1 + X_2 = 1$, and we can rewrite the equation in terms of one unknown, the fractional amount of carbonate groundwater (X_1):

$$R_m = X_1R_1(C_1/C_m) + (1 - X_1)R_2(C_2/C_m)$$

Inserting values for the mixed water (ER-5-3 #2), the carbonate groundwater end-member (ER-3-1), and the Cenozoic groundwater end-member (ER-5-3), we obtain a value of $X_1 = 0.59$, or 59% carbonate groundwater. This implies that approximately 41% of the groundwater in ER-5-3 #2 originated from the overlying Cenozoic units. If we use WW-C1 as the carbonate groundwater end-member, we obtain a more modest estimate of 25% Cenozoic groundwater. Note that the Cenozoic groundwater composition used in this calculation (ER-5-3) is from a maximum depth of 2549 ft, and probably includes a significant component of groundwater from the alluvial aquifer. Groundwater leaking into the carbonate aquifer at the base of the volcanic section may have a somewhat lower $^{36}Cl/Cl$ ratio and higher chloride concentration.

The lowest $^{36}Cl/Cl$ ratio among the Cenozoic groundwater samples was observed in well ER-5-4 (3.94×10^{-13}), which plots on the mixing line in Figure 6. If we assume this is similar to the $^{36}Cl/Cl$ groundwater ratio near the base of the volcanic section, we can recalculate the mixing proportions for ER-5-3 #2 groundwater. Using WW-C1 as the carbonate groundwater end-member, we calculate a revised Cenozoic mixing component of 44%. Assuming a more "evolved" Cenozoic end-member clearly does little to change the estimated mixing proportions. Unfortunately, we cannot independently test the $^{36}Cl/Cl$ mixing models using $\delta^{18}O$ or δD data because the groundwater from these wells all have nearly identical stable isotope compositions (Table 4).

In general, the $^{36}Cl/Cl$ mixing models suggest that between 25 and 44% of the groundwater in ER-5-3 #2 must be derived from the overlying Cenozoic aquifers in order to account for the observed enrichment in ^{36}Cl relative to WW-C1 and ER-3-1. We assume that the Cenozoic groundwater component was not introduced during pumping (i.e. due to drawdown from the overlying volcanic units). ER-5-3 #2 was recompleted in March 2001 (prior to sampling) with the specific objective of isolating access to the carbonate aquifer (IT Corporation, 2001). It is likely that some fraction of the Cenozoic groundwater component was added along the flowpath, before the water reached the Frenchman Flat basin. However, we would emphasize the fact that the mixing ratios for ER-5-3 #2 were calculated relative to nearby wells with similar flowpath histories. Since *all* of these wells are likely to contain a previously inherited component of groundwater from the overlying Cenozoic aquifers, the elevated $^{36}Cl/Cl$ ratio in ER-5-3 #2 may reflect an additional mixing component that was introduced within the Frenchman Flat basin.

Hydrologic mass balance considerations

On the basis of hydraulic data, Winograd and Thordarson (1975) estimated a net vertical groundwater flux of "no more than" 70 ac-ft/yr (8.6×10^5 m^3/yr) from the Cenozoic aquifers and aquitards to the underlying carbonate aquifer in Frenchman Flat. Assuming vertical crossflow through a 180 km^2 area in Frenchman Flat and an effective interstitial

porosity of 10%, this corresponds to an average vertical velocity of 4.8×10^{-3} m/yr.* In Yucca Flat, the magnitude of vertical transport was estimated to be in the range of 25 to 65 ac-ft/yr. Assuming that downward leakage also occurs in the four valleys that lie between Pahranagat Valley and the NTS (Tikaboo Valley, Emigrant Valley, northern Three Lakes Valley, and northern Indian Springs Valley), then the cumulative leakage is estimated to be between 150 and 400 ac-ft/yr (Winograd and Thordarson, 1975; p. 93). Laczniak et al. (1996) point out that this estimate assumes water moves only through primary interstices, and does not take into account increases in permeability associated with fractures and faults.

Estimates of carbonate aquifer underflow through the NTS from Pahranagat Valley vary from a low value of 3,730 ac-ft/yr (4.6×10^6 m^3/yr; Kirk and Campana, 1990) to a high value of 13,620 ac-ft/yr (1.68×10^7 m^3/yr; Sadler et al., 1992). Winograd and Friedman (1972) estimated an underflow rate of about 6,000 ac-ft/yr (7.4×10^6 m^3/yr) on the basis of a deuterium mass balance model for the Ash Meadows springs. The value used in the UGTA regional flow model was 7,990 ac-ft/yr (9.86×10^6 m^3/yr; DOE/NV, 1997). These estimates include underflow into *both* Yucca and Frenchman Flats from the east. If we accept the UGTA model value of 7,990 ac-ft/yr, then the cumulative downward leakage rate from the Cenozoic aquifers predicted by Winograd and Thordarson (1975) would constitute only 2 to 5% of the total carbonate aquifer flux. This is significantly less than the 25 to 44% mixing component estimated for ER-5-3 #2 groundwater on the basis of ^{36}Cl/Cl mass balance calculations. There are several possible explanations for this discrepancy.

One obvious possibility is that Winograd and Thordarson's (1975) vertical flux estimate somewhat under-predicts the actual transport rates. To achieve the 25 to 44% mixing component predicted from the ^{36}Cl/Cl data, the total vertical flux within the six basins contributing Cenozoic groundwater would need to be in the range of 2,000 to 3,500 ac-ft/yr. If we assume that roughly one-sixth of the flux occurs in Frenchman Flat, this translates to a vertical transport flux of between 330 and 585 ac-ft/yr, and an average vertical velocity between 2.3×10^{-2} and 4.0×10^{-2} m/yr (using the same cross-sectional area and effective interstital porosity values given above). We can use these calculated velocities to estimate the average time needed for a water particle to move from the top to the bottom of the volcanic section. The saturated thickness of the volcanic section is ~790 m in ER-5-3 #2, although this value may more than double near the center of the basin. Assuming a 790 m thickness, the average vertical travel time will be between 20,000 and 34,000 years. Integrated travel times may be greater than this if groundwater in the Cenozoic aquifers flows laterally to a hydraulic sink prior to vertical transport.

Winograd and Thordarson (1975; p. 56) noted that increased recharge during the pluvial period may have raised the water table by "hundreds of feet" relative to present day levels. Because the head differential between the Cenozoic strata and the lower carbonate aquifer probably was greater during and immediately after the last pluvial

* The vertical velocity is determined from the equation $Q = Apv$, where Q is the groundwater flux, A is the cross-sectional area, p is the effective interstitial porosity, and v is the average linear velocity.

period (~10,000 years ago), groundwater near the base of the tuff aquitard today may have moved through the Cenozoic section in less time than these calculations suggest (see Winograd and Thordarson, 1975; p. 114). Nevertheless, the estimated flow velocities are generally very small, even with the increased vertical fluxes required to account for the $^{36}Cl/Cl$ mixing relationships.

Another possible explanation for the large apparent fraction of Cenozoic groundwater in ER-5-3 #2 is that transport processes have *locally* enhanced the relative abundance of Cenozoic groundwater in the carbonate aquifer. For example, there may be a nearby fault or fracture system acting as a conduit for vertical transport (cf. Fabryka-Martin et al., 1993). Alternatively, the portion of the carbonate aquifer penetrated by ER-5-3 #2 may have an unusually low transmissivity, allowing a gradual accumulation of the Cenozoic groundwater-mixing component over time. Hershey and Acheampong (1997) estimated linear groundwater flow velocities of 0.9 to 5.8 m/yr along a flow path between WW-C1 and Army Well #1 using groundwater ^{14}C model ages. Using the same method, Thomas et al. (1996) predicted an average linear velocity of 26 m/yr for the regional flow path between Pahranagat Valley and Ash Meadows. Although both flow paths pass through portions of Frenchman Flat, the flow velocity estimates vary by approximately an order of magnitude. This could imply that groundwater flow rates are slower in the carbonate aquifer underlying Frenchman Flat relative to the entire Death Valley regional flow system. Winograd and Pearson (1976) suggested that water moving through Frenchman Flat is transported primarily along preferred pathways in the lower carbonate aquifer. Flow channeling is likely to be strongly controlled by faults, and hence, understanding the structural controls on groundwater flow patterns in the basin is likely to be important in predicting transport rates within the carbonate aquifer.

Lastly, it is possible that ER-5-3 #2 contains less of a Cenozoic groundwater component than predicted, and its $^{36}Cl/Cl$ ratio simply reflects geochemical evolution along a different flowpath than that of WW-C1 or ER-3-1. However, the difference in hydraulic head between the volcanic and carbonate aquifers in Frenchman Flat together with the high Na^+ and SO_4^{2-} concentrations in ER-5-3 #2 tend to support Winograd and Thordarson's (1975) original argument for vertical leakage.

Conclusions and Recommendations

The interpretations presented here were developed on the basis of a small data set and include a number of assumptions. In spite of these limitations, the $^{36}Cl/Cl$ results provide a useful independent measure of groundwater transport processes and flow rates that assist the verification of CAU-scale flow and transport modeling. Our primary conclusion is that the vertical transport rates of soluble, non-sorbing radionuclides in Frenchman Flat are very slow, requiring tens of thousands of years to move through the saturated column of alluvium and volcanic rocks. If transport rates in the vicinity of ER-5-3 #2 have been augmented by groundwater flow along faults, it would imply that flow rates through the rock matrix are even slower than we have estimated. Given the time scales for conservative transport, we infer that highly sorptive radionuclides are unlikely to ever pass through the Cenozoic section in measurable concentrations.

As is always the case, our interpretations could be improved by additional data, in particular from the carbonate aquifer and the lower portion of the volcanic section. With the planned development of well ER-5-4 #2 in FY 2002, it may be possible to determine whether the $^{36}Cl/Cl$ results from well ER-5-3 #2 are typical of deep groundwater beneath Frenchman Flat, or if the observed Cenozoic groundwater "enrichment" is localized at this well. If the latter is true, it would suggest that fault-controlled vertical transport is an important consideration during CAU-scale modeling in Frenchman Flat. In general, our understanding of transport processes through the volcanic section underlying Frenchman Flat is very poor. The UGTA project has initiated a study of the tuff confining unit (TCU) in Yucca Flat in an attempt to better understand vertical transport in that basin. Hence, there may be value in attempting to demonstrate the transferability of the Yucca Flat TCU data analysis to Frenchman Flat. To help meet this goal, it may be desirable to evaluate the physical and mineralogical properties of core samples returned from drilling at ER-5-4 #2. This would permit a direct comparison of samples from the volcanic section in both basins.

The main conclusions of this study are as follows:

(1) Groundwaters in the Cenozoic alluvial and volcanic aquifers typically exhibit high $^{36}Cl/Cl$ ratios (5.27 to 8.43×10^{-13}) and low Cl concentrations (10 to 23 mg/L). In some cases, lower $^{36}Cl/Cl$ ratios may result from reaction with carbonate rock clasts in the alluvium, as seen at well ER-5-4 (3.94×10^{-13}). This process is likely to depend on the relative abundance of carbonate rock detritus along a particular flowpath.

(2) Many of the alluvial and volcanic aquifer groundwaters have $^{36}Cl/Cl$ ratios greater than the value expected for modern recharge in this area (~5.0 to 6.0×10^{-13}). The elevated ratios are consistent with predicted increases in atmospheric ^{36}Cl production during late Pleistocene time, implying significant groundwater recharge occurred during the last pluvial period. This interpretation is corroborated by groundwater oxygen isotope data.

(3) Carbonate aquifer groundwaters typically exhibit relatively low $^{36}Cl/Cl$ ratios (1.66 to 4.23×10^{-13}) and high Cl concentrations (24 to 44 mg/L) that are inherited from water-rock interaction with the carbonate host rock. Groundwater from well ER-5-3 #2 in northern Frenchman Flat is enriched in $^{36}Cl/Cl$ (2.29×10^{-13}) relative to nearby wells completed in the carbonate aquifer (e.g. WW-C1). This enrichment can be modeled as a mixing process related to the vertical leakage of groundwater from the tuff aquitard to the lower carbonate aquifer. Mixing models suggest that 25 to 44% of the water in ER-5-3 #2 originated from the overlying Cenozoic aquifers.

(4) Mass balance calculations developed from the ER-5-3 #2 mixing results and regional flow estimates indicate vertical transport fluxes in Frenchman Flat are on the order of 330 to 585 ac-ft/yr. Assuming vertical crossflow through a 180 km^2 area in Frenchman Flat and an effective interstitial porosity of

10%, this flux corresponds to an average vertical velocity of 0.02 to 0.04 m/yr. This implies a mean travel time of 20,000 to 34,000 yrs for a water particle moving vertically through the 790 m volcanic section in ER-5-3 #2. These calculated flow rates are 5 to 8 times greater than those predicted by Winograd and Thordarson (1975), but still imply very slow vertical transport of contaminants.

(5) Geologic structures beneath Frenchman Flat may locally enhance the vertical transport of groundwater through the alluvial and volcanic section. It is not possible to distinguish whether the $^{36}Cl/Cl$ enrichment at ER-5-3 #2 is due to vertical leakage along a fast flowpath, or simply the gradual accumulation of groundwater that percolated downward at ambient flow velocities. The latter case may suggest slow lateral transport rates within the carbonate aquifer beneath Frenchman Flat. Faults may also serve as flow barriers that compartmentalize lateral groundwater transport, accounting for some of the observed heterogeneity in geochemical signatures

(6) Chloride leaching experiments were performed on twelve different rock samples from the ER-5-3 #2 borehole. The highest concentrations of chloride were extracted from carbonate rock (22.6 ppmw) and one sample of alluvium (22.3 ppmw). Tuffaceous volcanic rocks yielded lower chloride concentrations, ranging from 3.0 to 11.7 ppmw on eight samples.

(7) $^{36}Cl/Cl$ ratios were successfully measured on only two leachate samples, but when combined with earlier leaching results these data show that the ^{36}Cl in the rock is not in equilibrium with the ^{36}Cl in the surrounding groundwater. This implies the rate of exchange between the two ^{36}Cl reservoirs is relatively slow. Groundwater from the volcanic aquifers is generally farthest from equilibrium with the host rock.

References

Bentley, H.W., and Davis, S.N. (1982) Applications of AMS to hydrology. In: Kutschera, W. (ed.), *2nd Annual Symposium on Acceleration Mass Spectrometry.* Argonne National Laboratory, ANL-PHY 81-1, pp 193-227.

Bentley, H.W., Phillips, F.M., Davis, S.N., Gifford, S., Elmore, D., Tubbs, L.E., and Gove, H.E., (1982) Thermonuclear ^{36}Cl pulse in natural water. Nature, 300, pp 737-740.

Bentley, H.W., Phillips, F.M., and Davis, S.N. (1986) Chlorine-36 in the terrestrial environment. In: P.Fritz and J.Ch. Fontes (eds.), Handbook of Environmental Isotope Geochemistry, Volume 2, The Terrestrial Environment, B. Elsevier, Amsterdam, pp 427-480.

Bryant, E.A. (1992) The Cambric Migration Experiment – A Summary Report. Los Alamos National Laboratory, LA-12335, September 1992.

Claassen, H.C. (1986) Late-Wisconsin paleohydrology of the west-central Amargosa Desert, Nevada, U.S.A. Chem. Geol., 58, pp 311-323.

Cornett, R.J., Andrews, L.A., Chant, L.A., Davies, W.G., Greiner, B.R., Imahori, Y., Koslowsky, V.T., Kotzer, T., Milton, J.C.D., and Milton, G.M. (1997) Is ^{36}Cl from weapons test fallout still cycling in the atmosphere? Nucl. Inst. and Meth. in Phys. Res. B, 123, pp 378-381.

Davis, S.N., Cecil, D., Zreda, M., and Sharma, P. (1998) Chlorine-36 and the initial value problem. Hydrogeology Journal, 6, 104-114.

Davisson, M.L., Smith, D.K., Kenneally, J.M., and Rose, T.P. (1999) Isotope hydrology of southern Nevada groundwater: stable isotopes and radiocarbon. Water Resour. Res., 35, pp 279-294.

Dettinger, M.D., Harrill, J.R., Schmidt, D.L., and Hess, J.W. (1995) Distribution of carbonate-rock aquifers and the potential for their development, southern Nevada and adjacent parts of California, Arizona and Utah. U.S. Geol. Survey Water-Resources Investigations Report 91-4146, 100 p.

DOE/NV (1997) Regional Groundwater Flow and Tritium Transport Modeling and Risk Assessment of the Underground Test Area, Nevada Test Site, Nevada. U.S. Department of Energy, Nevada Operations Office, Environmental Restoration Division, DOE/NV-477, October 1997, Las Vegas, NV.

DOE/NV (1999) Corrective Action Investigation Plan for Corrective Action Unit 98: Frenchman Flat, Nevada Test Site, Nevada. U.S. Department of Energy, Nevada Operations Office, Environmental Restoration Division, DOE/NV-478-Rev.1, July 1999, Las Vegas, NV, 219 p.

DOE/NV (2000) United States Nuclear Tests, July 1945 through September 1992. U.S. Department of Energy, Nevada Operations Office, DOE/NV-209-Rev.15, December 2000, Las Vegas, NV, 162 p.

Elmore, D., Fulton, B.R., Clover, M.R., Marsden, J.R., Gove, H.E., Naylor, H., Purser, K.H., Kilius, L.R., Beukins, R.P., and Litherland, A.E. (1979) Analysis of ^{36}Cl in environmental water samples using an electrostatic accelerator. Nature, 277, pp 22-25.

Fabryka-Martin, J., Wightman, S.J., Murphy, W.J., Wickham, M.P., Caffee, M.W., Nimz, G.J., Southon, J.R., and Sharma, P. (1993) Distribution of chlorine-36 in the unsaturated zone at Yucca Mt.: An indicator of fast transport paths. FOCUS '93: Site Characterization and Model Validation, Las Vegas, NV, 26-29 Sept 1993.

French, R.H. (1985) Daily, seasonal, and annual precipitation at the Nevada Test Site, Nevada. Desert Research Institute, Water Resources Center Publication 45042, July 1985, 57 p.

Hainsworth, L.J., Mignerey, A.C., Helz, G.R., Sharma, P., and Kubik, W. (1994) Modern chlorine-36 deposition in southern Maryland, USA. Nuclear Instruments and Methods in Phys. Res. Sect. B - Beam Interactions with Materials and Atoms, 92, pp 345-349.

Harrill, J.R., Gates, J.S., and Thomas, J.M. (1988) Major groundwater flow systems in the Great Basin region of Nevada, Utah, and adjacent states. U.S. Geol. Survey Hydrologic Investigations Atlas, HA-694-C, 2 sheets, scale 1:1,000,000.

Hershey, R.L., and Acheampong, S.Y. (1997) Estimation of groundwater velocities from Yucca Flat to the Amargosa Desert using geochemistry and environmental isotopes. Desert Research Institute, Water Resources Center Publication 45157, 49 p.

Ingraham, N.L., Lyles, B.F., Jacobson, R.L., and Hess, J.W. (1991) Stable isotopic study of precipitation and spring discharge in southern Nevada. Jour. Hydrol., 125, pp 243-258.

IT Corporation (1999) Underground Test Area Project Corrective Action Unit 98: Frenchman Flat, Volume II – Groundwater Data Documentation Package, Draft Rev. 0. Las Vegas, NV April 1999, 387 p.

IT Corporation (2000a) Frenchman Flat Well Cluster ER-5-3 Data Report – Preliminary Rev. 0. Las Vegas, NV, September 2000, 208 p.

IT Corporation (2000b) Geochem00b.mdb and a User's Guide to the Comprehensive Chemistry Database for Groundwater at the Nevada Test Site, Rev. 2. Las Vegas, NV, September 2000.

IT Corporation (2001) Addendum to the Frenchman Flat Well Cluster ER-5-3 Data Report – Preliminary Rev. 0. Las Vegas, NV, August 2001, 101 p.

Kenneally, J. (1995) Preliminary report evaluating the use of strontium and chloride concentrations and $^{87}Sr/^{86}Sr$ ratios as analogs for the dissolution of inorganic carbon. Lawrence Livermore National Laboratory, report prepared for the U.S. Department of Energy, Nevada Operations Office, Environmental Restoration Division, Underground Test Area Operable Unit, April 1995, 14 p.

Kirk, S.T., and Campana, M.E. (1990) A deuterium-calibrated groundwater flow model of a regional carbonate-alluvial system. Jour. Hydrol., 119, pp 357-388.

Laczniak, R.J., Cole, J.C., Sawyer, D.A., and Trudeau, D.A. (1996) Summary of hydrogeologic controls on groundwater flow at the Nevada Test Site, Nye County, Nevada. U.S. Geol. Survey Water-Resources Investigations Report 96-4109, 59 p.

Lyles, B.F., McKay, W.A., Chapman, J.B., and Tyler S.W. (1991) Hydrogeologic characterization of wells HTH-1, UE18r, UE6e, and HTH-3, Nevada Test Site. Desert Research Institute, Water Resources Center Publication 45087, June 1991, 73 p.

Mazaud, A., Laj, C., Bard, E., Arnold, M., and Tric, E. (1991) Geomagnetic field control of ^{14}C production over the last 80 ky: Implications for the radiocarbon time-scale. Geophys. Res. Lett., 18, 1885-1888.

Mifflin, M.D. and Hess, J.W. (1979) Regional carbonate flow systems in Nevada. Jour. Hydrol., 43, pp 217-237.

Mifflin, M.D. and Wheat, M.M. (1979) Pluvial lakes and estimated pluvial climates of Nevada. Nevada Bureau of Mines and Geology Bulletin 94, 57 p.

Moran, J.E., and Rose, T.P. (2000) A chlorine-36 study of regional groundwater flow in southern Nevada. Lawrence Livermore National Laboratory, report prepared for the U.S.

Department of Energy, Nevada Operations Office, Environmental Restoration Division, Underground Test Area Project, September 2000, 25 p.

Quade, J., Mifflin, M.D., Pratt, W.L., McCoy, W., and Burckle, L. (1995) Fossil spring deposits in the southern Great Basin and their implications for changes in water-table levels near Yucca Mountain, Nevada, during Quaternary time. Geol. Soc. Am. Bull., 107, pp 213-230.

Rose, T.P., Kenneally, J.M., Smith, D.K., Davisson, M.L., Hudson G.B., and Rego, J.H. (1997) Chemical and Isotopic Data for Groundwater in Southern Nevada. Lawrence Livermore National Laboratory, UCRL-ID-128000, 35 p.

Sadler, W.R., Campana, M.E., Jacobson, R.L., and Ingraham, N.L. (1992) A deuterium-calibrated discrete-state compartment model of regional groundwater flow, Nevada Test Site and vicinity. Desert Research Institute, Water Resources Center Publication 45088, 77 p.

Smith, D.K. (2001) Evaluation of the radiochemistry of near-field water samples at the Nevada Test Site applied to the definition of a Hydrologic Source Term. Lawrence Livermore National Laboratory report prepared for the National Nuclear Security Agency, Nevada Operations Office, Environmental Restoration Division, July 2001.

Spaulding, W.G. (1985) Vegetation and climates of the last 45,000 years at the Nevada Test Site and vicinity. U.S. Geological Survey Professional Paper 1329, 83 p.

Thomas, J.M., Welch, A.H., and Dettinger, M.D. (1996) Geochemistry and isotope hydrology of representative aquifers in the Great Basin region of Nevada, Utah, and adjacent states. U.S. Geol. Survey Professional Paper 1409-C, 100 p.

Tyler, S.W., Chapman, J.B., Conrad, S.H., Hammermeister, D.P., Blout, D.O., Miller, J.J., Sully, M.J., and Ginanni, J.M. (1996) Soil-water flux in the southern Great Basin, United States: Temporal and spatial variations over the last 120,000 years. Water Resour. Res., 32, pp 1481-1499.

Winograd, I.J., and Friedman, I. (1972) Deuterium as a tracer of regional groundwater flow, southern Great Basin, Nevada and California. Geol. Soc. Am. Bull., 83, pp 3691-3708.

Winograd, I.J., and Pearson, F.J., Jr. (1976) Major carbon-14 anomaly in a regional carbonate aquifer – Possible evidence for megascale channeling, south central Great Basin. Water Resour. Res., 12, pp 1125-1143.

Winograd, I.J., and Thordarson, W. (1975) Hydrogeologic and hydrochemical framework, south-central Great Basin, Nevada-California, with special reference to the Nevada Test Site. U.S. Geol. Survey Professional Paper 712-C, 126 p.

Appendix A

Descriptions of Lithologic Samples used in Chloride Leaching Studies

The following are brief descriptions of lithologic samples obtained from ER-5-3 #2 drill cuttings that were used in chloride leaching experiments. Samples are archived at the U.S. Geological Survey Core Library in Mercury, Nevada. Descriptions are based on observations of the authors, supplemented by unpublished data provided by Bechtel Nevada geologists (H.H. Gang and L.B. Prothro), and lithologic descriptions found in the preliminary data report for the ER-5-3 well cluster (IT Corporation, 2000a).

Depth Interval: 940-990 ft
Lithology: Alluvium
Stratigraphic Unit: Quaternary-Tertiary Alluvium (Qta)

Description: Sandy alluvium, moderately sorted, moderately indurated. Pale yellowish-brown matrix contains fine-grained felsic crystal fragments (quartz, feldspar) with subrounded volcanic and carbonate lithic fragments, typically ≤5 mm in size. Abundant calcite cement. Intact matrix pieces are uncommon.

Depth Interval: 1330-1360 ft
Lithology: Alluvium
Stratigraphic Unit: Quaternary-Tertiary Alluvium (Qta)

Description: Sandy and gravel, moderately sorted, moderately indurated. Grayish orange matrix contains abundant angular to subrounded, gray carbonate and quartzite lithic fragments, with much less abundant volcanic fragments and rare felsic crystal fragments. Lithics are generally ≤5 mm in size. Matrix is commonly cemented with calcite.

Depth Interval: 2110-2150 ft
Lithology: Ash-Flow Tuff
Stratigraphic Unit: Ammonia Tanks Tuff (Tma)

Description: Moderately-welded ash-flow tuff. Pale brown to greyish-brown color. Contains abundant feldspar phenocrysts to 2 mm in size (15%), minor quartz (<5%), and bronze-colored biotite phenocrysts to 2 mm (2-3%). Contains ~10% lt. brown to white pumice fragments; 10% volcanic lithic fragments.

Depth Interval: 2310-2340 ft
Lithology: Bedded Tuff
Stratigraphic Unit: Ammonia Tanks Tuff (Tma)

Description: Reworked, bedded tuff, pale gray to pale orangish gray in color. Contains common feldspar and quartz crystal fragments, <1-2 mm in size (5-10%) in a weakly calcareous, zeolitized matrix. Contains sparse biotite crystals (1-2%), and volcanic lithic fragments.

Depth Interval: 2520-2560 ft
Lithology: Ash-Flow Tuff
Stratigraphic Unit: Rainier Mesa Tuff (Tmr)

Description: Moderately-welded ash-flow tuff, light gray in color. Contains feldspar phenocrysts to 1.5 mm (~5%) with sanidine > plagioclase; glassy quartz grains to 1 mm (1-2%); biotite grains <1 mm in size (1%). Contains ~5% white to pale brown pumice fragments to 2 mm, commonly flattened; minor lithic fragments (~2%).

Depth Interval: 2830-2860 ft
Lithology: Bedded Tuff
Stratigraphic Unit: Tuff of Holmes Road (Tmrh)

Description: Bedded tuff, pale brown to grayish orange. Contains common feldspar and quartz phenocrysts to 2 mm (5-10%), and biotite crystals <1 mm in size (~3%). Common white pumice fragments (5%) up to 5 mm are strongly zeolitized, and sometimes rimmed with secondary Mn-oxides. Also contains common gray and grayish-brown lithic fragments (5%), ≤1 mm in size.

Depth Interval: 2920-2960 ft
Lithology: Ash-Flow Tuff
Stratigraphic Unit: Topopah Spring Tuff (Tpt)

Description: Moderately-welded ash-flow tuff. Reddish-brown to greyish-orange in color. Contains common feldspar phenocrysts up to ~2 mm in size (10%), rare quartz (~2%), and rare biotite up to 1 mm (<2%). Small brown pumice fragments are rarely observed (~1%); also contains rare volcanic lithic fragments (1-2%). Secondary fracture linings of chalcedony are fairly common.

Depth Interval: 3250-3280 ft
Lithology: Bedded Tuff
Stratigraphic Unit: Wahmonie Formation (Tw)

Description: Bedded (reworked) tuff and/or tuffaceous sediment. Brick-red to reddish brown in color. Contains common feldspar crystals, typically <0.5 mm in size (5-10%); minor quartz and biotite (2%); common volcanic lithic fragments.

Depth Interval: 3720-3760 ft
Lithology: Ash-Flow Tuff
Stratigraphic Unit: Tunnel Formation (Tn)

Description: Non-welded ash-flow tuff. Pinkish-brown to pale reddish-brown color. Contains ~5% feldspar phenocrysts, generally ≤ 1 mm in size; plagioclase crystals are commonly altered to a white, chalky color; quartz and biotite are very rare (<1%). Contains common white to pale brown pumice fragments (10%), generally < 3 mm in size, that appear to be devitrified to zeolite minerals. Minor volcanic lithic fragments (<5%).

Depth Interval: 4150-4200 ft
Lithology: Bedded and/or Non-Welded Tuff
Stratigraphic Unit: Bullfrog Tuff (Tcb)

Description: Grayish olive tuff with common white to pale pink zeolitized pumice fragments. Contains abundant phenocrysts of feldspar and quartz, typically ≤ 1 mm in size (5-10%), common biotite grains to 1 mm (~5%), and common silicified volcanic rock fragments.

Depth Interval: 4780-4820 ft
Lithology: Paleozoic Carbonate
Stratigraphic Unit: Sevy Dolomite (Dss)

Description: Pale pinkish-orange to orangish gray dolomite, medium-grained (recrystallized); well indurated, moderately porous.

Depth Interval: 5350-5390 ft
Lithology: Paleozoic Carbonate
Stratigraphic Unit: Laketown Dolomite (Sl)

Description: Light to dark gray banded dolomite, with thin calcite veinlets; fine-grained, well indurated, low porosity.

Chapter 8

Stable Isotope Investigation of Precipitation and Recharge Processes in Central Nevada

Timothy P. Rose

Executive Summary

Precipitation, spring water, and shallow infiltration samples were collected at four locations in central Nevada on a biannual basis beginning in 1999. Stable isotope analyses of these samples are used to determine the relative contribution of cool and warm season precipitation to the recharge budget, and to evaluate the timing and extent of evaporation during recharge. Cool-season precipitation (October to May) accounts for 75 to 80% of the precipitation total, most of which occurs as snowfall during the winter months. All precipitation samples have δD-δ^{18}O values that plot along the global meteoric water line, and exhibit little or no evidence of evaporation prior to infiltration. The average isotopic compositions (weighted by amount) for warm- and cool-season precipitation differ by 5.3 to 8.8‰ in δ^{18}O and 38 to 70‰ in δD, with isotopically lighter values occurring during the cool season. The mean annual precipitation is strongly weighted toward the cool season average.

Perched mountain springs located near each of the precipitation monitoring sites show little variation in their stable isotope compositions over time, and provide reasonable proxies for the average recharge composition at a given location. Three of the springs have isotopic signatures that indicate moderate amounts of evaporation during recharge, while a fourth spring is non-evaporated. The non-evaporated spring discharges from fractured granitic rock, and infiltration rates at this location may be sufficiently rapid to where evaporation is minimized. Projecting the isotopic values of the evaporated springs back to the global meteoric water line along typical evaporation trajectories reveals the initial composition of the precipitation. The results show that cool-season precipitation accounts for virtually all of the recharge at three of the sites, and >90% of the recharge at a fourth site.

Shallow soil infiltration samples collected in lysimeters show moderate to large variations in infiltration amount from year-to-year, independent of the total precipitation amount. The rate at which the snowpack melts may be an important control on the net infiltration flux, and on the corresponding amount of evaporation that is observed. When the amount of infiltration is relatively small (≤ 0.5 cm precipitation equivalent) the samples are evaporated. In contrast, larger amounts of infiltration show no evidence of evaporation and plot along the global meteoric water line. Slow infiltration rates will allow more time for evaporation, resulting in a larger net vapor loss that translates to lower infiltration fluxes. The lysimeter data also reveal that heavy isotope enrichment

processes that occur during aging of the snowpack cannot account for the evaporated isotopic signatures, as previously hypothesized, since this process will not be infiltration volume-dependent. Water vapor loss through the soil zone during slow infiltration is inferred to be the dominant control on evaporation.

Introduction

Reliable estimates of groundwater recharge rates are one of the key elements in any water budget model. Water budgets in turn provide the hydrologic framework necessary to develop numerical flow and transport models, such as those being used to predict contaminant transport at the Nevada Test Site (U.S. Department of Energy, 1997; D'Agnese et al., 1997). It is well known that only a fraction of the total precipitation that falls on a particular area actually reaches the water table. Recharge rates depend on a combination of factors including precipitation rate and intensity, infiltration rate, evapotranspiration, soil properties (porosity, thickness, storage capacity, hydraulic conductivity), and bedrock permeability (cf. Hevesi et al., 2002). Early estimates of recharge in Nevada were based on the Maxey-Eakin method (Maxey and Eakin, 1950), an empirically calibrated model that divides recharge areas into different zones on the basis of mean annual precipitation rates. While this approach is still used, more refined techniques have subsequently been developed that include modified versions of the Maxey-Eakin method (Hevesi and Flint, 1998), chloride mass balance calculations (Dettinger, 1989), and numerical modeling approaches (Hevesi et al., 2002).

The stable isotopes of hydrogen ($^{2}H/^{1}H$) and oxygen ($^{18}O/^{16}O$) have been widely used in recharge studies to identify groundwater source areas, to quantify recharge amounts, and to understand the role of evaporation during recharge (for review see Fontes, 1980; Ingraham et al., 1998; Coplen et al., 2000). A recent study comparing the stable isotope values of spring waters and precipitation in the Spring Mountains near Las Vegas concluded that springtime snowmelt may account for up to 90% of all groundwater recharge in southern Nevada (Winograd et al., 1998).

This report describes the preliminary results of a study designed to evaluate recharge processes at four sites in central Nevada using stable isotopes. The study area (Figure 1) is inferred to be the principal recharge center for a regional groundwater flow system that extends >200 km from mountainous regions in central Nevada, through the Nevada Test Site, and into the low desert along the Nevada-California border (Davisson et al., 1999; Rose and Davisson, 2002). The primary objectives of this study are: (1) to develop a data set to describe variations in precipitation and spring water isotopic compositions over time; (2) use these data to estimate the relative contributions of summer vs. winter precipitation to the net recharge budget; and (3) evaluate the timing and extent of evaporation (isotopic enrichment) processes occurring during recharge. Particular attention is given to the possibility that isotope fractionation processes during snow metamorphism may help to account for the evaporated stable isotope values of many Nevada groundwaters.

Hydrologic Setting

The study area is located in central Nevada, near the geographic center of the Basin and Range province. The physiography of this region is characterized by a series of subparallel north-south trending mountain ranges that are separated by broad alluvial basins (Figure 1). Elevations vary from about 1450 m to more than 3500 m above sea level. The climate in central Nevada is arid to semi-arid, with average precipitation rates ranging from 12 cm/yr in the driest valleys to >50 cm/yr in the highest ranges (Lamke and Moore, 1965). Summer convective storms account for up to one third of the annual

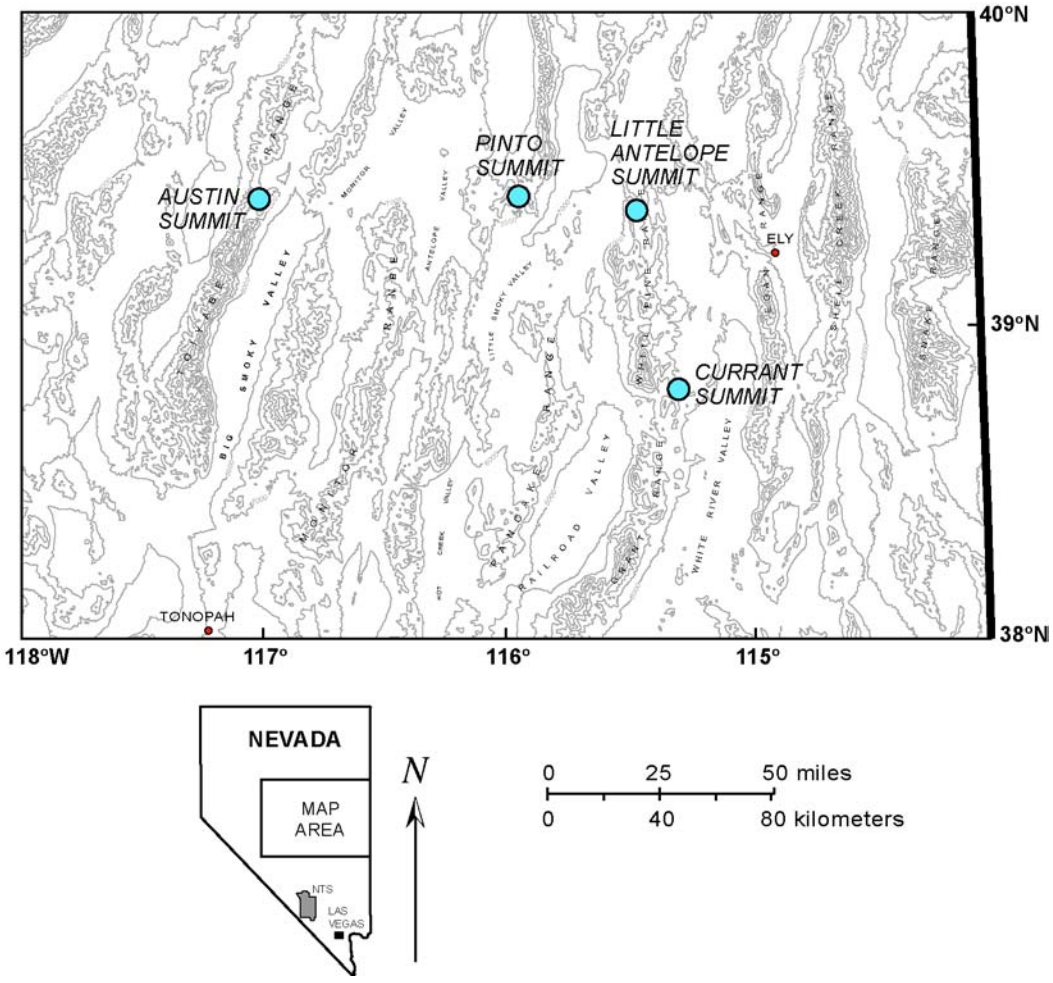

Figure 1. Topographic map of central Nevada showing the locations of monitoring sites for this study.

precipitation, but are typically of short duration and limited areal extent. High evapotranspiration rates during the summer months (Shevenell, 1996) tend to limit summer recharge contributions, except in the case of rare high intensity events. Winter storms associated with areally extensive low-pressure systems account for approximately

two thirds of the annual precipitation in Nevada (Houghton, 1969). These storms tend to be lower intensity, longer duration events that produce relatively large snowfall accumulations at high elevations. Rapid melting of the snowpack in the spring and early summer probably accounts for a majority of the annual recharge budget. Winograd et al. (1998) inferred that snowmelt provides up to 90% of all groundwater recharge in the Spring Mountains near Las Vegas.

High elevation areas in eastern and central Nevada form major recharge centers for regional flow systems that transport groundwater into southern Nevada (e.g. Eakin, 1966; Mifflin and Hess, 1979). These systems are typified by fracture-dominated flow through deep carbonate rock aquifers, driven by hydraulic gradients that are laterally continuous over hundreds of kilometers (Harrill et al., 1988). Continuity in the oxygen isotope ($\delta^{18}O$) values of groundwater along these flowpaths is consistent with major source areas in central Nevada (Davisson et al., 1999). Determining the recharge contribution to the regional water budget in this area is important to the interpretation of groundwater flow patterns through the Nevada Test Site. In particular, considerable uncertainty still exists regarding the amount of 'flow from the north' into the Pahute Mesa underground test area (e.g. Thomas et al., 2002) and water budgets for this area are presently constrained only by observed discharge rates at nearby springs (Reiner et al., 2002). In addition to contaminant transport issues, constraining the regional water budget is also important in terms of determining the availability of water resources to meet future needs. A reliable supply of water resources is critical to sustaining DOE/DOD operations in southern Nevada, and is also highly relevant to meeting the needs of the growing urban population in this region.

Stable Isotopes in the Hydrologic Cycle

Stable isotopes of hydrogen ($^{2}H/^{1}H$) and oxygen ($^{18}O/^{16}O$) are ideal hydrologic tracers because they are uniquely intrinsic to the water molecule. Oxygen and hydrogen isotope measurements are conventionally reported as delta (δ) values, representing the per mil (‰, or parts per thousand) difference in the isotope ratio of a sample (x) relative to a reference standard (std):

$$\delta = 1000[(R_x/R_{std}) - 1]$$

where R refers to the measured isotope ratio ($^{2}H/^{1}H$ or $^{18}O/^{16}O$). The internationally accepted standard for δD and $\delta^{18}O$ analyses of waters is Standard Mean Ocean Water (SMOW), which has a δ-value of zero for both hydrogen and oxygen. In general, meteoric waters from continental interiors have negative δ-values because they contain lower abundances of the heavy isotopes (^{2}H or ^{18}O) relative to the ocean.

In the water cycle, hydrogen and oxygen isotopes are fractionated (partitioned) between the liquid and vapor phases during evaporation and condensation processes, in accordance with well-known temperature-dependent relationships (cf. Criss, 1999). This leads to predictable variations in the stable isotope ratios of atmospheric precipitation as a function of latitude, elevation, and distance from the ocean (Dansgaard, 1964). Most large storm systems originate over the ocean. As a storm moves inland, the removal of

precipitation from the clouds gradually depletes the remaining water vapor in heavy isotopes (e.g. Ingraham and Taylor, 1991). This process reflects the tendency of the heavy isotopes to preferentially fractionate into the more condensed phase. In general, cooler air temperatures are associated with larger fractionation effects, such that winter precipitation often exhibits lighter (more negative) δD and $\delta^{18}O$ values than warm season precipitation.

Craig (1961) showed that the $\delta^{18}O$ and δD values of precipitation samples conform to the empirical linear relationship $\delta D = 8\delta^{18}O + 10$, known as the global meteoric water line (GMWL). This relationship approximately holds for modern precipitation samples from Nevada (e.g. Benson and Klieforth, 1989; Ingraham et al., 1991), although both the slope and y-intercept of the line can vary slightly with geographic location. The y-intercept of the GMWL is often referred to as the deuterium excess, or *d*-value, where $d = \delta D - 8\delta^{18}O$ (Dansgaard, 1964).

The process of evaporation is characterized by a kinetic isotope separation effect that concentrates the residual liquid in the heavier isotopes (Craig et al., 1963). Evaporated waters are shifted to the right of the GMWL along trajectories with a slope between about 3 and 6, with deuterium excess (*d*) values < 10. Evaporation effects are well documented in desert environments, and may occur both during the descent of rain droplets (Stewart, 1975), and during runoff and infiltration processes (e.g. Gat and Dansgaard, 1972; Barnes and Allison, 1988; Smith et al., 1992). Kinetic isotope enrichment effects also occur during snowpack aging due to mass transport processes within the snowpack (e.g. Stichler et al., 1981; Friedman et al., 1991). Since net evaporative losses are one of the dominant factors affecting water budgets, tracking the changes in stable isotope ratios at various steps in the recharge process can provide insight into the timing and relative amount of evaporation that occurs during recharge.

Previous Observations of Stable Isotope Variations in Central Nevada

Figure 2 shows a plot of $\delta^{18}O$ versus δD values of groundwater samples collected from perched mountain springs and regional carbonate springs in central Nevada (data from Rose and Davisson, 2002). Most samples have isotopic values that plot to the right of the GMWL, with *d*-values for individual samples ranging from +8 to -3, and an average *d*-value near +4. This is similar to the *d*-values observed in groundwater from arid basins throughout the world (e.g. Margaritz, et al., 1989; Sami, 1992). Note that the regional groundwaters exhibit a *d*-shift that is comparable to that of the mountain springs in the recharge areas. This suggests a link between the regional groundwaters and modern recharge centers in central Nevada, and implies the observed *d*-shift is inherited through evaporation processes during recharge.

Rose et al. (1999) studied the isotopic variations in winter snowpacks in central Nevada to determine whether the observed enrichments in spring waters may be related to processes occurring during snowpack aging and ablation. Snow recrystallizes over time due to heat transfer from the ground, producing temperature and vapor pressure gradients within the snowpack (Benson and Trabant, 1973). This so-called 'snow metamorphism'

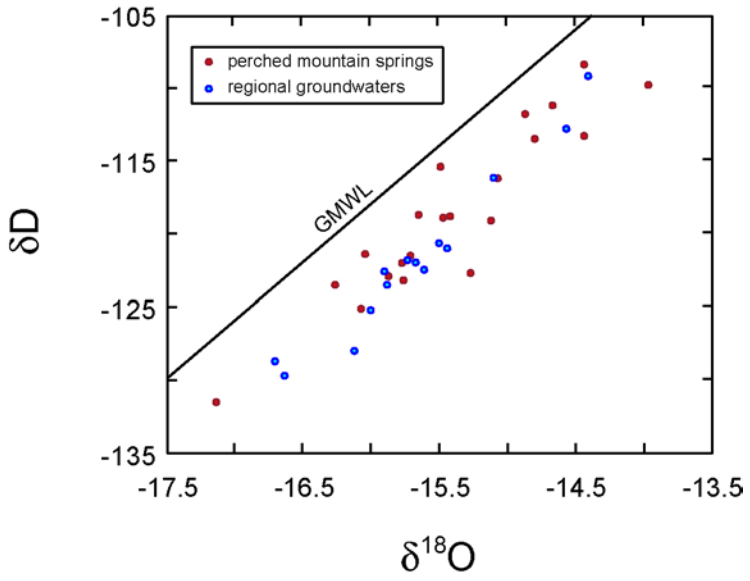

Figure 2. Plot of δD vs. $\delta^{18}O$ values of groundwater samples from perched mountain springs and regional aquifers in central Nevada. Groundwater samples are shifted to the right of the global meteoric water line (GMWL) with an average deuterium excess (*d*-value) of near +4.

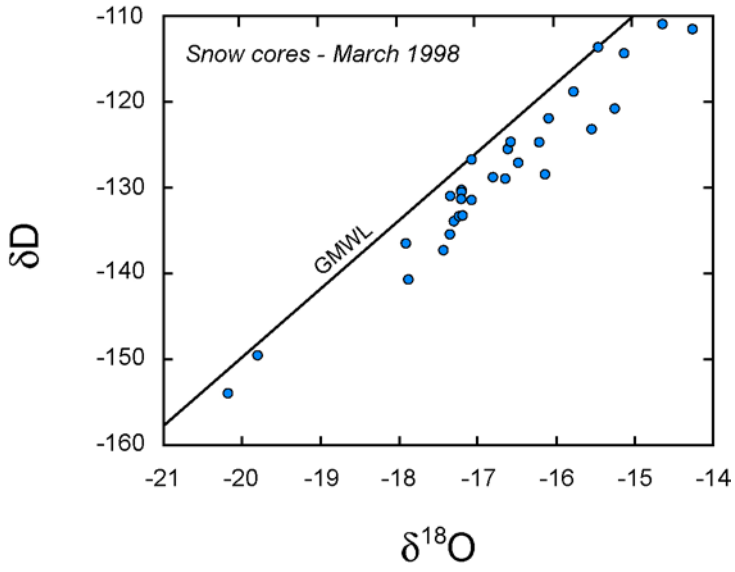

Figure 3. Plot of δD vs. $\delta^{18}O$ values of snow core samples collected throughout central Nevada during March 1998. Many of the data points are shifted to the right of the global meteoric water line (GMWL) due to kinetic isotope fractionation effects during aging of the snowpack. The average *d*-value for these samples (+5) is nearly the same as for the groundwaters in Figure 2.

process is accompanied by kinetic isotope fractionation effects that gradually enrich the snowpack in heavy isotopes over time (Friedman et al., 1991).

Figure 3 shows a $\delta^{18}O$-δD plot for 28 bulk snow cores collected throughout central Nevada in March 1998 (Rose et al., 1999). Many of the data points are shifted to the right of the GMWL, with an average *d*-value near +5. This *d*-value is similar to that of the groundwaters plotted in Figure 2, suggesting that snow metamorphism may account for the observed shift off the GMWL in Nevada groundwaters. However, to fully test this hypothesis it is necessary to compare the isotopic value of bulk winter precipitation with that of snowmelt infiltration. Snowfall collected in a precipitation gauge will not undergo mass loss due to snow metamorphism, and the initial isotopic composition of the snow will be preserved. In contrast, snowmelt collected in a shallow lysimeter should exhibit the final isotopic composition of the water that infiltrates the soil zone following snow metamorphism.

Sample Locations and Methods

Precipitation gauges were installed in January 1999 at three locations along the Hwy 50 corridor (Austin Summit, Pinto Summit, and Little Antelope Summit) and one location along Hwy 6 (Currant Summit). Site locations are shown in Figure 1. The precipitation gauges consist of 1 m segments of 15.7 cm diameter PVC pipe that are capped at one end, and mounted vertically in a stone foundation. Evaporation effects are minimized by adding mineral oil to the bottom of the gauges. Site coordinates were determined using a portable GPS, and are given in Table 1. Elevations at the gauging stations range from 2140 to 2285 m above sea level, and represent the highest elevationpoints that are readily accessible by major highways within the geographic region of interest. Integrated samples of cool and warm season precipitation are collected on a biannual basis, usually during May and October. The entire sample (typically between 1 and 5 L of water) is removed from the gauge using a peristaltic pump and taken to back to the lab for an accurate volume determination. The precipitation amount, x (in cm) is then calculated from the volume measurement (V) using the equation $x = V/\pi r^2$, where r is the radius of the gauge.

Shallow infiltration samples are collected during the winter season using small lysimeters that are buried near the precipitation gauges. The lysimeter consists of a 15.7 cm diameter funnel attached to a 2L-HDPE bottle with silicone sealant and wrapped with watertight tape along the seal. A 6 mm OD copper tube (approximately 0.5 m in length) is inserted through a separate hole at the top of the bottle to maintain a constant pressure between the interior of the bottle and the atmosphere. The vent tube is also of great assistance in finding the lysimeter on the return visit, since it's the only part of the assembly that extends above the surface. A small amount of mineral oil is added to the bottom of the lysimeter to prevent evaporation, and the mouth of the funnel is filled with smooth pebbles to facilitate drainage of water from the top of the funnel into the bottle. The lysimeter is then buried with the top of the funnel situated approximately 10 cm below the soil surface. The soil layer above the lysimeter is carefully replaced, loosely packed and then leveled to avoid forming a depression.

Table 1. Locations of precipitation gauges and springs.

Sample Name/Type	**Latitude** (dms)	**Longitude** (dms)	**Elevation** (m)
Austin Summit			
Precipitation gauge/lysimeter	39 28 53	117 02 22	2285
Spring	39 28 51	117 02 39	2240
Pinto Summit			
Precipitation gauge/lysimeter	39 27 03	115 56 06	2255
Spring	39 27 25	115 56 18	2240
Little Antelope Summit			
Precipitation gauge/lysimeter	39 23 46	115 28 01	2267
Spring	39 24 57	115 29 35	2200
Currant Summit			
Precipitation gauge/lysimeter	38 49 05	115 16 58	2140
Spring	38 49 22	115 18 04	2085

Mountain springs located near each gauging station are also sampled biannually to compare the isotopic composition of the local (perched) water table with that of the precipitation and infiltration samples. Discharge rate and water quality parameters (temperature, conductivity, alkalinity, and pH) are measured in the field. Spring locations are given in Table 1.

Results

Precipitation Data

The weighted mean isotopic compositions and mean precipitation amounts for samples from all four precipitation monitoring sites are reported in Table 2. The full data set is found in Table 3. Weighted mean isotopic values are calculated using the expression:

$$\delta_{mean} = \frac{\sum \delta_1 X_1}{\sum X_1}$$

where δ_i is the measured isotopic value for a given sample, and x_i is the corresponding precipitation amount (in cm). Each site has been visited a total of seven times since the

gauges were installed in January 1999. The first set of samples, collected in July 1999, likely represents a mixture of cool and warm season precipitation, and these data are not used in calculating mean values (with the exception of the 'full record' isotopic values in Table 2). A sample was not obtained at Currant Summit in July 1999 due to vandalism; fortunately, this has not been a recurrent problem.

Table 2. Mean Precipitation Amounts and Isotopic Values

	Austin Summit		**Pinto Summit**		**Little Antelope Summit**		**Currant Summit**	
	Mean Precipitation Amounts (past 3 years)							
	(cm)		(cm)		(cm)		(cm)	
Annual	16.8		29.3		28.1		22.2	
Warm Season	3.3		6.4		6.7		5.3	
Cool Season	13.5		22.9		21.4		16.9	
	Weighted Mean Isotopic Values							
	$\delta^{18}O$ (‰)	δD (‰)	$\delta^{18}O$ (‰)	δD (‰)	$\delta^{18}O$ (‰)	δD (‰)	$\delta^{18}O$ (‰)	δD (‰)
Full Record	-14.6	-108	-15.0	-109	-14.8	-108	-14.3	-103
Past 3 Years	-14.6	-108	-14.8	-107	-14.6	-106	-14.3	-103
Warm Season (3 yrs)	-10.3	-77	-10.6	-74	-8.2	-53	-7.6	-51
Cool Season (3 yrs)	-15.6	-115	-16.0	-116	-16.7	-123	-16.4	-120

Mean precipitation amounts range from 16.8 cm/yr at Austin Summit to 29.3 cm/yr at Pinto Summit, although the relative proportion of warm vs. cool season precipitation is fairly consistent at all four locations. On average, between 20 and 24% of the precipitation fell during the warm season, compared with 76 to 80% during the cool season. These statistics may be influenced by a drier-than-average summers in 1999 and 2001, particularly at Austin and Pinto Summit (Table 3), and in all likelihood the precipitation record is simply too brief to determine meaningful long-term averages.

Two of the precipitation gauges (Austin and Pinto Summits) are located near weather monitoring stations in Austin and Eureka, allowing a comparison of our data with longer-term records. The data were obtained from the Western Regional Climate Center website (www.wrcc.dri.edu). The average precipitation rate in Austin is 32.0 cm/yr, or nearly double the value measured at Austin Summit during this study. This implies the past three years have been unusually dry in this area. Warm season precipitation (June to October) accounts for 27% of the annual total at Austin – somewhat higher than the 20% value measured at Austin Summit. In Eureka, the average annual precipitation is 30.1 cm/yr, which is fairly close to the value measured at Pinto Summit (29.3 cm/yr).

Table 3. Precipitation Data

Location / Sample Date	Time Period	Precipitation Amount (cm)	$\delta^{18}O$ (‰)	δD (‰)
Austin Summit				
16-Jul-99	01/99 - 07/99	13.7	-14.7	-107
1-Nov-99	07/99 - 10/99	0.7	-5.9	-41
15-May-00	11/99 - 05/00	11.0	-17.1	-131
16-Oct-00	05/00 - 10/00	7.1	-12.0	-92
14-May-01	10/00 - 05/01	12.1	-15.8	-116
24-Oct-01	05/01 - 10/01	2.1	-6.2	-39
22-May-02	10/01 - 05/02	17.3	-14.6	-105
Pinto Summit				
16-Jul-99	01/99 - 07/99	20.7	-15.9	-119
2-Nov-99	07/99 - 10/99	2.6	-8.3	-50
15-May-00	11/99 - 05/00	19.5	-16.1	-117
16-Oct-00	05/00 - 10/00	12.6	-12.3	-89
14-May-01	10/00 - 05/01	25.9	-16.7	-121
24-Oct-01	05/01 - 10/01	3.9	-6.6	-43
23-May-02	10/01 - 05/02	23.4	-15.2	-111
Little Antelope Summit				
16-Jul-99	01/99 - 07/99	21.4	-15.7	-116
2-Nov-99	07/99 - 10/99	6.1	-6.7	-37
16-May-00	11/99 - 05/00	17.2	-17.4	-128
16-Oct-00	05/00 - 10/00	9.0	-10.6	-75
14-May-01	10/00 - 05/01	23.4	-17.6	-131
24-Oct-01	05/01 - 10/01	5.1	-5.6	-35
23-May-02	10/01 - 05/02	23.6	-15.2	-111
Currant Summit				
17-Jul-99	01/99 - 07/99	---	---	---
3-Nov-99	07/99 - 10/99	3.1	-6.6	-41
16-May-00	11/99 - 05/00	16.7	-16.1	-118
17-Oct-00	05/00 - 10/00	7.2	-9.4	-66
15-May-01	10/00 - 05/01	21.4	-16.6	-120
24-Oct-01	05/01 - 10/01	5.5	-5.8	-36
23-May-02	10/01 - 05/02	12.7	-16.5	-121

However, warm season precipitation accounts for 35% of the Eureka total, which is higher than the 22% average determined for Pinto Summit.

The weighted mean δD and $\delta^{18}O$ values for cool season, warm season, and annual precipitation are plotted in Figure 4. All of the data plot near the global meteoric water line, indicating that little evaporation occurred during descent of the precipitation through the atmosphere. Not surprisingly, cool season precipitation exhibits significantly lighter (more negative) isotopic values than warm season precipitation, in accordance with the temperature dependence of isotopic fractionations. The annual mean for each site is strongly skewed toward the winter mean, since this is when the majority of the precipitation falls. In addition, both the winter and annual mean values are fairly consistent between locations (only ~1‰ variation in $\delta^{18}O$, and 8‰ in δD within each group), even though the four sites are up to 150 km apart. This may reflect the tendency for winter low-pressure systems to be regional in extent.

Spring Water Data

Groundwater samples were collected from low volume springs located near each precipitation gauge beginning in the Fall of 1999. A total of six samples had been collected from each spring at the time of this report. Seepage through the vadose zone tends to homogenize differences in the isotopic composition of individual precipitation events (Yonge et al., 1985). Hence, local perched springs are generally considered to be good indicators of the average isotopic composition of recharge in a given area. When coupled with seasonal precipitation data, the springs can be used to deduce the relative contribution of summer vs. winter precipitation to the net recharge budget.

Measured flow rates, water quality parameters, and isotopic values for the springs are given in Table 4. All of the springs have low flow rates (averaging ~0.3 to 6 L/min), and show small fluctuations in discharge and water quality over time. Little Antelope Spring has a notably higher solute content than the other springs, implying a somewhat longer (or deeper?) flowpath. The $\delta^{18}O$ and δD values of each spring are fairly consistent over time, implying well-mixed groundwater systems. A notable exception is the May 2002 sample from Austin Summit, which was collected only a few days after a late spring snowstorm produced locally heavy accumulations. The cool-season precipitation, spring, and lysimeter samples collected from Austin Summit at the time all had nearly identical stable isotope values. The isotopic compositions of the spring and lysimeter samples probably reflected the rapid melting and infiltration of snow deposited by this storm. Figure 5 is a plot of the average δD vs. $\delta^{18}O$ values for the spring waters, together with the weighted mean values of winter and total precipitation for each site. With the possible exception of Currant Spring, the recharge contribution from summer precipitation appears to be negligible at these sites. Three of the springs (Currant, Pinto, and Little Antelope) have isotopic values that are shifted to the right of the global meteoric water line (GMWL), indicating evaporative enrichment before or during recharge. The *d*-values for these springs are all quite low, ranging from +0.8 to +2.1. In contrast, Austin Spring plots very close to the GMWL (with d = +9.8), and has an isotopic composition that is nearly identical to the mean cool season precipitation at

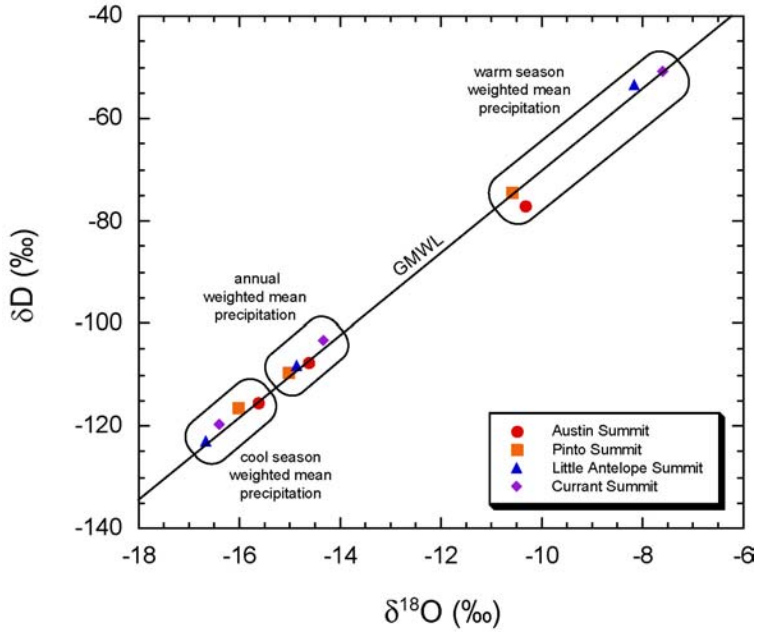

Figure 4. Weighted mean δD and $\delta^{18}O$ values for cool season, warm season, and annual precipitation from four monitoring sites in central Nevada. Data generally plot along the global meteoric water line (GMWL). The annual precipitation data are strongly skewed toward the cool season mean, reflecting the fact that most of the precipitation occurs during the winter months.

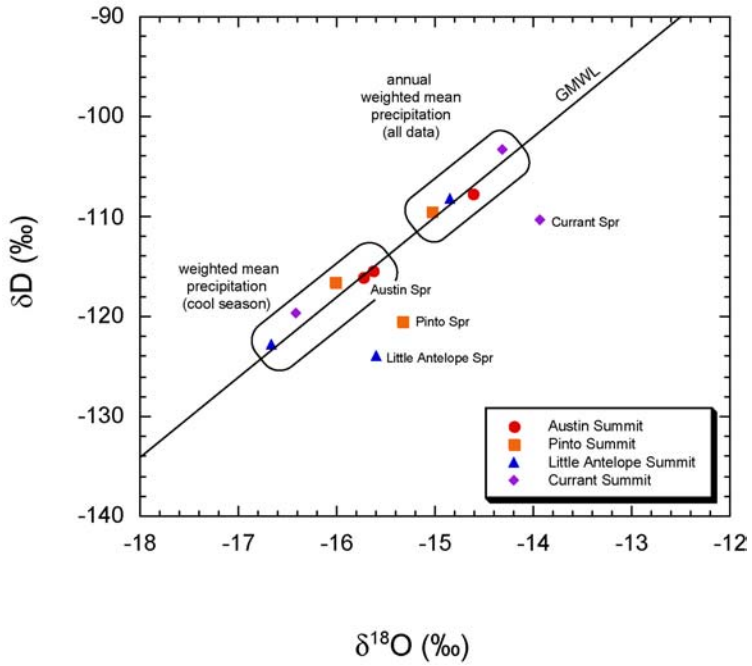

Figure 5. Comparison of δD and $\delta^{18}O$ values of precipitation samples and local springs at monitoring sites in central Nevada. Three of the springs (Currant, Pinto, and Little Antelope) are shifted to the right of the global meteoric water line (GMWL), reflecting evaporation processes during recharge. In contrast, the isotopic composition of Austin Spring is nearly the same as the cool season precipitation at Austin Summit.

Table 4. Spring water data.

Location / Sample Date	Est. Flow Rate (L/min)	Temp. (°C)	pH	Cond. (µS/cm)	Alkalinity (mg/L)	$\delta^{18}O$ (‰)	δD (‰)
Austin Summit Spring							
1-Nov-99	1.0	9	7.83	239	125	-16.0	-118
15-May-00	0.2	13	7.05	275	115	-16.1	-117
16-Oct-00	0.1	6	7.20	315	n.d.	-15.9	-116
14-May-01	< 0.1	18	7.05	277	140	-15.9	-118
24-Oct-01	< 0.1	7	7.80	377	150	-15.9	-120
22-May-02	0.3	7	7.15	311	130	-14.6	-107
Pinto Summit Spring							
2-Nov-99	5.0	4	8.10	299	175	-15.2	-120
15-May-00	15.0	7	7.50	395	150	-15.7	-120
16-Oct-00	2.0	5	7.69	372	n.d.	-15.4	-122
14-May-01	3.0	12	8.02	373	185	-15.4	-121
24-Oct-01	3.0	5	8.02	418	180	-15.2	-119
23-May-02	6.0	15	7.50	460	175	-15.1	-121
Little Antelope Spring							
2-Nov-99	1.0	9	7.08	1421	350	-15.5	-122
16-May-00	1.0	8	6.98	1661	400	-15.7	-122
16-Oct-00	1.0	9	6.76	1665	n.d.	-15.6	-124
14-May-01	0.9	8	6.95	1684	350	-15.6	-125
24-Oct-01	1.0	9	7.05	1520	400	-15.6	-126
23-May-02	0.8	8	7.05	1521	400	-15.6	-125
Currant Summit Spring							
3-Nov-99	0.5	12	7.51	381	170	-13.9	-108
16-May-00	0.1	2	7.20	477	160	-13.9	-110
17-Oct-00	0.3	8	7.21	446	n.d.	-14.0	-112
15-May-01	1.2	13	7.72	456	160	-14.0	-112
24-Oct-01	0.3	8	7.51	402	175	-13.9	-111
23-May-02	0.1	7	7.52	388	175	-13.9	-109

n.d. = not determined

Austin Summit (Figure 5). The lack of evaporation may reflect the nature of the soil and bedrock at Austin Summit. The area is underlain by granitic bedrock with common surface exposures, and has a relatively thin, coarse-grained soil cover. Once the soil zone becomes saturated, water may percolate downward fairly rapidly to the underlying fractured bedrock, thereby minimizing evaporative losses.

To estimate the mean isotopic values of Currant, Pinto, and Little Antelope Springs prior to evaporation, we projected the observed values back to the GMWL along an assumed evaporation trajectory. Evaporation lines have slopes that vary from approximately 3 to 6 depending on the temperature and relative humidity conditions (Gat, 1971). Lowerslopes are more typical in arid environments due to lower humidity. Assuming an evaporation line with a slope of 4, the following pre-evaporation values (on the GMWL) are obtained:

Currant Spring [$\delta^{18}O$ = -16.1‰, δD = -119‰];
Pinto Spring [$\delta^{18}O$ = - 17.3‰, δD = -128‰];
Little Antelope Spring [$\delta^{18}O$ = -7.9‰, δD = -133‰].

The pre-evaporation isotopic values for Currant Spring are slightly heavier than the cool season precipitation average, implying a small contribution of warm-season recharge. Using the cool-season and warm-season precipitation averages, we estimate a maximum warm season recharge contribution of only 3.5%. Decreasing the assumed slope of the evaporation line from 4 to 3 would increase the warm-season recharge fraction to a maximum value of 8%. In contrast, the evaporation-corrected isotopic values for Pinto Spring and Little Antelope Spring are actually lower than the cool season precipitation average for these sites by 1.3‰ in $\delta^{18}O$ and 10 to 12‰ in δD. This may imply that average cool-season precipitation at these locations is normally isotopically lighter (more negative) than the current precipitation record suggests. Possible alternative explanations include: (1) the preferential recharge of isotopically light snowmelt, and (2) short-term (decade-scale) variations in climate.

The volume of water that reaches the soil-bedrock interface is largely determined by the balance between the timing of evapotranspiration and infiltration through the soil profile (Hevesi et al., 2002). Assuming that soil zone infiltration is driven largely by piston flow, it follows that early-season infiltration should reach the soil-bedrock interface first. It is well known that as a snowpack begins to melt, the initial melt water is isotopically lighter than the bulk snow composition, with the heavy isotope content of the melt water steadily increasing over time (Stichler et al., 1981; Herrmann et al., 1981). Thus, the initial wetting front in the soil zone should be isotopically lighter than the infiltration that comes later in the season. This process could lead to the preferential recharge of isotopically light 'early' snowmelt, although this hypothesis has not been tested.

Another possibility is that the water discharging at Pinto and Little Antelope Springs may have a longer residence time than that of Austin and Currant Springs. If groundwater residence times are the order of decades, the possibility arises that short-term variations in climate could influence the isotopic compositions of the springs. Decade-scale changes in the stable isotope composition of spring waters were recently recognized in

the Sierra Nevada, and were attributed to increases in mean annual air temperature and changes in atmospheric circulation patterns between the 1960s and 1990s (Rademacher et al., 2002). $\delta^{18}O$ and δD values were observed to increase by 1.2‰ and 11‰ over this time frame, which is nearly identical to the difference between the evaporation-corrected spring compositions and average cool-season precipitation at Pinto and Little Antelope Summits. Comparison of the tritium content of modern precipitation with that of the springs would help to determine whether this is a viable model for central Nevada.

Lysimeter Data

Shallow infiltration samples were collected during the past three winter seasons using small lysimeters that were buried in close proximity to each of the precipitation gauges. The main objective was to obtain samples of snowmelt *as it entered the soil zone* to determine whether kinetic isotope enrichments during snow metamorphism (Figure 3) are inherited during recharge. Mineral oil is added to the bottom of the lysimeters to prevent further evaporation once the sample enters the container. The lysimeter data are summarized in Table 5.

Infiltration amounts vary significantly from year to year at a given location, and are not strongly correlated with precipitation amount – although larger amounts of infiltration tend to occur during winters with higher than average precipitation. The ratio of infiltration to precipitation amount ranges from <1% to 59%. Austin and Pinto Summits show the largest range in infiltration amounts, whereas Little Antelope and Currant Summits tend to show a more consistent range in values (Table 5). Several factors may affect the amount of shallow infiltration that accumulates in the lysimeter, including soil properties, evapotranspiration rates, snowpack distribution (e.g. drifting), and the rate at which the snowpack melts. As previously noted, the large amount of infiltration collected at Austin Summit in May 2002 is thought to reflect the rapid melting of a late season snowstorm.

The δD and $\delta^{18}O$ values of the lysimeter samples are also quite variable, and include values that are both above and below the average cool season precipitation value for a given location. In part this reflects year-to-year differences in the isotopic composition of the cool-season precipitation (Table 3), although the lysimeter samples rarely have the same isotopic composition as the precipitation for a given year. On two occasions, the amount of water in the lysimeter was too small to perform stable isotope measurements.

The stable isotope compositions of the lysimeter samples are plotted in Figure 6. The data generally plot either along the GMWL or below it, although one sample from Little Antelope Summit is well above the line (with a *d*-value of +16.4). The four samples with evaporated isotopic signatures are associated with small infiltration volumes ($\leq$ 0.5 cm of precipitation equivalent) and low infiltration/precipitation ratios ($\leq$ 4%). In comparison, the five samples that plot along the GMWL have infiltration volumes ranging from 0.7 to 10.4 cm of precipitation equivalent, and infiltration/precipitation ratios between 6 and 59%. Hence, there is a clear correlation between infiltration amount and the extent of evaporation. The evaporated samples may reflect the slow infiltration of moisture that

sat in the shallow soil environment for an extended period of time, whereas the non-evaporated samples indicate more rapid infiltration of larger fluid volumes.

In general, the lysimeter data do *not* substantiate the hypothesis that evaporated groundwaters in central Nevada are derived from fractionation processes during snowmetamorphism. If this were the case, we would expect all of the lysimeter data to plot below the GMWL in Figure 6. Instead, we observe that larger volume lysimeter samples all have isotopic values that cluster along the GMWL. This suggests the integrated flux of snowmelt infiltration will have a *d*-value very similar to that of the original precipitation (d = +10) *in the absence of further evaporation effects*. (It is important to remember that the lysimeters contained mineral oil that prevented additional evaporation once the sample had reached the container). The results of this study point to evaporative losses through the soil profile and during runoff as the dominant mechanisms for isotopic enrichment. It should be noted that plant transpiration returns water to the atmosphere essentially unchanged with respect to its isotopic composition, and is not associated with fractionation effects (Zimmermann et al., 1967).

Table 5. Lysimeter data.

Location / Sample Date	Time Period	Infiltration Amount (cm)	Infiltration / Precipitation (ratio)	$\delta^{18}O$ (‰)	δD (‰)
Austin Summit					
15-May-00	11/99 - 05/00	0.2	0.02	-16.2	-132
14-May-01	10/00 - 05/01	0.7	0.06	-16.9	-124
22-May-02	10/01 - 05/02	10.3	0.59	-14.5	-105
Pinto Summit					
15-May-00	11/99 - 05/00	<0.1	<0.01	-12.6	-101
14-May-01	10/00 - 05/01	10.4	0.40	-15.6	-115
23-May-02	10/01 - 05/02	<0.1	<0.01	---	---
Little Antelope Summit					
16-May-00	11/99 - 05/00	<0.1	<0.01	---	---
14-May-01	10/00 - 05/01	0.1	<0.01	-18.3	-130
23-May-02	10/01 - 05/02	0.2	0.01	-15.2	-119
Currant Summit					
16-May-00	11/99 - 05/00	2.8	0.17	-16.2	-120
15-May-01	10/00 - 05/01	1.2	0.06	-15.3	-112
23-May-02	10/01 - 05/02	0.5	0.04	-13.4	-116

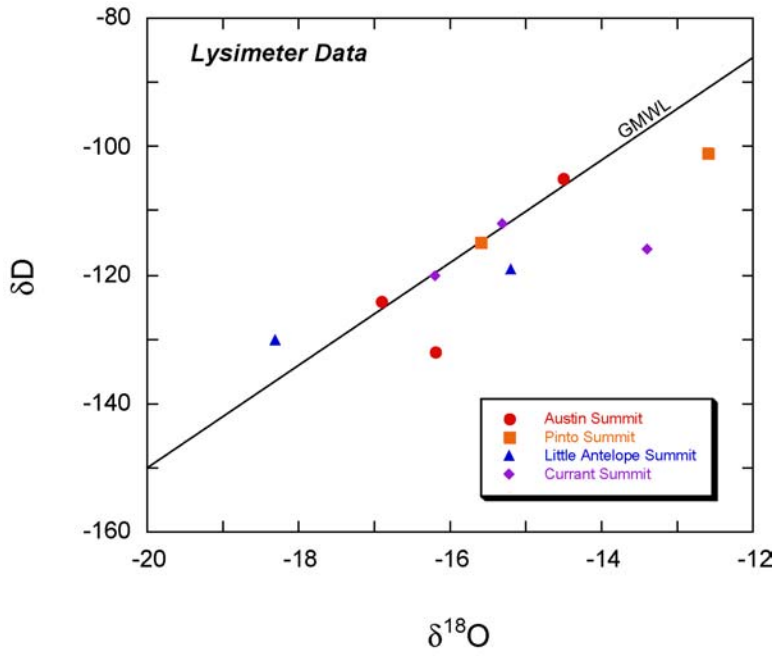

Figure 6. Plot of δD vs. $\delta^{18}O$ values of lysimeter samples from monitoring locations in central Nevada. Evaporated samples plotting below the global meteoric water line (GMWL) correlate with small infiltration volumes. Samples representing larger infiltration volumes tend to cluster along the GMWL. See text for discussion.

The data from this study and Rose et al. (1999) suggest a complex isotopic evolution during snow metamorphism and melting. The combined data sets show that the initial isotopic composition of winter precipitation lies along the GMWL (Figure 4), and that subsequent recrystallization of the snowpack causes the an isotopic enrichment characterized by *d*-values of <10 (Figure 3). However, the lysimeter data imply this enrichment is essentially reversed during melting, yielding snowmelt infiltration with a *d*-value similar to that of the original precipitation (near +10). The explanation for this reversal may be related to the late-stage evolution of the snowpack. Rose et al. (1999) collected snow samples on multiple occasions from the same locations during a single season and found that the late season snow plotted along δD-$\delta^{18}O$ trajectories with slopes greater than 8. This evolutionary pathway is consistent with a late-season increase in the deuterium excess values of the snowmelt, and may account for the fact that the 'large volume' lysimeter samples do not appear to be evaporated.

Conclusions

The results of this study suggest that the evaporated isotopic signatures of spring waters in Nevada are either inherited during runoff events, or by evaporative losses through the soil zone. Net infiltration along stream channels is not considered a significant component of the overall recharge budget because the area affected by active channels is small relative to the interchannel areas (Hevesi et al., 2002). Hence, direct (*in situ*)

infiltration of snowmelt is probably the dominant recharge mechanism, and most of the evaporation that occurs is probably related to losses through the soil profile. Collecting water samples along a depth profile through the soil zone would yield insights into the isotopic distribution within the upper soil zone during springtime infiltration. Barnes and Allison (1983, 1988) have used this approach to model evaporation through the soil profile. However, evaporation through unsaturated soils is a complicated process because isotopic transport occurs by diffusion of both liquid water and water vapor (see Criss, 1999). Developing a quantitative isotope model for soil evaporation would require a more involved monitoring and sampling program than the current scope of this study, and would necessitate setting up instrumentation to measure variations in soil moisture and humidity conditions over time.

The main conclusions of this study are as follows.

(1) The existing data indicate that warm season precipitation accounts for approximately 20 to 25% of the precipitation total, although these statistics may be biased by drier than average summers over the course of the study. The isotopic composition of the mean annual precipitation is strongly weighted toward the cool season average.

(2) Cool season precipitation dominates the recharge budget in central Nevada, accounting for essentially all of the recharge at three of the study locations, and >90% of the recharge at one site. This result is consistent with conclusions drawn by Winograd et al. (1998) for recharge in the Spring Mountains of southern Nevada.

(3) Stable isotope compositions of integrated precipitation samples show little evidence of evaporation prior to infiltration. The majority of evaporation evidently occurs during infiltration through the soil zone. The extent of evaporation is likely to be dependent on the rate at which the snowpack melts, which determines the infiltration rate. Slower infiltration rates translate to larger evaporative losses. Kinetic isotope effects during snow metamorphism do not appear to have an important influence on the bulk isotopic composition of snowmelt infiltration.

Extending this work into the future will result in a more rigorous database that better reflects the mean isotopic compositions of precipitation, spring water, and infiltration samples at each of these sites. Basic data of this type are critical to the development of quantitative recharge models. Estimates of infiltration rates and their corresponding isotopic compositions can be improved by deploying multiple lysimeters at a given site, which will help to offset localized effects related to heterogeneous snow cover and soil properties. In addition, tritium analyses should be performed to determine whether observed differences in the isotopic compositions of springs and average winter precipitation are related to climate variations or simply the length of the current monitoring record.

Acknowledgments

The Hydrologic Resources Management Program at the U.S. Department of Energy, Nevada Operations Office provided the funding for this work. I wish to thank Bruce Hurley, Bonnie Thompson, Dave Smith, and Annie Kersting for their support and encouragement of this study. Dave Smith, Ross Williams, Gail Eaton, and Lee Davisson provided field assistance on various occasions, and Gail Eaton helped prepare the figures for this report. This work was performed under the auspices of the U.S. Department of Energy by Lawrence Livermore National Laboratory under contract number W-7405-Eng-48.

References

Barnes, C.J., and Allison, G.B. (1983) The distribution of deuterium and ^{18}O in dry soils. Theory. Journal of Hydrology, 60, pp 141-156.

Barnes, C.J., and Allison, G.B. (1988) Tracing water movement in the unsaturated zone using stable isotopes of hydrogen and oxygen. Journal of Hydrology, 100, pp 143-176.

Benson, C.S., and Trabant, D.C. (1973) Field measurements of the flux of water vapor through dry snow. In: *Proceedings, Symposia on the Role of Snow and Ice in Hydrology*, Banff, September 1972, vol. 1. Unesco-WMO-IAHS Publication no. 107, pp 291-298.

Benson, L. and Klieforth, H. (1989) Stable isotopes in precipitation and ground water in the Yucca Mountain region, southern Nevada: paleoclimatic implications. In: D.H. Peterson (ed.), *Aspects of Climate Variability in the Pacific and Western Americas*. American Geophysical Union, Geophysical Monograph v. 55, pp 41-59.

Coplen, T.B., Herczeg, A.L., and Barnes, C. (2000) Isotope engineering – using stable isotopes of the water molecule to solve practical problems. In: P.G. Cook and A.L. Herczeg (eds.), Environmental Tracers in Subsurface Hydrology. Kluwer, Boston, pp 79-110.

Craig, H. (1961) Isotopic variations in meteoric waters. Science, 133, pp 1702-1703.

Craig, H., Gordon, L.I., and Horibe, Y. (1963) Isotope exchange effects in the evaporation of water. 1. Low-temperature experimental results. Journal of Geophysical Research, 68, pp 5079-5087.

Criss, R.E. (1999) Principles of Stable Isotope Distribution. Oxford Press, New York, 254 p.

D'Agnese, F.A., Faunt, C.C., Turner, A.K., and Hill, M.C. (1997) Hydrogeologic evaluation and numerical simulation of the Death Valley regional ground-water flow system, Nevada and California. U.S. Geological Survey Water-Resources Investigations Report 96-4300, 124 p.

Dansgaard, W. (1964) Stable isotopes in precipitation. Tellus, 16, 436-468.

Davisson, M.L., Smith, D.K., Kenneally, J., and Rose, T.P. (1999) Isotope hydrology of southern Nevada groundwater: stable isotopes and radiocarbon. Water Resources Research, 35, pp 279-294.

Dettinger, M.D. (1989) Reconnaissance estimates of natural recharge to desert basins in Nevada, U.S.A., by using chloride-balance calculations. Journal of Hydrology, 106, pp 55-78.

Eakin, T.E. (1966) A regional interbasin groundwater system in the White River area, southeastern Nevada. Water Resources Research, 2, pp 251-271.

Fontes, J.Ch. (1980) Environmental isotopes in groundwater hydrology. In: P. Fritz and J.Ch. Fontes (eds.), *Handbook of Environmental Isotope Geochemistry, Vol. 1, The Terrestrial Environment, A*. Elsevier, Amsterdam, pp 75-140.

Friedman, I., Benson, C., and Gleason, J. (1991) Isotopic changes during snow metamorphism. In: H.P. Taylor, Jr., J.R. O'Neil, and I.R. Kaplan (eds.), *Stable Isotope Geochemistry: A Tribute to Samuel Epstein*. Geochemical Society Special Publication No. 3, pp 211-221.

Gat, J.R. (1971) Comments on the stable isotope method in regional groundwater investigations. Water Resources Research, 7, pp 980-993.

Gat, J.R., and Dansgaard, W. (1972) Stable isotope survey of the fresh water occurrences in Israel and the northern Jordan Rift Valley. Journal of Hydrology, 16, pp 177-212.

Harrill, J.R., Gates, J.S., and Thomas, J.M. (1988) Major ground-water flow systems in the Great Basin region of Nevada, Utah, and adjacent states. U.S. Geological Survey Hydrologic Investigations Atlas, HA-694-C, scale 1:1,000,000, 2 sheets.

Herrmann, A., Lehrer, M., and Stichler, W. (1981) Isotope input into runoff systems from melting snow covers. Nordic Hydrology, 12, pp 309-318.

Hevesi, J.A., and Flint, A.L. (1998) Geostatistical estimates of future recharge for the Death Valley Region. In: *High Level Radioactive Waste Management*, Proceedings of the Ninth Annual International Conference, Las Vegas, NV, May 11-15, 1998, pp 173-177.

Hevesi, J.A., Flint, A.L., and Flint, L.E. (2002) Preliminary estimates of spatially distributed net infiltration and recharge for the Death Valley region, Nevada-California. U.S. Geological Survey Water-Resources Investigations Report 02-4010, 36 p.

Houghton, J.G. (1969) Characteristics of rainfall in the Great Basin. Desert Research Institute, University of Nevada, Reno, 205 p.

Ingraham, N.L., and Taylor, B.E. (1991) Light stable isotope systematics of large-scale hydrologic regimes in California and Nevada. Water Resources Research, 27, pp 77-90.

Ingraham, N.L., Lyles, B.F., Jacobson, R.L., and Hess, J.W. (1991) Stable isotopic study of precipitation and spring discharge in southern Nevada. Journal of Hydrology, 125, pp 243-258.

Ingraham, N.L., Caldwell, E.A., and Verhagen, B.T. (1998) Arid catchments. In: C. Kendall and J.J. McDonnell (eds.), *Isotope Tracers in Catchment Hydrology*. Elsevier, Amsterdam, pp 435-465.

Lamke, R.D., and Moore, D.O. (1965) Interim inventory of surface water resources of Nevada. Nevada Department of Conservation and Natural Resources, Water Resources Bulletin no. 30, 38 p.

Margaritz, M., Aravena, R., Pena, H., Suzuki, O., and Grilli, A. (1989) Water chemistry and isotope study of streams and springs in northern Chile. Journal of Hydrology, 108, pp 323-341.

Maxey, G.B., and Eakin, T.E. (1950) Groundwater in White River Valley, White Pine, Nye, and Lincoln Counties, Nevada. Nevada State Engineer, Water Resources Bulletin no. 8, 59 p.

Mifflin, M.D., and Hess, J.W. (1979) Regional carbonate flow systems in Nevada. Journal of Hydrology, 43, pp 217-237.

Rademacher, L.K., Clark, J.F., and Hudson, G.B. (2002) Temporal changes in stable isotope composition of spring waters: Implications for recent changes in climate and atmospheric circulation. Geology, 30, pp 139-142.

Reiner, S.R., Laczniak, R.J., DeMeo, G.A., Smith, J.L., Elliott, P.E., Nylund, W.E., and Fridrich, C.J. (2002) Ground-water discharge determined from measurements of evapotranspiration, other available hydrologic components, and shallow water-level changes, Oasis Valley, Nye County, Nevada. U.S. Geological Survey Water-Resources Investigations Report 01-4239, 65 p.

Rose, T.P., and Davisson, M.L. (2002) Isotopic and geochemical evidence for Holocene-age groundwater in regional flow systems of south-central Nevada. In: Y. Enzel, S.G. Wells, and N. Lancaster (eds.), *Paleoenvironments and Paleohydrology of the Mojave and Southern Great Basin Deserts*. Geological Society of America Special Paper, *in press*.

Rose, T.P., Davisson, M.L., Criss, R.E., and Smith, D.K. (1999) Isotopic investigation of recharge to a regional groundwater flow system, Great Basin, Nevada, USA. In: *Proceedings, International Symposium on Isotope Techniques in Water Resources Development and Management*, Vienna, 10-14 May 1999. International Atomic Energy Agency, IAEA-CSP-2/C, session 2, pp 63-72.

Sami, K. (1992) Recharge mechanisms and geochemical processes in a semi-arid sedimentary basin, Eastern Cape, South Africa. Journal of Hydrology, 139, pp 27-48.

Shevenell, L. (1996) Statewide potential evapotranspiration maps for Nevada. Nevada Bureau of Mines and Geology Report 48, 32 p.

Smith, G.I., Friedman, I., Gleason, J.D., and Warden, A. (1992) Stable isotope compositions of waters in southeastern California: 2. Groundwaters and their relation to modern precipitation. Journal of Geophysical Research, 97, pp 5813-5823.

Stewart, M.K. (1975) Stable isotope fractionation due to evaporation and isotopic exchange of falling waterdrops: Applications to atmospheric processes and evaporation of lakes. Journal of Geophysical Research, 80, pp 1133-1146.

Stichler, W., Rauert, W., and Martinec, J. (1981) Environmental isotope studies of an alpine snowpack. Nordic Hydrology, 12, pp 297-308.

Thomas, J.M., Benedict, F.C., Jr., Rose, T.P., Hershey, R.L., Paces, J.B., Peterman, Z.E., Farnham, I.M., Johannesson, K.H., Singh, A.K., Stetzenbach, K.J., Hudson, G.B., Kenneally, J.M., Eaton, G.F., and Smith, D.K. (2002) Geochemical and isotopic interpretations of groundwater flow in the Oasis Valley flow system, southern Nevada. Desert Research Institute, University of Nevada, Water Resources Center Publication 45190.

U.S. Department of Energy (1997) Regional groundwater flow and tritium transport monitoring and risk assessment of the Underground Test Area, Nevada Test Site, Nevada. U.S Department of Energy, Nevada Operations Office, Environmental Restoration Division Report DOE/NV-477, 396 p.

Winograd, I.J., Riggs, A.C., and Coplen, T.B. (1998) The relative contributions of summer and cool-season precipitation to groundwater recharge, Spring Mountains, Nevada, USA. Hydrogeology Journal, 6, pp 77-93.

Yonge, C.J., Ford, D.C., Gray, J., and Schwarcz, H.P. (1985) Stable isotope studies of cave seepage water. Chemical Geology, 58, pp 97-105.

Zimmermann, U., Ehhalt, D., and Münnich, K.O. (1967) Soil water movement and evapotranspiration: Change in the isotopic composition of the water. In: *Isotopes in Hydrology*. International Atomic Energy Agency, Vienna, pp 567-585.